Optimization of Core Tripping Using a Thermoporoelastic Approach

By

Rahman Ashena

A Thesis Submitted to the Department of Petroleum Engineering

Chair of Drilling and Completion Engineering

Montanuniversität Leoben

In Partial Fulfilment of the Requirements for the Degree of Doktor der montanistischen Wissenschaften

April 2017

Affidavit

I declare in lieu of oath, that I wrote this thesis and performed the associated research myself, using only literature cited in this volume.

……

Rahman Ashena, 2017

Acknowledgments

All honor and grace goes to God, with his love and infinite power, everything can be done. Accomplishments are rarely achieved without assistance from others. I would like to thank all the people who contributed to the work described in this thesis. First and foremost, I would like to express my sincere gratitude to the Department of Petroleum Engineering, Montanuniversität Leoben, for giving me the opportunity to do research for my PhD study. Sincere thanks to *Dr. Claudia Gruber* and *A.Prof. Michael Prohaska* for editing my thesis and providing valuable comments.

I would like express my appreciation to *Prof. Holger Ott* and *Dr. Siroos Azizmohammadi,* and *Mr. Rudolf-Nikolaus Knezevic, OMV* for their technical support and kind consultations on reservoir engineering and geological aspects of the work. I also wish to thank *Prof. Vamegh Rasouli*, from *University of North Dakota*, who gave me kind technical help and support on the geomechanical aspects of the research. My sincere gratitude also goes to *Mr. George Williamson* and *Mr. Auden Kvinnesland* from *Baker Hughes*, *Mr. Corin Lewsey* and *Mr. Ian Ross* from *NOV*, *Mr. Tony Kennaird* from *CoreLab*, *Ms. Iza Zubizarreta* from *Senergy*; *Mr. Jos Nutbroek* from *Boart-Longyear*, *Mr. George Tophinke* and *Mr. Chris Daws* from *Sandvik*, who graciously helped me to learn about coring systems and tripping in the petroleum and mining industries. My cordial gratitude goes to my good friends, *Mr. Roman Manasipov* for helping me to debug my simulation codes, and *Mr. Mojtaba Kiani* for checking my mathematical derivations. Special thanks also go to *Dr. Christian Koller*, from *TDE-Group*, for his technical support. My acknowledgements also go to all my colleagues in the Department of Petroleum Engineering (DPE), particularly Chair of Drilling and Completion, and our nice secretary, *Frau. Patrizia Haberl,* for their sincere contributions and the working environment.

Last but not the least, my special gratitude goes to my beloved parents, *Sohrab* and *Maryam*, my beloved siblings, *Rahim* and *Mojdeh* , and my love *Golnaz* who patiently supported me by any means to continue my education. I sincerely thank their consistent patience, reassurance, and support during this time.

Abstract

The damage of core samples can occur during the cutting, tripping, and handling phases. The core damage must be prevented otherwise the properties would be adversely altered and thus the cores would not be representative. One of the most detrimental damages occurs during tripping when the core undergoes decompression and temperature drop from the bottomhole to the surface. This occurs when sufficient time is not allowed for the pore fluids in the center of the core to dissipate than in the annulus. As a result, excessive pore pressure differences and stresses are induced within the core body. This causes tensile failure manifesting as microfractures in its body. These adversely alter the core rock and mechanical properties.

Therefore, the sample should be tripped slowly enough so that the induced pore pressure and stress difference do not become excessive and the core does not undergo tensile failure. On the other hand, this slow enough tripping rate should meet the operational rig costs so that it does not cause invisible lost time. Therefore, the optimal tripping speeds should be determined for each case. This should be used as the basis of selection for different methods. The industry has so far utilized only generic methods for selecting their core tripping speeds. Just recently, there has been some research which failed to consider the thermal effect, the mud cake effect, and mechanical properties, they did not either evaluate the induced stresses or the optimal rates.

Therefore, in this work, a state-of-the-art thermoporoelastic model has been developed to find the optimal tripping rates, which also contributes to the candidate selection. This work includes 1) the modeling, derivation, and evaluation of the hydraulic and thermal effects including the neglected ones in the literature, i.e., the thermal, mechanical, and mud cake effects; 2) summing all the effects causing induced stresses; 3) checking the induced stresses with the failure criterion; 4) indicating if tensile failure occurs for a specified tripping rate. This process is repeated for different tripping rates until the optimal one is obtained. A standard procedure is proposed to determine the optimal tripping using a standard set of inputs and running the model. During the modeling process, the contributing parameters have been identified and their effects have been investigated. Among the parameters, the hydraulic diffusivity coefficient and the in-situ conditions have been detected and introduced as the main factors determining the optimal rates and the basis for coring candidate selection.

Kurzfassung

Während des Schneidens von Bohrkernen, dem Ausbau des Bohrgestänges und während der Weiterverarbeitung können Schäden am Bohrkern auftreten. Diese Schäden gilt es zu vermeiden damit die mit dem Bohrkern verbundenen Eigenschaften auch als repräsentativ gelten. Einer der schwerwiegendsten Schäden tritt während dem Ausbau des Bohrgestänges auf, wenn der Kern einem Druck- und Temperaturabfall, welche zwischen Kernteufe und Oberfläche herrschen, ausgesetzt wird. Dieser Umstand tritt dann auf wenn Porenflüssigkeit aus der Mitte des Bohrkerns nicht genügend Zeit erhält nach außen zu dringen. Als Folge treten starke Druckdifferenzen im Porenraum sowie induzierte Spannung im Kerninneren auf. Dies führt zu Zugversagen welches Mikrofrakturierung und daher eine Veränderung der Gesteinseigenschaften zur Folge hat.

Aus diesen Gründen sollte der Bohrkern mit einer Geschwindigkeit entnommen werden, die es zulässt dass Porendruck und induzierte Spannungen nicht zu Zugversagen führen. Gleichzeitig sollte eine derartige Reduzierung der Ausbaugeschwindigkeit nicht zu einer Erhöhung der bohrplattformspezifischen Kosten führen. Deshalb sollte die optimale Ausbaugeschwindigkeit für jeden Fall einzeln bestimmt werden. Dies sollte als Basis für die zukünftige Auswahl der optimalen Geschwindigkeit sowie der optimalen Methode dienen. Der bisherige Industriestandard sah vor, dass generische Methoden zur Bestimmung der Ausbaugeschwindigkeit führen. Erst kürzlich hat es ähnliche Untersuchungen gegeben, welche jedoch Themen wie thermische Einwirkung, Einwirkungen der Bohrschlamm-Filterbarriere und mechanischen Eigenschaften nicht berücksichtigen und auch die induzierte Spannung und optimale Ausbaugeschwindigkeit nicht bewerten.

Aus diesen Gründen wurde in dieser Arbeit ein modernstes thermo-poroelastisches Modell zur Bestimmung der optimalen Ausbaugeschwindigkeit entwickelt, das auch zur Auswahl der optimalen Methoden beiträgt. Diese Arbeit beinhaltet 1) die Modellierung, Ableitung und Evaluierung von hydraulischen und thermischen Effekten, welche auch jene Einflüsse berücksichtigt, die in der bisherigen Literatur vernachlässigt wurden, d.h. thermische-, mechanische- und Bohrschlamm-Filterbarriere betreffende Einflüsse; 2) eine Aufsummierung aller Einflüsse welche induzierte Spannungen bewirken; 3) eine Untersuchung von induzierten Spannungen in Bezug auf die jeweilige Versagensart; 4) die Feststellung ob

Zugversagen für bestimmte Ausbaugeschwindigkeiten auftritt. Dieser Prozess wird solange für unterschiedliche Ausbaugeschwindigkeiten wiederholt bis die optimale Geschwindigkeit gefunden wird. Des Weiteren wird eine Standardprozedur vorgestellt, die es ermöglicht die optimale Ausbaugeschwindigkeit anhand eines Modells, welches einen standardisierten Satz an Eingabevariablen benötigt, festzustellen. Während der Modellierung werden die einflussverantwortlichen Parameter identifiziert und ihr Effekt untersucht. Innerhalb dieser Parameter sind der Koeffizient der hydraulischen Leitfähigkeit sowie die In-situ Spannungen die Hauptfaktoren zur Bestimmung der optimalen Ausbaugeschwindigkeiten sowie die Basis für die Auswahl der optimalen Methode.

Table of Contents:

List of Figures:

List of Tables:

Chapter 1: Introduction and Objectives

1.1 Introduction

In the petroleum industry, it is widely understood that core damage is a major concern when measuring properties from cores (*Worthington et al., 1987; Fjaer et al., 2008; Hettema et al., 2002; Holt, 1994*). Core damage can occur during the different phases of core cutting, tripping, handling, etc. During tripping, fast retrieval of the cores may not allow sufficient time for the dissipation of the pore fluids within the sample and pressure equalization. This is the most severe in ultra-low-permeability cores or cores with very low-permeability mud cake (*McPhee et al., 2015*). This induces pore pressure difference and tensile stresses within the sample. As this may cause tensile failure and thus the creation of microfractures within the sample, it causes the alteration of the core properties and thereby core damage. This phenomenon is attributed to the gas expansion and viscous forces applied during expansion (*Rosen et al., 2007*).

The aforementioned core damage is serious. A very specific characteristic of these fractures is the fact that they initiate within the core instead of initiating on the core surface (*Bouteca et al., 1994*). Thus, cores may be damaged though there is no apparent damage (*Bouteca et al., 1994 & Mcphee et al., 2015*). The core properties particularly the rock and mechanical ones, e.g., porosity, permeability, compressive and tensile strength, Young's modulus, etc. would not be representative of the reservoir (inferred from *Hettema et al., 2002*; *Zubizarreta et al., 2013 & Byrne et al., 2015*). In addition, the microfractures may propagate, connect, and convert into fractures leading to core jamming during tripping. An example of CT scans from a damaged tight core due to the tripping is shown in **Figure 1-1**.

In order to prevent the tensile failure and the creation of microfractures in the cores during tripping, adjusting the tripping speed may help. It should be adjusted not to exceed the critical value at each depth. The optimal rate is the tripping speed that is sufficiently slow to avoid core damage due to tripping and at the same time as quick as possible to minimize operational rig costs.

The drilling industry has not been determined to overcome the lack of clarity regarding their core tripping schedules. This is due to the fact that their KPI (Key Performance Indicator) is based on the maximum footage drilled. However, their KPI for coring, as it should be, is gradually changing to the economic core quality recovered (*Mcphee et al., 2015*). Therefore, recently some attempts have been made in adjusting the tripping rate. To prevent exceeding the critical tripping velocities, several generic or rule of thumb methods are available in the industry or standard organizations. For example, in *API RP 40, (1998*), it is stated: '*The core barrel should be brought to the surface smoothly. During the last 500 feet (*$\approx 150\ m$*) the core should be surfaced slowly to minimize gas expansion that can severely damage unconsolidated cores if the pressure is reduced too quickly*'. Several companies have their own core tripping schedules which are based on rules of thumb or experience (*McPhee et al., 2015*). These and similar other schedules for core tripping are too general and not appropriate enough. Therefore, these schedules cannot either guarantee to protect the mechanical integrity of the core during tripping (i.e., cause core damage), or cause excessive tripping times, i.e., invisible lost time. In addition, as the industry does not have an engineered approach for selecting their tripping schedules for specified core properties, they do not possess a basis for selecting their coring methods (or candidate selection).

Therefore, a more engineered method is required to model the core tripping rate during retrieval. Recently, to fill the aforementioned gap, some works have been conducted using poroelastic modeling (*Hettema et al., 2002*), fluid flow by Computational Fluid Dynamics software (*Zubizarreta et al., 2013; Byrne et al., 2015)* and Finite Element modeling *(Hoeink et al., 2015)* which relate the failure to the pore pressure difference exceeding the tensile strength of the sample. There are some lacks in the literature: 1) In none of the previous works, the induced stresses due to tripping have been evaluated to compare with the rock strength, 2) the thermal effect has not been either modeled or just an approximation for the whole sample has been considered (*Hettema et al., 2002*), 3) the mud cake effect has been just assumed constant, this does not provide a valid estimation, 4) the effect of some mechanical

properties have not been considered, 5) the contributing parameters have not been clearly identified, 6) no determinative factors have been already introduced by which we can generally manage the core tripping schedule, and 7) no criterion exists for candidate selection of the core tripping or coring method.

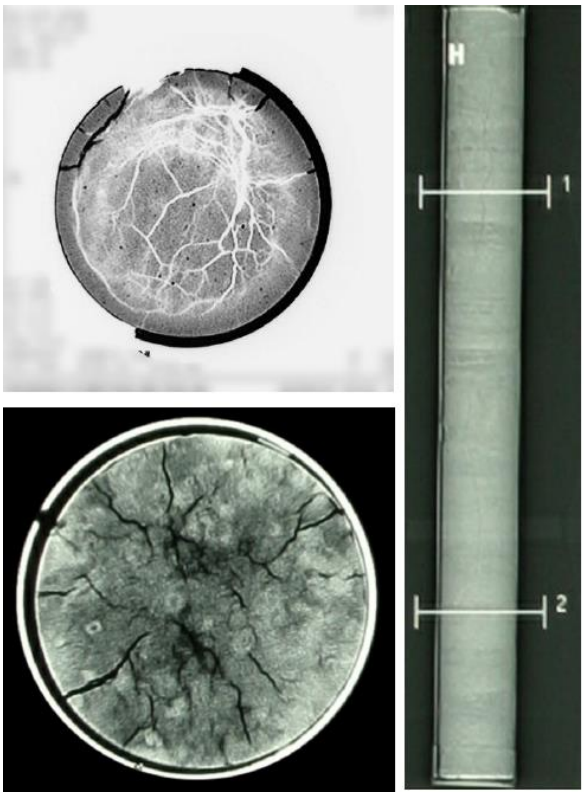

Figure 1-1: CT Scan Images Showing Microfractures Occurred in a Rock Section (*Mcphee et al., 2015; Zubizarreta et al., 2013; Byrne et al., 2015*)

1.2 Objectives and Analytical Modeling

Considering the aforementioned problem, another approach is required which considers all the effects and thus provides a more comprehensive solution to the problem. Therefore, in this work, a thermoporoelastic approach is selected. Following this approach, as an outline, the induced pore pressure and stresses within the core can be considered during its trip to the surface. Thanks to the comprehensiveness of this approach, in addition to the induced pore pressure and confining pressure drop, the mud cake and the thermal effects can also be taken into account. These effects have not been thoroughly considered in the literature. Then, a modeling procedure must be designed to create the thermoporoelastic model for the case of core tripping. This model would be able to evaluate the induced pore pressure and stresses for the time when the sample reaches the surface. Then, the induced effective stresses can be

checked with the failure criterion to indicate whether the sample can be retrieved in a preserved manner or not. This should be repeated in an iterative manner for various tripping speeds, while considering economic rig time limitations, until the optimal rate is reached (if it exists). This can practically provide a standard method to determine the optimal core tripping in real operations.

During the modeling process, all the contributing parameters and their effects can be identified. Then, among these factors, the most significant ones are selected as the determinative factors. These factors are those by which it is expected to generally understand in advance if there are or are not any optimal tripping rates, which both prevent core damage and are economical. This helps us for candidate selection of different coring methods.

In short, the objectives of the thesis are:

- ✓ Preventing the core damage and core preservation during its retrieval to the surface; providing economic and cost-effective core retrieval while considering operational rig costs and reduction of invisible lost time during core tripping
- ✓ Considering the effects that have not been thoroughly considered in the literature including the thermal effect, the mud cake effect, and the mechanical properties during the modeling in order to provide a better prediction of failure
- ✓ Developing a thermoporoelastic modeling approach for the case of core tripping to optimize the tripping. The resultant model is expected to be able to evaluate the induced stresses and pore pressures within the core sample, consider the failure criterion, and determine the optimal tripping rate
- ✓ Proposing a practical simple procedure for the optimal tripping rates determination using some given and also estimated input parameters
- ✓ Identifying the contributing parameters in the modeling process and also their effects on the core tripping schedule
- ✓ Detecting the determinative factors among the contributing parameters as the factors having the greatest effects on the induced stresses and failure during tripping. These factors are introduced as the main criteria which help proper candidate selection for the wireline continuous coring and pressure coring, i.e. the proper coring method(s) to be used for specified core samples/properties.

Chapter 2: Systems for Core Tripping

2.1 Introduction

It is one of the objectives of this research to investigate which of the coring or core tripping methods is/are appropriate for which core samples/properties. Therefore, it is crucial to know about these methods.

In order to investigate various core tripping rates that are practically possible considering the research objectives, it is crucial to know about these methods. There are two basic systems of core tripping/coring available in the market. These two systems are 1) conventional coring which retrieves the core sample to the surface via the drill pipe, and 2) wireline continuous coring which retrieves the core via using wireline. In both of these systems, there are two criteria to be considered: 1) the protection and preservation of the sample during its trip and 2) economic retrieving the sample based on the operational rig costs. As the first criterion can be safely disregarded in case of using pressure coring, it is important to discuss pressure coring in this chapter.

2.2 Conventional Coring

Conventional coring is a method of rotary coring by which the inner tube containing the core is retrieved together with the outer tube assembly following a conventional trip. A general schematic of conventional coring assembly has been shown in **Figure 2-1.** The core bit is connected to the *outer tube assembly*. The outer tube assembly is playing the role of the Bottom-Hole-Assembly (BHA). The outer tube assembly is connected to the drill pipes via the *cross-over sub* and the *top sub*. Conventional core cutting is accomplished using a coring bit/head with essentially the same principle as a drilling bit; however, the core bit cuts a hollow cylindrical rock and thus possesses smaller bearings and cutters. Prior to coring start,

the mud is allowed to pass through the inner tube to ensure no debris can enter the inner tube and it is clean. After coring commences, the mud circulation path is diverted to the annulus between inner and outer tubes by virtue of a *dropping ball*. The ball is a spherical metal of 1 ¼-in diameter that is either dropped from the surface to be seated on its seat or is activated hydraulically. The mud circulation path is diverted in order to prevent interfering with the cutting action and not to flush and damage the cut sample. In order to make the inner tube be remained stationary while the outer tube assembly is rotating freely during cutting, *bearing/swivels* are used near the top and bottom of the inner tube. After enough core is already cut by the core bit (i.e. end of coring), the drill string is overpulled so that the core can be cut by virtue of *core catchers* or *retainers* at the bottom end of the inner tube. Then, the drill string together with the core barrel is tripped and pulled out of hole. While tripping, it is important to let the expanded gas be vented to the mud and thus to prevent over-pressurization in the inner tube. Therefore, the inner tube should be in hydraulic communication with the hydrostatic mud column via the inner tube check valves (**Figure 2-1**).

It should be noted that the most prominent advantages of conventional coring, compared with the wireline continuous method, is the capability of recovering large core length and size. Sampling with the length of e.g. 120 ft is possible; and depending on the hole size diameter sizes of even greater than 5-in is possible.

The most prominent disadvantage of conventional coring is that the core barrel is retrieved to the surface through a conventional drill string trip (*Deliac et al., 1991; Baker Hughes, 2012; Farese et al., 2013; Harrigan & Cole, 2011*). This makes conventional coring timely and thus costly. In order to preserve the sample during its retrieval to the surface, the industry uses generic tripping schedules such as using the maximum tripping speed equal to 1.524 m/s, or as in **Table 2-1**. Some research works have been recently conducted considering some generic tripping schedules (e.g., as in **Table 2-2**). It is also recommended by the industry that for the tripping of very tight e.g. shale cores, conventional tripping is the solution. As one of the objectives of this research, these will be investigated.

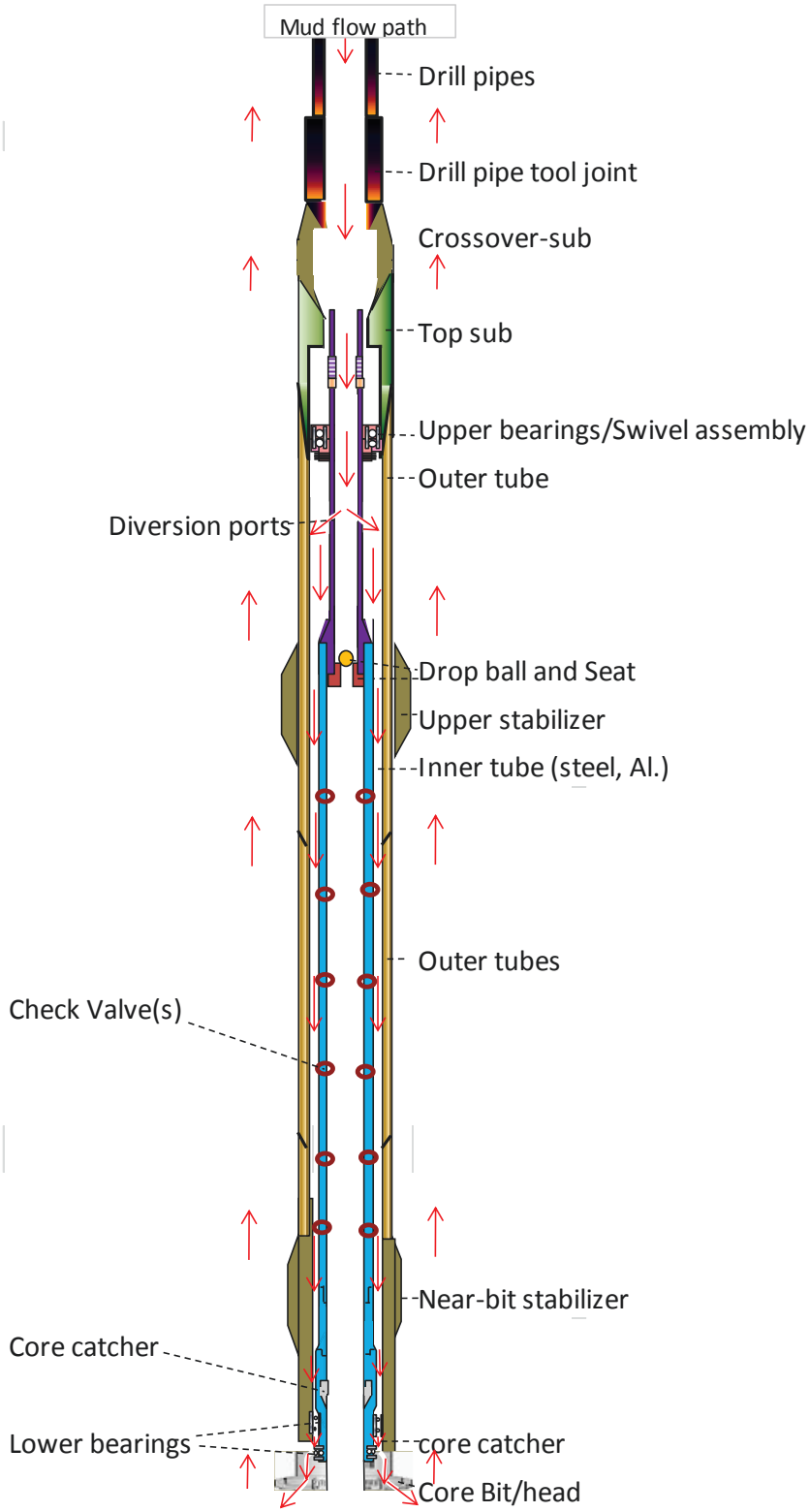

Figure 2-1: Conventional Coring during Cutting the Sample

Table 2-1: A Generic Industry's Trip Schedule- for Gas-Bearing Cores by a Company–Conventional Coring

Depth (TVD[1], m)	Trip Rate
Bottom – 400	0.45 m/s (1 min/stand)
400. – 100	0.15 m/s (3 min/stand)
100. – surface	0.0375 m/s (12 min/stand)

Table 2-2: One Generic Core Trip Schedule for Gas-Bearing Cores – Conventional Coring (*Zubizarreta, et al., 2013*)

Depth (TVD, m)	Trip Rate
Bottom – Top of BHA at surface	0.45 m/s (1 min/stand)
Top of BHA at surface – 150	0.075 m/s (6 min/stand)
150 – Surface	0.05 m/s (9 min/stand)

2.3 Wireline Continuous Coring

Wireline continuous coring (*WCC*) is a method of coring by which changing the inner tube assembly containing the core is accomplished via wireline. In this method, switching from the drilling mode to the coring mode and vice versa can be continuously conducted using wireline without any required conventional trips (*Randolf and Jourdan, 1991; Warren et al., 1998; Gelfgat, 2003*). On average, the wireline tripping rate ($\approx 1.5\ m/s$) can be about three times the conventional tripping rate ($\approx 0.45\ m/s$). This method was developed to reduce the excessive tripping times and its operational costs as is the case with the conventional coring method. This constitutes the main difference from the conventional method. In other aspects, the method is similar to the conventional method, e.g. the same outer assembly, the same core bit, etc.

Schematics of the core barrel used in this method have been illustrated in **Figure 2-2**. In order to switch from the drilling to the coring mode, first the *drill insert/plug* (which was inserted inside the core bit) is extracted out from the BHA by wireline and *overshot*[2]. Second, the inner tube/barrel assembly is tripped into the outer tube assembly again by wireline. Next, the mud circulation is done; thus, the mud pressure which is applied at the *squeeze nozzle*. This keeps the *pressure head* to be seated in the *locking seat* in order to start cutting the sample (**Figure 2-2**). In order to switch from the coring to the drilling mode, first the *inner tube assembly* (including the inner tube and bearing assembly) is retrieved by wireline and

[1] True Vertical Depth

[2] Overshot assembly is a tool run at the bottom end of the wireline in order to unlatch/latch the drill rod assembly or the inner tube assembly.

overshot assembly. Next, the *inner drilling assembly* (including drill plug and drill rods) is run in hole by wireline. Mud circulation is applied. This makes the inner drilling rod to be latched to the outer assembly in the *lobe sub* and the *locking grapple* to be activated and to latch to the *locking seat*. With these two points of contact, drilling can be started/resumed. It is also possible to run in with an empty inner tube assembly to cut additional cores (further coring).

The main advantage of wireline continuous coring is that it mitigates the tripping time as the invisible lost time during conventional coring (*Walker et al., 1990*; *Deliac et al., 1991; Baker Hughes, 1999, 2012 and 2013; Bencic et al., 1998; Farese et al., 2013*). This contribution is the most vivid for coring deep zones, coring alternative multiple and separate zones. Currently, the main disadvantage of wireline continuous method is the possible damage occurring to the samples due to their rapid tripping of tight cores (inferred from *Zubizarreta et al., 2013*). This has been normally ignored by the drilling personnel as it violates the philosophy of using wireline. However, the operators have recently started paying attention to this issue. Therefore, the industry as a generic method, uses slowing down considerably in the last 100 m interval near the surface (i.e., the low trip rate as in **Table 2-3**); as another generic method, it recommends the application of conventional coring for typical shale cores.

As the aforementioned rule of thumb methods do not suffice the needs for optimal tripping, some research using engineering approaches has been recently started (*Hettema et al., 2002; Zubizarreta et al., 2013; Byrne et al., 2015; Hoeink et al., 2015*). The candidate selection of core samples for the wireline method is one of the main objectives of this research. Therefore, we will distinguish the core properties that can be safely tripped by the wireline method.

Table 2-3: An Industry Generic Trip Schedule- for Gas-Bearing Cores–Wireline Coring

Depth (TVD, m)	High Trip Rate [m/s]	Low Trip Rate [m/s]
Bottom – 100	1.524	1.524
100-surface	1.524	0.035

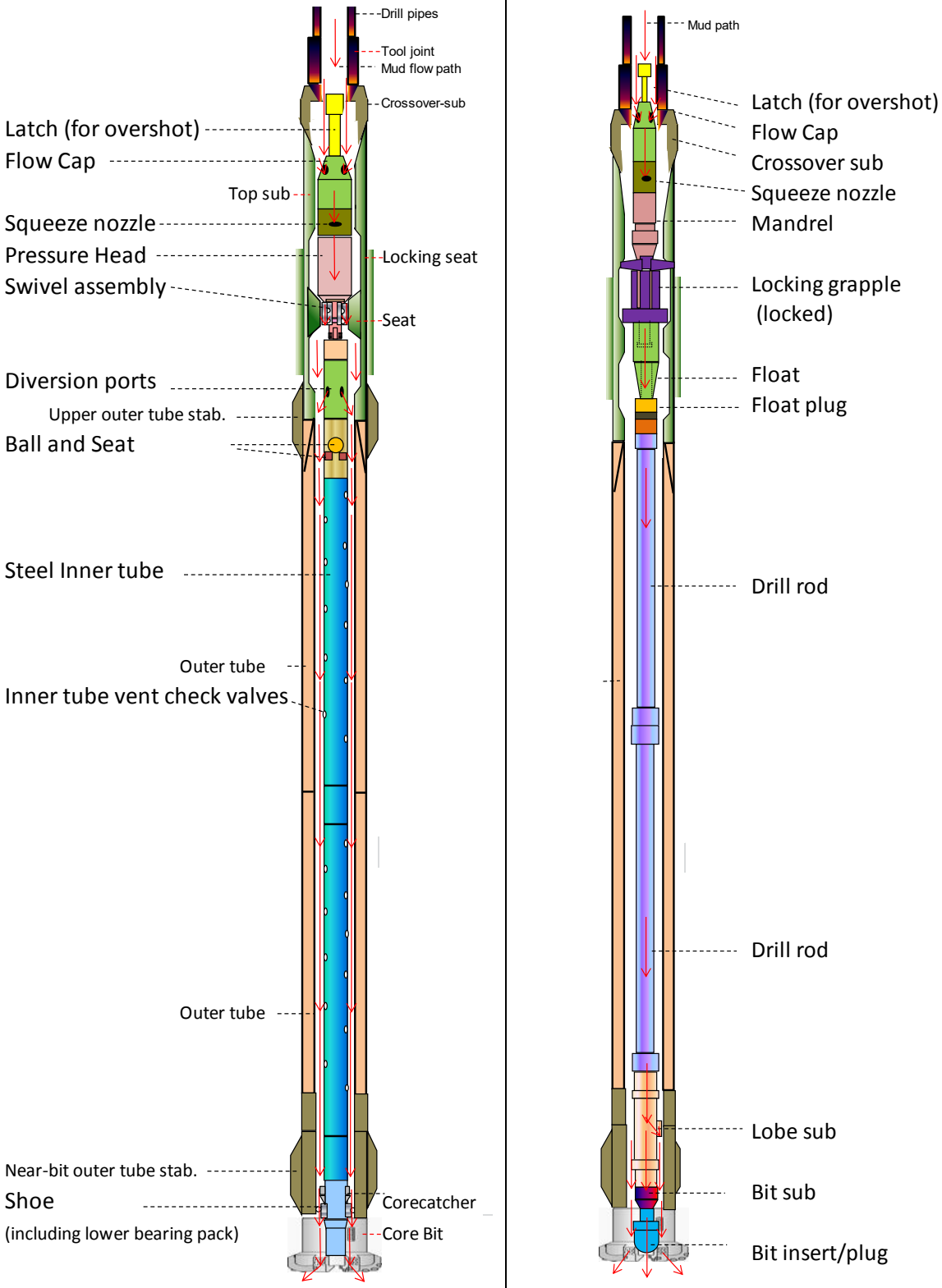

a) Coring Mode **b) Drilling Mode**

Figure 2-2: The Schematic of Wireline Continuous Coring

2.4 Pressure Coring

Pressure/in-situ coring is a feature of sampling from the rock by which the sample is retrieved to the surface in a sealed pressure-type container. Therefore, the sample can reach the surface with its in-situ pore pressure. This almost prevents any fluid diffusion out of the core and therefore the core be considered intact. Then, at the surface, such tight samples can be depressurized very slowly in desorption canisters so that their mechanical integrity is safely maintained. Therefore, the sample rock and mechanical properties such as Young's modulus or strength would be representative of the reservoir. This method has other advantages in terms of the liberated fluids and their sealing during tripping, but their discussion is out of the scope of this research.

There are some rocks with specified properties that cannot be tripped to the surface mechanically preserved. Such rocks and their properties must be known. In the literature, there are no clear candidate selection procedures for the pressure coring method. In this research, such rocks and their properties would be determined. These cores are sealed in the pressure coring method and pulled out of hole neglecting their tripping rates without any worries about their preservation (*Hyland, 1983; Bjorum, 2013 and 2014; Davis et al., 2013; Shinmoto et al., 2011 and 2012*). This means that the core can be retrieved as quickly as possible without causing damage to the sample via wireline continuous method. Then, the core pressure can be relieved very slowly at surface so that the sample is preserved mechanically. A schematic of a typical barrel for pressure coring method has been shown in **Figure 2-3**.

In the pressure coring so far discussed, the whole in-situ pressure is maintained[3]. In order to maintain more safety of handling the core barrel and enlarge the core size, it is also possible to partially keep the in-situ pressure, e.g., 1000 *psi*[4]*(Bjorum, 2013)*.

[3] *CoreVault* system, by *Halliburton*

[4] *QuickCapture* system, by *Corpro*

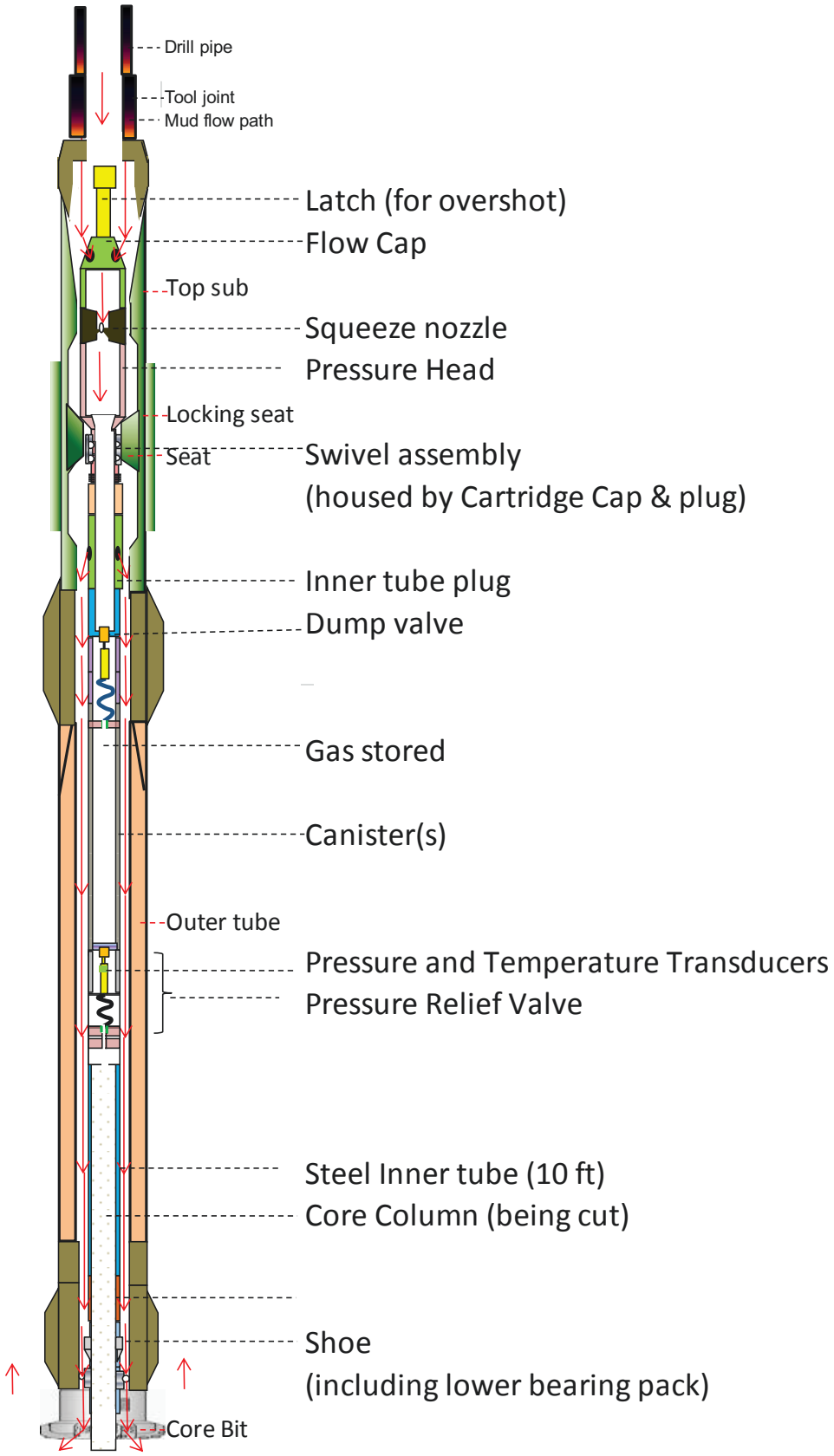

Figure 2-3: A Schematic of a Typical Pressure Coring via Wireline Continuous Method

Chapter 3: Theory of Thermoporoelasticity –Core Tripping

3.1 Introduction

In this chapter, the possibility of applying thermoporoelasticity to the case of core tripping is investigated. Therefore, first the thermoporoelasticity concept and method is generally defined. Then, the core tripping problem is described and the way to translate and match this method with the case of core tripping is investigated. Finally, the theory of thermoporoelasticity is further discussed by discussing the governing equations involved. Therefore, the conservative equations, constitutive equations, diffusivity equations, and the fluid modeling during tripping are explained. In **Chapter 5**, in an analytical approach using these equations, the induced stresses during tripping will be presented.

3.2 Definition

Thermoporoelasticity is the study of rock mechanical behavior and how the rocks undergo deformation and failure in response to the effects of imposing a change or difference to the confining stress, the pore pressure, and also the temperature (*Wang, 2000; Zoback, 2010*). In other words, it describes the interaction and coupling between the confining stress difference, the pore fluid pressure difference and the temperature difference. This coupling can be in two ways:

- ✓ *Solid to fluid coupling:*
  Imposing a change in confining stress at the boundary induces a change in pore fluid pressure or/and temperature change.
- ✓ *Fluid to solid coupling:*

Imposing a change in the pore fluid pressure or temperature induces a change in the volume of the porous body.

In thermoporoelasticity, the initial state constitutes the basis of the problem. Therefore, the thermoporoelastic parameters are considered as their difference from their initial values. These parameters include the confining stress/pressure difference ΔP_c, the pore pressure difference ΔP_p, and the temperature difference ΔT. Therefore, the initial thermoporoelastic parameters are considered zero. Then, it is also assumed that these imposed differences occurs immediately at the time of nearly zero ($t=0^+$). Then, the new conditions last for a specified period of time Δt (**Figure 3-1**). At the end of each time period that we are interested, the effects of the changes in the conditions on the interested parameters are analytically found. The interesting parameters for each problem can be the induced pore pressures or the induced stresses.

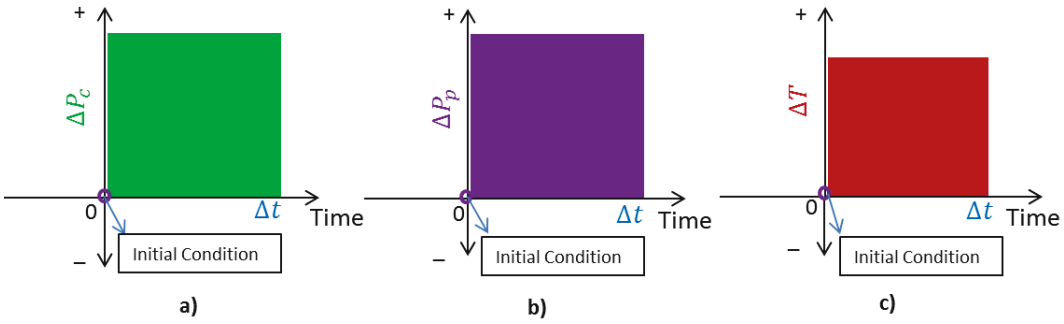

Figure 3-1: General Thermoporoelastic Initial and Boundary Conditions

3.3 Problem Description

The problem considered in this thesis is a cylindrical porous core sample that is decompressed out of its surrounding drilling mud pressure during its tripping to the surface. The sample is initially located at the bottomhole depth and surrounded by the drilling mud. Therefore, it is exposed to a constant hydrostatic compressive stress field, i.e., the hydrostatic mud pressure, and constant mud temperature. The sample has its initial pore pressure which can be equal to the bottomhole mud pressure. As the sample is being tripped, accordingly, at its boundary, 1) the compressive confining mud pressure is dropped, i.e., the release of the confining stress, 2) the pore fluids diffuse out and thus its pore pressure drops, and 3) the temperature of the mud surrounding the sample drops. The boundary of the sample experiences these drops suddenly.

Gradually, the aforementioned differences at the boundary extend towards the inside. The rate that these drops are transferred from the boundary to the inside depends on the given properties and the time. If this transfer does not occur quickly enough, it leaves lower drops in the inside than the outside. This is identical to higher values in the inside than the outside. Therefore, a difference in pore pressure and temperature is created between the boundary and the inside. This difference causes induced stresses distributed within the core. This process continues until the sample reaches the surface where the confining stress and temperature become those of the surface conditions. All these changes of core conditions cause induced tensile stresses within the sample, which may finally cause the sample failure during the trip.

To deal with the mentioned problem, we need to evaluate the induced stresses and predict the failure. As the core sample is porous and permeable, we cannot use the simple solid elastic models (**Appendix-A**). Therefore, in this research, a thermoporoelastic approach will be utilized to consider the effects of all aforementioned changes that induce stresses within the core. Translating the initial conditions to the language of thermoporoelasticity gives: 'the core sample is initially at zero stress difference, zero pore pressure difference, and zero temperature difference'. Translating the boundary conditions to the language of thermoporoelasticity gives: 'decompression of the core is done at once'. In **Figure 3-2**, the thermoporoelastic changes to the core sample during its trip to the surface, including the initial and boundary conditions, have been shown.

Therefore, at the time 0^+, the sample undergoes an immediate confining pressure difference, pore pressure difference, and temperature difference at its boundary. The initial and boundary conditions using the original thermoporoelasticity have been shown in **Figure 3-3**. Based on the application of the thermoporoelastic theory in its original form, all the induced differences to the core occur just immediately; then, these differences are maintained for a specified period. This represents the immediate retrieval of the core from bottomhole to the surface. Therefore, it cannot represent a real core tripping by which the core is being tripped gradually, not immediately. This is a problem regarding the representative application of thermoporoelasticity to the case of core tripping. In **Chapter 5**, the aforementioned problem will be dealt with and the analytical modeling of the induced stresses within the core will be comprehensively investigated.

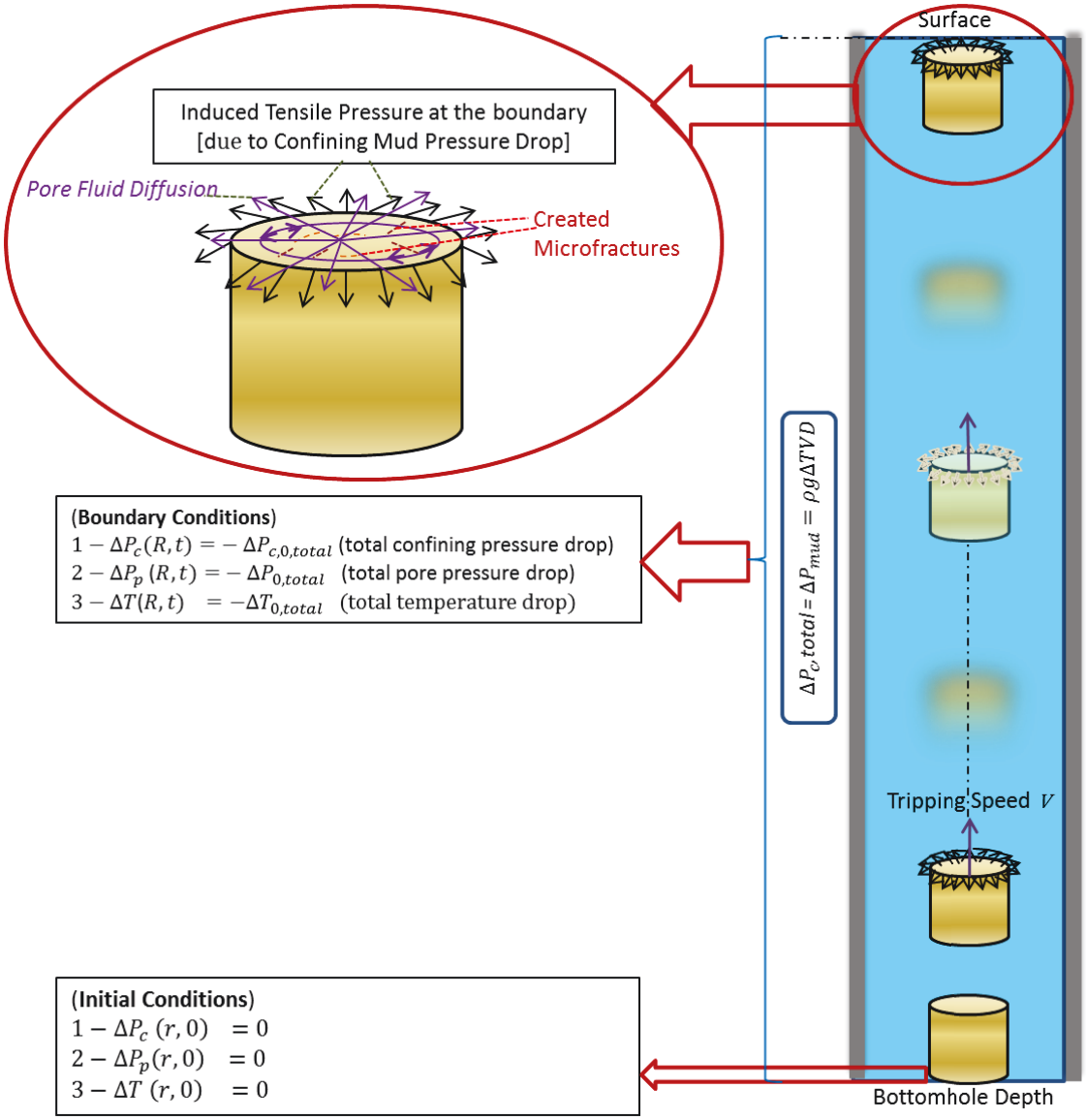

Figure 3-2: Core Decompression, its Thermoporoelastic Changes from Bottomhole to the Surface, and Created Microfractures

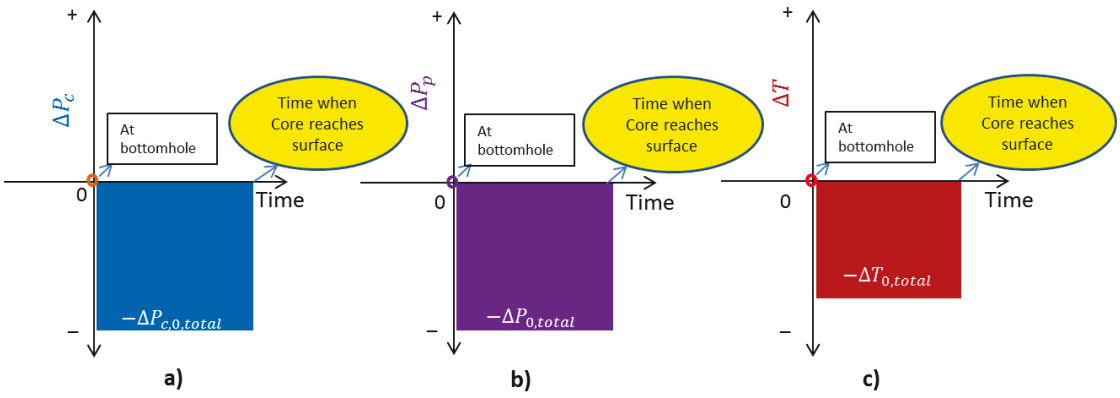

Figure 3-3: Initial and Boundary Conditions Assuming Immediate Core-Decompression from Bottomhole to the Surface Using Original Thermoporoelasticity

3.4 Governing Equations

It is important to consider the corresponding physical laws which govern the thermoporoelastic modeling. The corresponding equations describe the mathematical relationships between important parameters involved in the problem. These important parameters are a) confining stress drop, b) pore pressure drop, and c) temperature drop.

Basically, the governing equations are divided into the conservative laws, constitutive laws and diffusivity laws. These equations are common for all thermoporoelastic problems, only their boundary conditions may differ which make the solutions different.

3.4.1 Conservative Equations

In the development of thermoporoelasticity constitutive equations, the conservative laws for the continuity, momentum, and energy are considered as follows:

Continuity: $$\frac{\partial m}{\partial t} + q_{i,i} = 0 \qquad \textit{Eq. 3-1}$$

Momentum: $$\sigma_{ij,j} = 0 \qquad \textit{Eq. 3-2}$$

Energy: $$\frac{\partial \Delta T}{\partial t} = -\frac{1}{\rho_b c_b} h_{i,i} - \frac{1}{\rho_f \emptyset} (T q_i)_i \qquad \textit{Eq. 3-3}$$

In which ρ_b is the density of the bulk material, c_b is the specific heat capacity of the bulk material, $h_{i,i}$ is the heat flux, $q_{i,i}$ is the fluid mass flux, m is the fluid mass, t is the time, σ denotes the stresses, ΔT is the temperature difference, ρ_f is the fluid density, $\emptyset$ is the rock porosity.

3.4.2 Constitutive Equations

In thermoporoelasticity, the following constitutive equations hold between the stress difference and strain, pore pressure difference, and temperature difference (*Wang, 2000; Detournay & Cheng, 1993; Zoback, 2010; Chen & Ewy, 2005*):

$$\Delta\sigma + \alpha \Delta P_p = K\epsilon \qquad \textit{Eq. 3-4}$$

$$\zeta = \frac{1}{H}\sigma + \frac{1}{R}P \qquad \textit{Eq. 3-5}$$

$$\Delta\sigma = K_{T(}\epsilon_T - \frac{\alpha_m}{3}\Delta T) \qquad \textit{Eq. 3-6}$$

Where $\Delta\sigma$ is the stress difference which is the same as the confining mud pressure difference (for the core tripping case); ΔP_p is the pore pressure difference; K is *the bulk modulus of elasticity*; ϵ is the poroelastic strain; a is *the Biot's coefficient*; ζ is *the increment of water content*; $\frac{1}{H}$ is *the poroelastic expansion coefficient* (*Wang, 2000*); $\frac{1}{R}$ is the *specific storage coefficient*; ΔT is the temperature difference; K_T is *the isothermal bulk modulus;* ϵ_T is *the thermal strain*; α_m is *the bulk thermal expansion coefficient*.

Having applied the constitutive equations to the case of core tripping in polar coordinates, we have the following relationships in radial and hoop or tangential directions (*Boley & Weiner, 1985; Jaeger & Cook, 1976; Wang, 2000*):

$$\Delta\sigma_{rr} = 2G\epsilon_{rr} + 2G\frac{\upsilon}{1-2\upsilon}(\epsilon_{rr} + \epsilon_{\theta\theta}) - a\Delta P_p \qquad \textit{Eq. 3-7}$$

$$\Delta\sigma_{\theta\theta} = 2G\epsilon_{\theta\theta} + 2G\frac{\upsilon}{1-2\upsilon}(\epsilon_{rr} + \epsilon_{\theta\theta}) - a\Delta P_p \qquad \textit{Eq. 3-8}$$

Where $\Delta\sigma_{rr}$ and ϵ_{rr} are respectively the induced radial stress and strain; $\Delta\sigma_{\theta\theta}$ and $\epsilon_{\theta\theta}$ are respectively the induced hoop or tangential stress and strain; G is the shear modulus; υ is the Poisson's ratio; a is the Biot's coefficient.

3.4.3 Diffusivity Equations

As the core sample is being raised from bottom, its outside hydraulic head and temperature drops. This induces a pressure and temperature difference from inside to the outside. These differences cause pore fluid flow and heat transfer from inside to the outside (**Figure 3-4**). These in turn, cause transient pressure and temperature change within the core body.

The thermoporoelastic diffusivity equations describe the transient pore pressure change, i.e. pressure diffusivity equation, and transient temperature change from inside of the sample to its outside. Pressure diffusivity equation is found by combining the continuity law and the Darcy's law. Thermal diffusivity equation is analogically found by combining the thermal continuity equation and the Fourier's law. The pressure diffusivity equation is as follows (*Wang, 2000; Detournay & Cheng, 1993; Carslaw & Jaeger, 1959*):

$$\frac{\partial\Delta P_p}{\partial t} = \eta\left(\frac{\partial^2\Delta P_p}{\partial r^2} + \frac{1}{r}\frac{\partial\Delta P_p}{\partial r}\right) \qquad \textit{Eq. 3-9}$$

Considering the coupling effect of temperature change on the pore pressure change, the coupled-hydraulic diffusivity equation is (*Chen & Ewy, 2005; Li, 1998*):

$$\frac{\partial \Delta P_p}{\partial t} = \eta \left(\frac{\partial^2 \Delta P_p}{\partial r^2} + \frac{1}{r} \frac{\partial \Delta P_p}{\partial r} \right) + \eta' \frac{\partial \Delta T}{\partial t} \qquad \textit{Eq. 3-10}$$

The thermal diffusivity equation is:

$$\frac{\partial \Delta T}{\partial t} = \eta_T \left(\frac{\partial^2 \Delta T}{\partial r^2} + \frac{1}{r} \frac{\partial \Delta T}{\partial r} \right) \qquad \textit{Eq. 3-11}$$

Considering the coupling effect of the pore pressure change on the temperature change, it becomes (*Chen & Ewy, 2005*):

$$\frac{\partial \Delta T}{\partial t} = \eta_T \left(\frac{\partial^2 \Delta T}{\partial r^2} + \frac{1}{r} \frac{\partial \Delta T}{\partial r} \right) + \eta'_T \left[\frac{\partial T}{\partial r} \frac{\partial \Delta P_p}{\partial r} + T \left(\frac{\partial^2 \Delta P_p}{\partial r^2} + \frac{1}{r} \frac{\partial \Delta P_p}{\partial r} \right) \right] \qquad \textit{Eq. 3-12}$$

Where η is the hydraulic diffusivity coefficient; η' is the coupling coefficient by temperature change on pore pressure change; η_T is the thermal diffusivity coefficient; η'_T is the coupling coefficient by the pore pressure change on the temperature change.

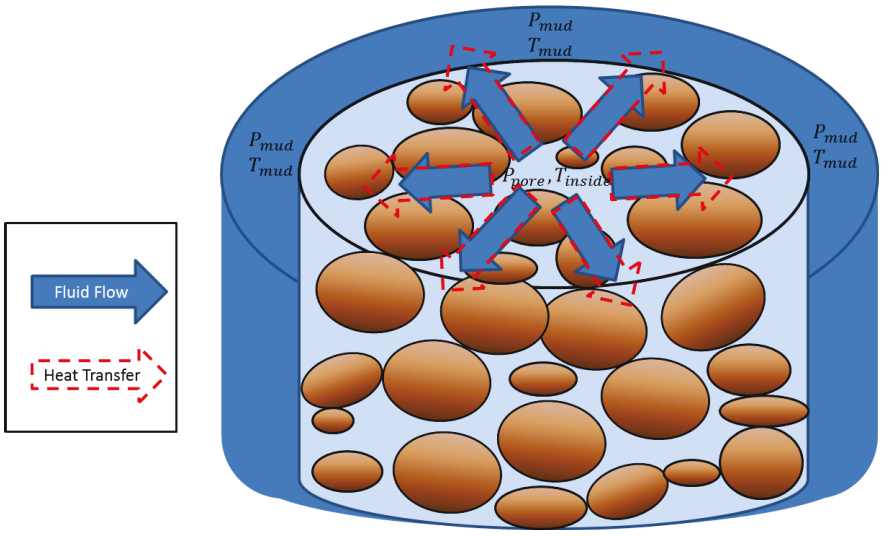

Figure 3-4: Pore Fluid Diffusion and Heat Transfer out of the Sample during Tripping

3.4.4 Fluid-Modeling Equations

As seen in **Eq. 3-10**, the hydraulic diffusivity coefficient η is the main coefficient in the diffusivity equation. This coefficient in turn depends on the four properties including porosity, permeability, *Viscosity*, and *isothermal compressibility* as (*Ahmed and McKinney, 2005)*:

$$\eta = 9.869 \times 10^{-13} \frac{K}{\varphi \mu C_t} \qquad \textit{Eq. 3-13}$$

Where η shows the hydraulic diffusivity coefficient $[m^2/s]$, K is permeability $[mD]$, , φ is porosity, μ is viscosity $[cp]$; and C_t is the total compressibility [1/Pa].

During the core trip to the surface, the pressure and temperature conditions change. Therefore, the viscosity and compressibility of the fluid (gas) change during the trip. During the trip from the bottomhole, this causes the hydraulic diffusivity coefficient η to change. These changes are modeled as follows: The porosity and permeability change during the trip are considered negligible in this work.

Viscosity

The fluid viscosity is defined as the fluid resistance against flow or shear. If water is the fluid contained in the sample, its viscosity remains rather unchanged during its trip to the surface. However, if it is gas, it varies, i.e., drops, with pressure and temperature. Therefore, the gas viscosity is evaluated in terms of pressure and temperature by (*Dempsey's equation, 1965*):

$$ln\left(T_{pr}\frac{\mu_g}{\mu_1}\right) = a_0 + a_1P_{pr} + a_2{P_{pr}}^2 + a_3{P_{pr}}^3 + T_{pr}\left(a_4 + a_5P_{pr} + a_6{P_{pr}}^2 + a_7{P_{pr}}^3\right) + {T_{pr}}^2\left(a_8 + a_9P_{pr} + a_{10}{P_{pr}}^2 + a_{11}{P_{pr}}^3\right) + {T_{pr}}^3(a_{12} + a_{13}P_{pr} + a_{14}{P_{pr}}^2 + a_{15}{P_{pr}}^3) \quad \textit{Eq. 3-14}$$

Where μ_1 is found by (*Standing, 1977*):

$$\mu_1 = 8.118 \times 10^{-3} - 6.15 \times 10^{-3}\log(\gamma_g) + \left[1.709 \times 10^{-5} - 2.062 \times 10^{-6}\gamma_g\right](T - 460) \quad \textit{Eq. 3-15}$$

The constants in the **Eq. 3-14** are given in **Table 3-1**.

Table 3-1: Constants Required for Dempsey's Gas Viscosity Calculation

$a_0 = -2.46211820$	$a_4 = +2.80860949$	$a_8 = -0.0793385648$	$a_{12} = +0.0839387178$
$a_1 = +2.970547414$	$a_5 = -3.49803305$	$a_9 = +1.39643306$	$a_{13} = -0.186408848$
$a_2 = -0.286264054$	$a_6 = +0.360373020$	$a_{10} = -0.149144925$	$a_{14} = +0.0203367881$
$a_3 = +0.00805420522$	$a_7 = -0.01044324$	$a_{11} = +0.00441015512$	$a_{15} = -0.000609579263$

Isothermal and Total Compressibility

The hydraulic diffusivity coefficient η is conversely proportional to the total compressibility of the core. Total compressibility C_t is in turn a function of the compressibility of the rock matrix (C_r) and the isothermal compressibilities of the fluids contained (*Dake, 1998*):

$$C_t = C_r + C_w S_w + C_g S_g \qquad \textit{Eq. 3-16}$$

Where C_w and C_g are respectively the water and gas isothermal compressibilities in 1/Pa; S_w and S_g are respectively the water and gas saturations.

If the fluid that is contained in the sample is water, its isothermal compressibility is practically fixed during its trip to the surface. However, if it is gas, it varies with pressure and temperature. Thus, the isothermal compressibility for a real gas is considered in terms of the pressure and temperature as (*McCain, 1990*):

$$C_g = \frac{1}{P} - \frac{1}{Z}\left(\frac{\partial Z}{\partial P}\right) = \frac{1}{P} - \frac{1}{P_{pc} Z}\left(\frac{3.53}{10^{0.9813 T_{pr}}} + \frac{0.548 P_{pr}}{10^{0.8157 T_{pr}}}\right) \qquad \textit{Eq. 3-17}$$

For a gas-bearing core, the gas isothermal compressibility C_g is considerably greater than the rock and water isothermal compressibility values. Therefore, during the sample trip, in our modeling, the rate of increase of the total compressibility is assumed equal to the rate of increase of the gas compressibility.

Chapter 4: Failure Criteria during Core Tripping

4.1 Introduction

As the core sample is being tripped, the boundary of the sample experiences a sudden drop in the confining mud pressure, a pore pressure drop, and a temperature drop. This occurs with a rate that only depends on the tripping rate. However, the rate that these drops extend from the boundary to the inside depends on the tripping rate and the sample properties. Therefore, this rate difference causes the pore pressure and temperature difference between the boundary and the inside of the core. These differences are responsible for inducing tensile stresses distributed within the core which can possibly cause tensile failure.

Therefore, in the direction of the objectives of this research to predict the core mechanical failure during tripping, we need to 1) determine the appropriate failure criterion and its framework, and 2) evaluate the normal stresses that are induced within the core sample. Therefore, in this chapter, first the appropriate failure criterion is determined. Then, in **Chapter 5**, we develop the equations for the principal induced stresses within the sample. These equations can fit into the tensile failure framework.

4.2 Principal Stresses during Core Tripping

In two-dimensional cylindrical coordinates, there are two particular orientations where the shear stresses are absent. The two corresponding orientations are called *principal planes*. These planes are perpendicular to each other. The corresponding stresses normal to these planes are called the *principal stresses*. For the case of tripping of the cylindrical core, the two principal planes are in the radial and hoop directions. Therefore, the principal stresses are the radial stress σ_{rr} and the hoop or tangential stress $\sigma_{\theta\theta}$ (as shown in the two dimensional view

in **Figure 4-1**, and in the three dimensional view in **Figure 4-2**). Therefore, the stress tensor becomes:

$$\sigma_{ij} = \begin{bmatrix} \sigma_{rr} & 0 \\ 0 & \sigma_{\theta\theta} \end{bmatrix} \qquad \textit{Eq. 4-1}$$

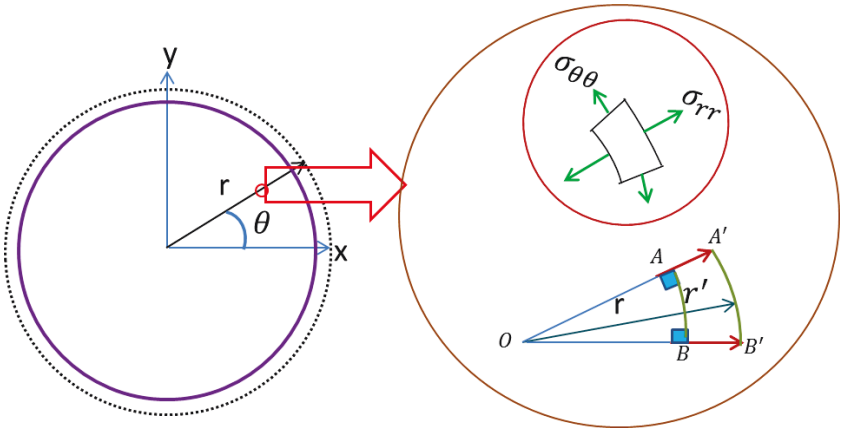

Figure 4-1: Induced Stresses within the Core Cross-Section due to its Decompression

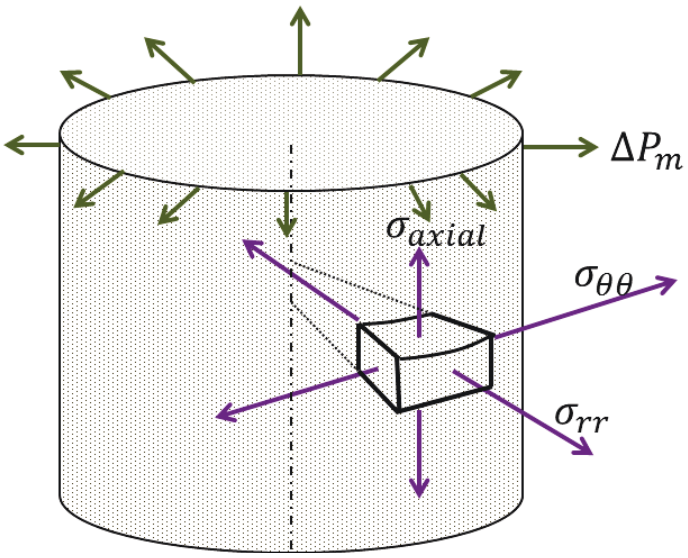

Figure 4-2: Principal Stresses in the Core Body during Tripping. The Tensile Stress is Considered Positive in this Work.

4.3 Tensile Failure

Tensile failure is a type of rock failure which occurs when the sample undergoes a tensile stress and it exceeds a critical limit called tensile rock strength (T0). Tensile failure occurs across some plane(s) in the sample (inferred from *Fjaer et al., 2008*). However, in isotropic materials, this plane is perpendicular to the stress direction (**Figure 4-3 a**).

In this research, the difference of the pore pressure-drop and temperature-drop between the inside and outside of the sample, are responsible for inducing tensile stresses within the

sample. If the effective tensile stresses exceed the tensile strength of the sample, tensile failure occurs and the microfractures would appear (also confirmed by *Bouteca et al., 1994; Hettema et al., 2002; Zubizarreta et al., 2013; Byrne et al.; 2015; Hoeink et al., 2015).* This is schematically shown in **Figure 4-3 b**.

As in this thesis, we need to deal with tensile stresses due to the nature of the research, we will consider the tensile stress as positive and the confining pressure difference as negative (**Chapter 5**).

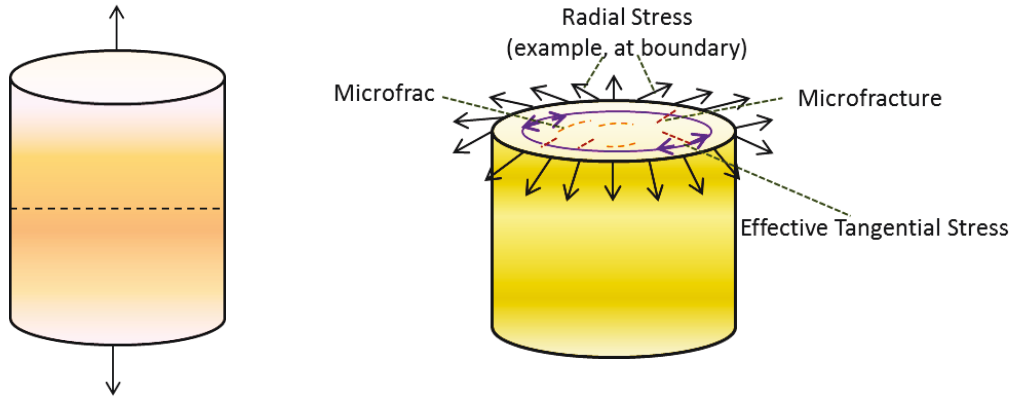

Figure 4-3: Tensile Failure. a) Typical Longitudinal b) Tripping Induced Tensile Failure in the Core

4.4 Failure Criteria

In order to select the appropriate tensile failure criterion for the case of core tripping, there are several failure criteria available. We discuss several common ones as follows:

- ***Von Mises***:

  Based on this failure criterion, yielding of materials begins when *the second deviatoric stress invariant* J_2[5] reaches a critical value. This criterion has been developed for tensile failure in solid plastic materials (*Malvern, L.E., 1969, Von Mises et al., 1913*). This criterion is also called *distortion energy theory*. As Von Mises failure criterion has been developed for solid plastic materials, it should not be used for the core tripping case.

[5] $\sqrt{(\sigma_1-\sigma_2)^2+(\sigma_2-\sigma_2)^2+(\sigma_3-\sigma_1)^2}$

- ***Gurson:***

  This criterion is used for plastic metals and has been even modified for porous ones (*Chien et al., 2000*). But, its appropriate usage is more for metals.

- ***Haigh[6]:***

  Haigh or *strain energy theory* is based on the assumption that strains are recoverable up to the elastic limit, and the energy absorbed by the material at failure is a single valued function independent of the stress system causing it.

- ***Rankine[7]:***

  Based on this criterion, the material yields when the maximum principal stress in a system reaches the value of the maximum strength at elastic limit in simple tension. This criterion is approximately correct for cast iron and brittle materials. This criterion is also called *maximum principal stress theory*.

- ***Griffith:***

  This failure criterion has been developed for brittle rocks (*Fjaer et al., 2008 & Griffith, 1921*) and is considered as the selected criterion in this thesis model.

Therefore, among the aforementioned criteria, the Griffith' criterion is selected for our application for the case of brittle cores.

Griffith Criterion

Using the Griffith' tensile criterion (*Griffith, 1921*), there are two-segment equations in terms of σ_1' and σ_3' , for isotropic rocks as follows (**Figure 4-4 a**):

$$\Delta\sigma_3' - T_s = 0 \qquad if(\Delta\sigma_1' + 3\Delta\sigma_3') > 0 \qquad \textit{Eq. 4-2}$$

$$(\Delta\sigma_1' - \Delta\sigma_3')^2 = 8T_s(\Delta\sigma_1' + \Delta\sigma_3') \qquad if\Delta\sigma_1' + 3\Delta\sigma_3' < 0 \qquad \textit{Eq. 4-3}$$

Where the condition $\sigma_1' + 3\sigma_3' > 0$ or $(\Delta\sigma_1' + 3\Delta\sigma_3') > 0$ means that the overall value of $\Delta\sigma_1' + 3\Delta\sigma_3'$ is tensile (using positive sign convention for tension).

In $\tau - \Delta\sigma'$ coordinates, the Griffith critrion has the following form (**Figure 4-4 b**):

$$\tau^2 = 4T_s(\Delta\sigma' + T_s) \qquad \textit{Eq. 4-4}$$

[6] http://www.roymech.co.uk/Useful_Tables/Mechanics/stress.html (Last Accessed on Oct. 22, 2016)

[7] http://www.roymech.co.uk/Useful_Tables/Mechanics/stress.html (Last Accessed on Oct. 22, 2016)

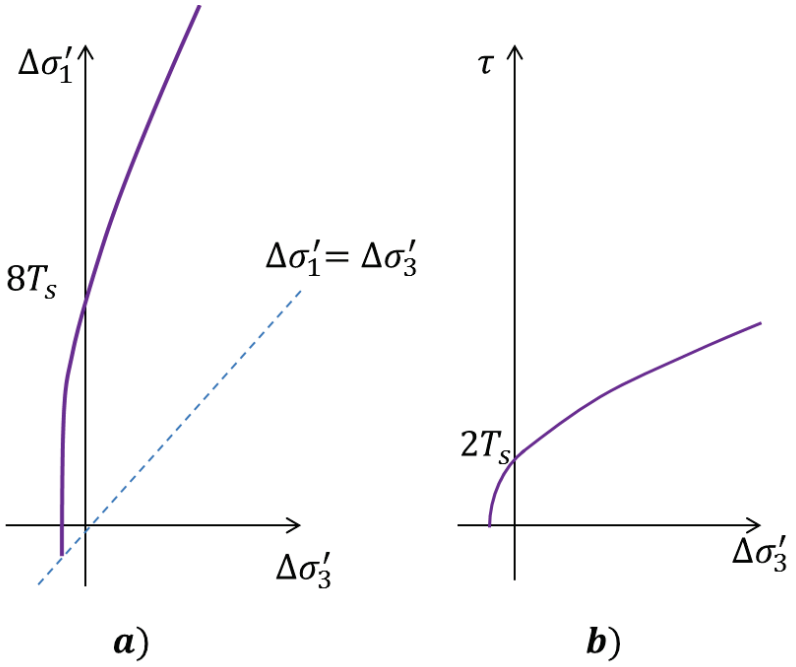

Figure 4-4: Griffith Tensile Failure Criterion: a) σ_1' versus σ_3', b) τ versus σ_3'

In order to apply the Griffith' criterion to the case of core tripping, first it is assumed that initially the core is at its initial pressure and temperature conditions bottomhole. This is the basis which means that initially we assume that the effective hoop and radial stresses are zero. As the sample is being tripped, the hydrostatic mud confining pressure drops from its basis value. The drop in the hydrostatic mud pressure creates tension. As a result, this makes the effective stresses in the radial and hoop directions tensile, i.e. $\Delta\sigma_1' = \Delta\sigma_3' > 0$. Thus, we have: $\Delta\sigma_1' + 3\Delta\sigma_3' > 0$. Using this, the first segment of Griffith' criterion (i.e. **Eq. 4-4**) is applicable as the failure criterion in this research. In two-dimensional cylindrical coordinates, the effective minimum principal stress ($\Delta\sigma_3'$) can be either the induced radial or hoop stresses as follows:

$$\Delta\sigma_3' = \Delta\sigma_{rr}' = \Delta\sigma_{rr} + \Delta P_p \qquad \textit{Eq. 4-5}$$

$$\Delta\sigma_3' = \Delta\sigma_{\theta\theta}' = \Delta\sigma_{\theta\theta} + \Delta P_p \qquad \textit{Eq. 4-6}$$

In summary, the equation for the tensile criterion is either of the following (shown in **Figure 4-5**):

$$\Delta\sigma_{rr}' \geq T_s \qquad \textit{Eq. 4-7}$$

$$\Delta\sigma_{\theta\theta}' \geq T_s \qquad \textit{Eq. 4-8}$$

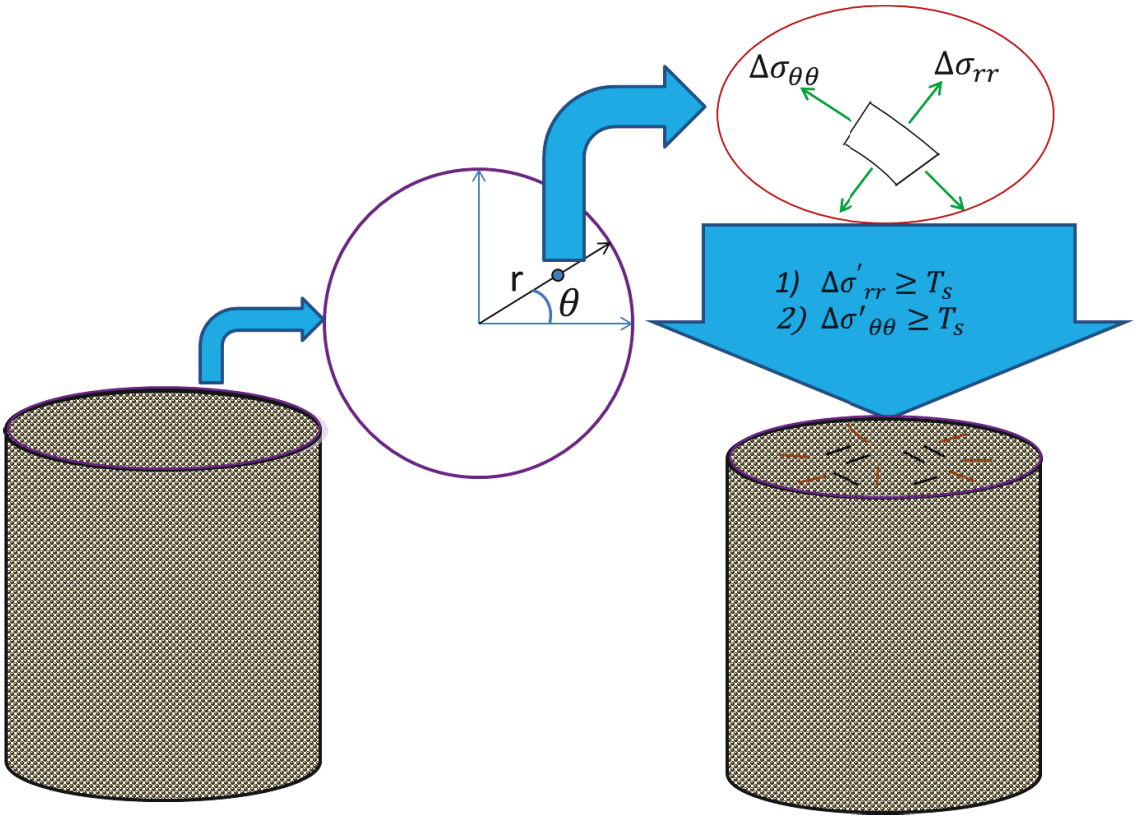

Figure 4-5: Application of the Griffith' Tensile Failure Criterion to Predict Failure during Core Tripping

Chapter 5: Analytical Approach and Model Development

5.1 Introduction

In **Chapter 3**, the core tripping problem was described with its initial and boundary conditions; the diffusivity equations that can potentially equate the distribution of the pore pressure and temperature difference within the core sample; the thermoporoelastic constitutive equations were presented which relate the induced stresses to the pore pressure difference and temperature difference distribution; it was also mentioned as one problem that the application of the original thermoporoelasticity to the core tripping case cannot represent the real conditions. Afterwards, in **Chapter 4**, the *Griffith*' criterion was determined as the core failure criterion of the problem; and the induced radial and hoop stresses were clarified as the effective minimum principal stress ($\Delta\sigma_3'$) responsible for causing the sample failure during its tripping. However, these stresses have not yet been equated and also their evaluation procedure must be still presented.

Therefore, in this chapter, first we will adjust the original thermoporoelasticity so that it can represent the real conditions for core tripping. Next, in an analytical approach, the solutions to the thermoporoelastic equations will be found considering the initial and boundary conditions. This will finally provide us with the equations for the induced stresses. Therefore, using the developed equations within the adjusted thermoporoelasticity, the evaluation of the induced stresses is possible at any time. Finally, by fitting the evaluated stresses into the failure criterion for different tripping velocities, the thermoporoelastic model development for optimizing core tripping is completed.

5.2 Representative Thermoporoelasticity

It was discussed in **Chapter 3** that as the original thermoporoelasticity can just consider the immediate tripping of the sample to the surface, it is not representative of the real conditions. To overcome this issue, we need to modify the original thermoporoelasticity to match with our application. Therefore, it is assumed that the core is being raised from the bottomhole in a number of discrete steps n and after implementation of each single step, the conditions of the sample are maintained for a specified duration until the next step is taken. This continues until the core reaches the surface. The number of n should be chosen arbitrarily large enough. Depending on the chosen value of N, each step causes three effects of drops of the confining mud pressure, the pore pressure and the temperature at the boundary of the core (as shown in **Figure 5-1**). The duration that the mentioned effects due to each step will last is from the implementation time until the sample reaches the surface or at any other specified time. This duration will be considered in the thermoporoelastic modeling. In addition, depending on the selected tripping velocities, bottomhole depth and n, the time interval between taking two successive steps is determined.

Therefore, when the core starts to be raised from bottomhole (during the first raising step from the bottomhole, $n=1$), the confining pressure, pore pressure, and temperature at the core boundary experience a specified difference or drop (this step is shown in **Figure 5-1**). The sample will continue experiencing these drops at its boundary until the time when it reaches the surface, or at any other time we are interested to investigate. Therefore, the duration that the effects of the first step will last (that must be considered in thermoporoelastic modeling) is equal to the whole tripping time. As the core is being raised for the second step ($n=2$), the same changes are induced to the sample and it will continue experiencing them until it reaches the surface. Obviously, the duration that the effects of the second step will last (that should be considered in the thermoporoelastic modeling) is less than that of the first step. This process, shown in **Figure 5-2**, continues so forth until the core reaches the surface.

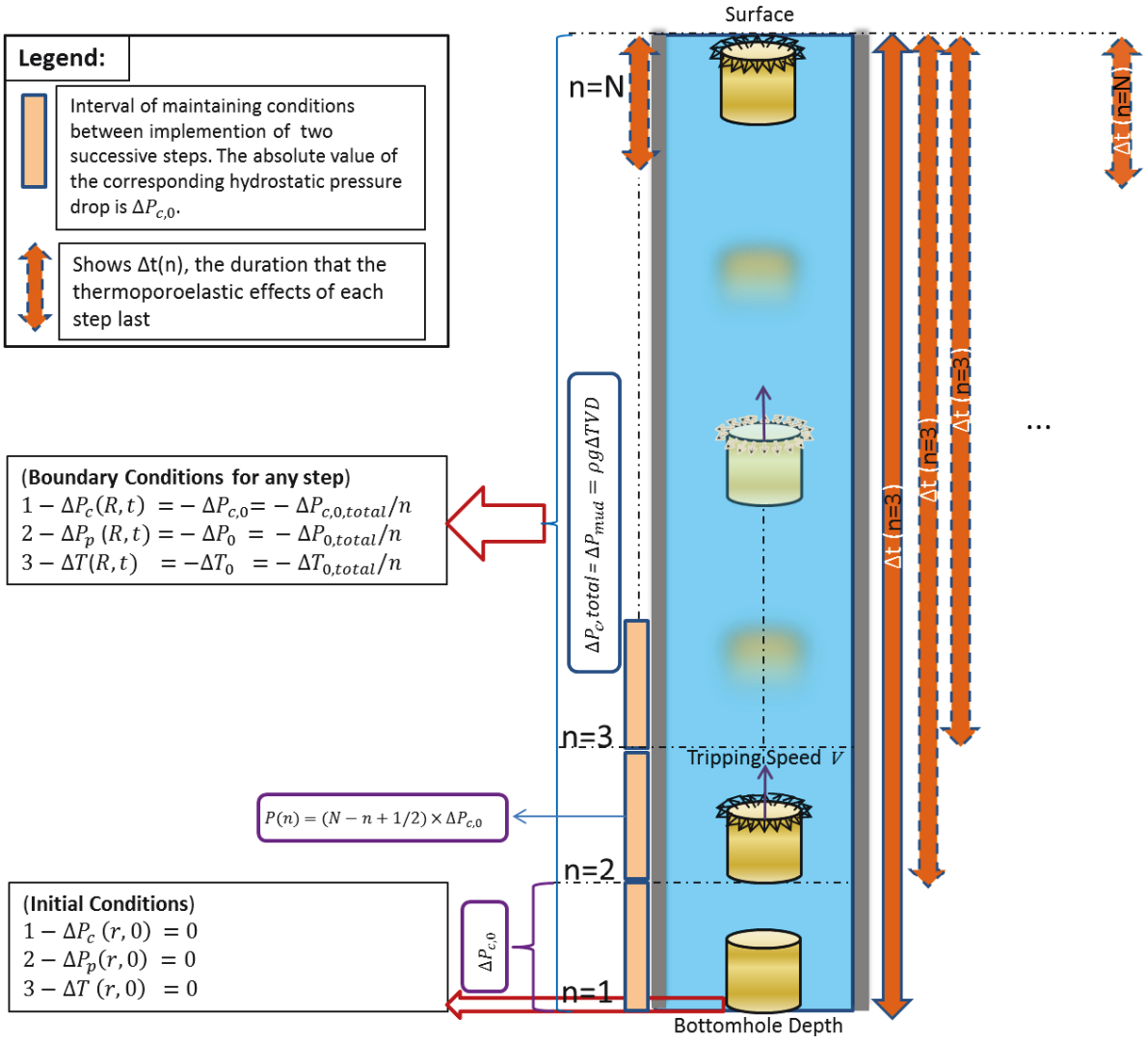

Figure 5-1: Core Decompression, Initial Conditions, the Boundary Conditions Indicating Thermoporoelastic Changes at the Boundary from Bottomhole to the Surface, and the Duration of Effects of Steps Δt(n)

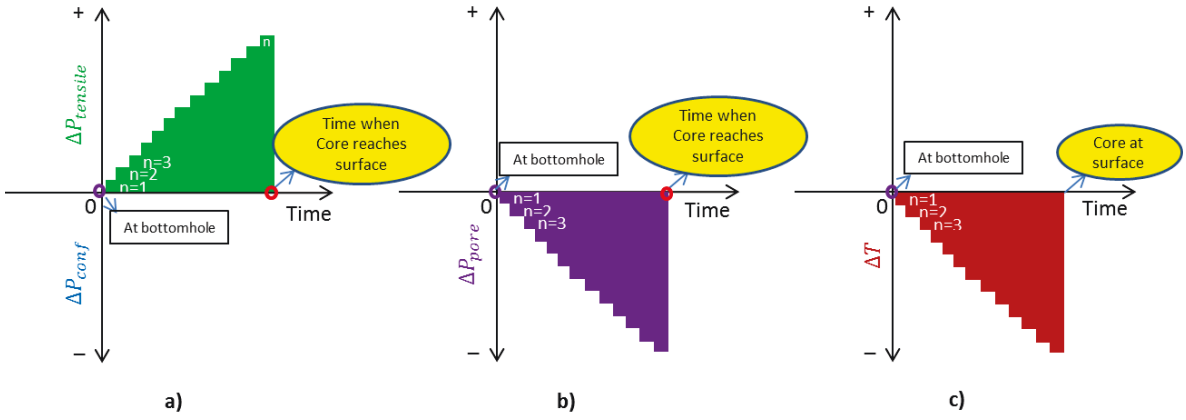

Figure 5-2: Initial and Boundary Conditions Considering Step-Wise Core -Decompression from Bottomhole to the Surface, Simulating the Real Gradual Core Tripping Using Thermoporoelasticity

5.3 Developing the Thermoporoelastic Modeling

Following the modification to the original thermoporoelasticity to match our core tripping application, it is necessary to develop a thermoporoelastic model to predict the induced pore pressures and stresses. Before illustrating the modeling process, several assumptions are made as follows:

In this approach, the following assumptions are made.

1) The derivation is made within the linear poroelastic framework.
2) The rock is assumed to be isotropic and homogeneous.
3) Pore fluid diffusion out of the core occurs only along the core radius. Therefore, axial flow with respect to the radial flow is considered negligible.
4) Single-phase fluids (dry gas or water) are considered.
5) Core pulling occurs with a constant rate or speed.
6) The stress state is the hydrostatic mud pressure. Therefore, the confining pressure applied on the sample is the mud pressure.
7) The initial pore pressure of the core sample at the bottomhole is assumed equal to the hydrostatic mud pressure.
8) Locked-in stresses remained in the sample are ignored, i.e., the core stress memory after cutting the sample is ignored. Therefore, the induced stresses can be safely considered zero.

Therefore, for the modeling process, the necessary flowchart has been developed, as shown in **Figure 5-3**. The required input data are inserted into the flowchart. These include the input bottomhole TVD, the tripping speed, the hydrostatic pressure drop between the implementation of two steps $\Delta P_{c,0}$, mud weight, some core properties including the sample porosity, viscosity, compressibility, and thus the hydraulic diffusivity coefficient[8] η (at surface conditions). Next, using the arbitrary $\Delta P_{c,0}$ (taken here as 50 KPa), the number of steps is calculated as N for the bottomhole depth. The initial values for the induced pore pressure $\Delta P_p(r,t)$, the induced radial stress $\Delta\sigma_{rr}(r,t)$, and the induced hoop stress $\Delta\sigma_{\theta\theta}(r,t)$ are assumed and considered zero; these represent those of the bottomhole conditions.

[8] The value of hydraulic diffusivity coefficient is given to the thermoporoelastic model at surface conditions.

Using the initial assumptions or calculations, moving from the bottomhole, the induced pore pressures and stresses corresponding to each step can be evaluated and summed-up to find the total values. For the evaluation corresponding to each step, we need to find the equations for the induced pore pressures and stresses (to be developed in the next section), the duration of the effect of each step $\Delta t(n)$, and the corresponding modified value of the hydraulic diffusivity coefficient[9] (which depends on the average pressure $P(n)$). For this purpose, a *for-loop* has been used in the algorithm of **Figure 5-3**. Therefore, the summation gives the total induced pore pressures and stresses at the surface. Next, the effective stresses $\Delta\sigma'$ can be found by adding the induced stresses $\Delta\sigma$ to the induced pore pressure ΔP_p. Finally, by entering the evaluated stresses into the Griffith' failure criterion, we can determine if safe tripping of core (i.e. without failure) or unsafe tripping (i.e. with failure) can be accomplished. For the purpose of enhanced simulation, coding and conversion of the flowchart algorithm to a software program has been accomplished in MATLAB-2015 environment.

[9] For each step n, the value of the hydraulic diffusivity η depends on the modified values of the fluid viscosity and compressibility for the pressure $P(n)$. This has been discussed in **Chapter 3 (Fluid-Modeling Equations)**.

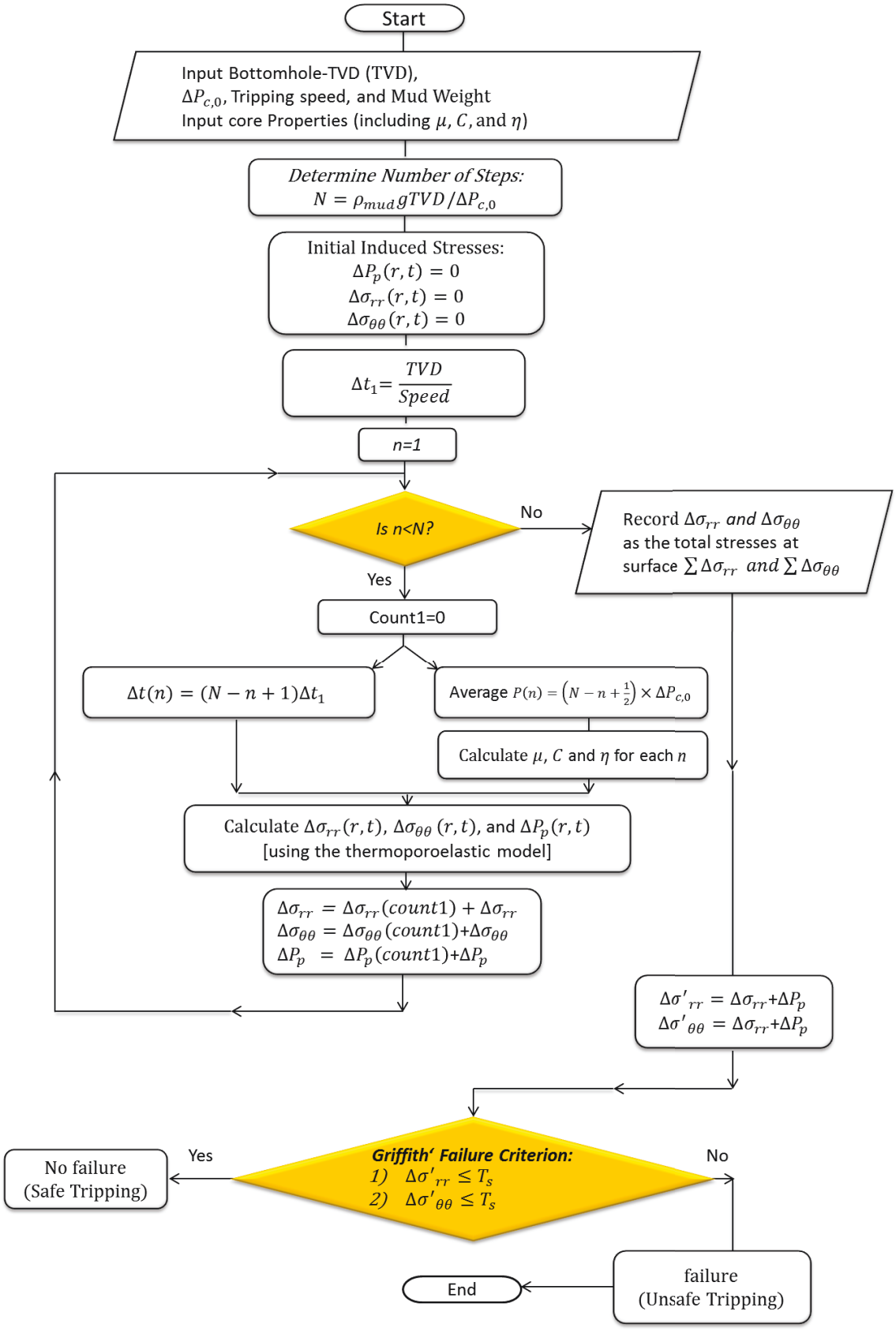

Figure 5-3: Developed Algorithm for the Induced Stress and Failure Prediction at the Time When the Sample has Reached the Surface

5.4 Equating Induced Pore Pressures and Stresses

To fill the gap in the model development process, it is required to find and develop the equations for the induced pore pressures and stresses during the sample tripping. This is done in this section. To accomplish this, an algorithm has been devised to show the required eight stages (as shown in **Figure 5-4**).

Initially, we consider the diffusivity equations, initial and boundary conditions, and the constitutive equations. After that, the problem's boundary conditions are decomposed into three classes called *unloading modes*. These modes consist of: 1) hydraulic, confining pressure drop, 2) hydraulic, pore pressure drop, and 3) thermal, temperature drop. Each of the three unloading modes is individually considered for a specified diffusivity equation (which is a Partial Differential Equation PDE). Using the unloading modes in section **5.4.1,** the hydraulic diffusivity equation is combined with the unloading modes I and II to create two Boundary Value Problems (BVPs). Similarly, the thermal diffusivity equation is combined with unloading mode III to generate the third BVP. Therefore, three individual problems represented in BVPs, are created.

Next, in order to facilitate solving the BVPs, we take Laplace transformations from the diffusivity equations. Then, the solutions of the BVPs are analytically found. These solutions provide us with Laplace of the distribution of the pore pressure and temperature differences within the sample. Next, we apply these solutions to the constitutive equations to develop and equate the Laplace of induced radial stress, hoop stress, and pore pressure. Next, using the superposition principle, the total Laplace of the induced stresses is found as the summation of the individual ones. Finally, we apply the *Stehfest*' *algorithm* (**Appendix-B,** *Jacquot et al., 1983*) to numerically take the Laplace inverse transformation and give out the induced pore pressures and stresses.

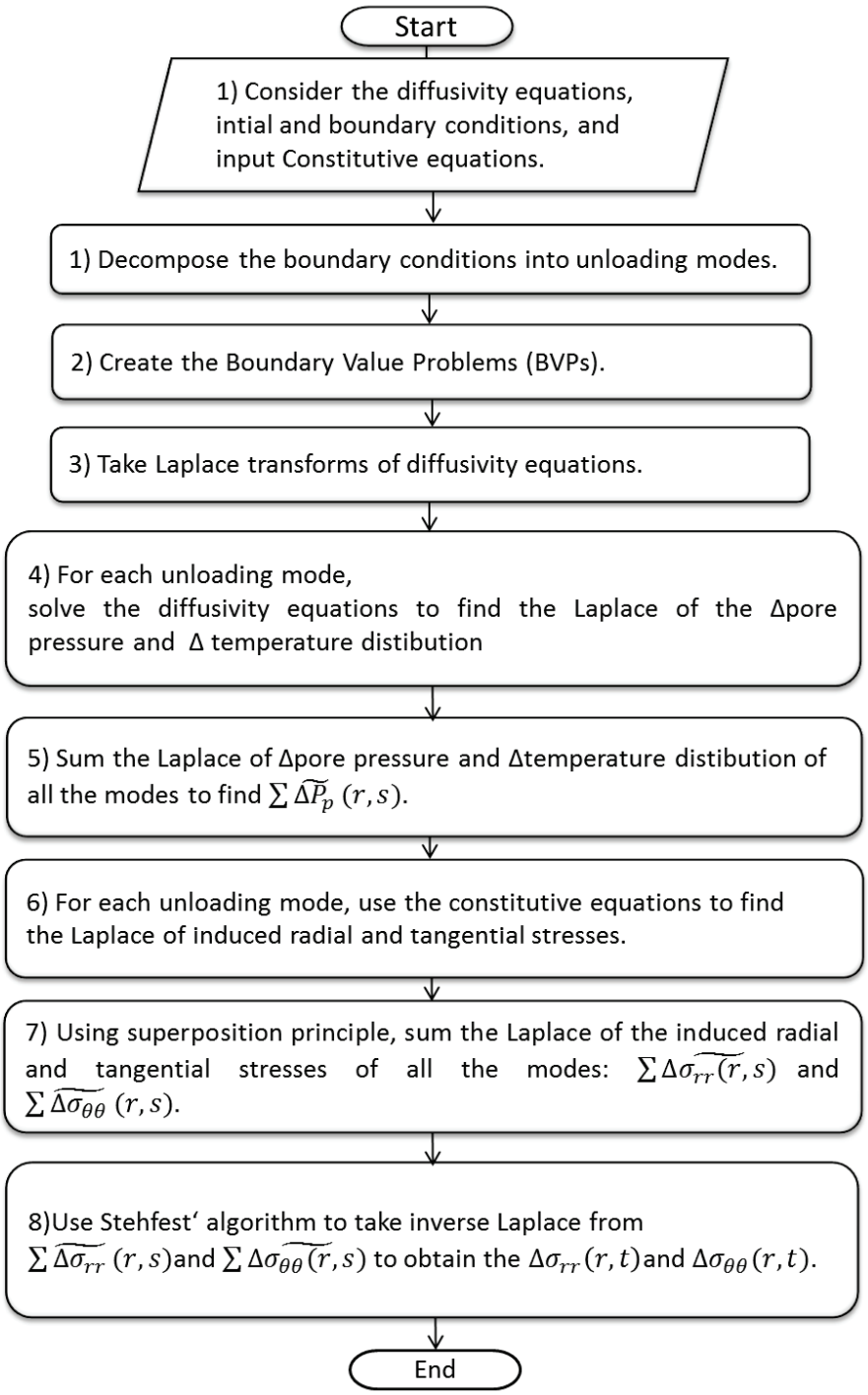

Figure 5-4: Flowchart for Equating the Thermoporoelastic Induced Stresses

5.4.1 Unloading Modes

Using the initial and boundary conditions (as shown in **Figure 5-1**), it is too complex to solve the thermoporoelastic PDEs as the three variables vary at the boundary simultaneously The variables are the confining pressure difference ΔP_c, the pore pressure difference ΔP_p, and temperature difference ΔT. Therefore, to facilitate solving the PDEs, the boundary conditions

are decomposed into three parts, called *the unloading modes*. For each unloading mode, it is assumed that only one variable is changed at the core boundary. The unloading modes are:

Unloading Mode I (Confining Pressure Drop):

Unloading mode I considers the drop of the confining mud pressure at the core boundary. In this mode, it is assumed that the pore pressure and the temperature are maintained constant and thus their differences are zero at the boundary. The conditions for this mode are:

- ✓ *The confining pressure difference at* the *boundary (for t>0):*

$$\Delta P_c(R,t) = \Delta P_{c,0} \qquad \textit{Eq. 5-1}$$

- ✓ *The pore pressure difference at the boundary (for t>0):*

$$\Delta P_p(R,t) = 0 \qquad \textit{Eq. 5-2}$$

- ✓ *The temperature difference at the outer boundary (for t>0):*

$$\Delta T(R,t) = 0 \qquad \textit{Eq. 5-3}$$

Unloading Mode II (Pore Pressure Drop):

Unloading mode II considers the drop of the pore pressure at the core boundary. In this mode, it is assumed that the confining mud pressure and the temperature are maintained constant and thus their differences are zero at the boundary. The conditions for this mode are:

- ✓ *The confining pressure difference at* the *boundary (for t>0):*

$$\Delta P_c(R,t) = 0 \qquad \textit{Eq. 5-4}$$

- ✓ *The pore pressure difference at the boundary (for t>0):*

$$\Delta P_p(R,t) = -\Delta P_0 \qquad \textit{Eq. 5-5}$$

- ✓ *The temperature difference at the outer boundary (for t>0):*

$$\Delta T(R,t) = 0 \qquad \textit{Eq. 5-6}$$

Unloading Mode III (Temperature Drop):

As the core sample is being tripped, due to the contact of the cooler drilling mud with the core sample, its boundary undergoes cooling, i.e., its temperature drops. To assume that the sample

boundary temperature is equal to the drilling mud temperature, the thermal convection coefficient of the drilling mud h is considered infinity.

Unloading mode III considers the drop of the temperature at the core boundary. In this mode, it is assumed that the confining mud pressure and the pore pressure are maintained constant and thus their differences are zero at the boundary. The conditions for this mode are:

- ✓ *Applied tensile stress (change) at* the outer *boundary (for t>0):*

$$\Delta P_c(R,t) = 0 \qquad \textit{Eq. 5-7}$$

- ✓ *Pore pressure (change or drop) at the outer boundary (for t>0):*

$$\Delta P_p(R,t) = 0 \qquad \textit{Eq. 5-8}$$

- ✓ *Temperature (change or drop) at the outer boundary (for t>0):*

$$\Delta T(R,t) = -\Delta T_0 \qquad \textit{Eq. 5-9}$$

5.4.2 Boundary Value Problems and Solutions

The three boundary value problems and the solutions for the induced pore pressure and stresses are presented as follows:

BVP I: Hydraulic, Confining Pressure Drop

Having combined (the Laplace transform of) the hydraulic diffusivity equation (**Eq. 3-9**) with the unloading mode I, the first BVP is created. Solving this BVP gives the Laplace of the pore pressure difference distribution $\widetilde{\Delta P}_{p_{(r,s)}}^{(hyd.1)}$ due to this effect as (*Wang, 2000; Detournay & Cheng, 1993*):

$$\widetilde{\Delta P}_{p_{(r,s)}}^{(hyd.1)} = -\frac{2\Delta P_c}{3sA}(1-\upsilon)\upsilon_u B(1-f_{mc})\left[I_0\left(\sqrt{\frac{s}{\eta}}R\right) - I_0\left(\sqrt{\frac{s}{\eta}}r\right)\right] \qquad \textit{Eq. 5-10}$$

Where

$$A = (1-\upsilon)I_0\left(\sqrt{\frac{s}{\eta}}R\right) - 2(\upsilon_u - \upsilon)\frac{I_1\left(\sqrt{\frac{s}{\eta}}R\right)}{\sqrt{\frac{s}{\eta}}R}$$

The equation for the induced displacement within the sample due to unloading mode II has been given by Wang *(2000)* and *Detournay & Cheng (1993)* as:

$$\widetilde{\Delta U_{rr}}_{(r,s)}^{(hyd.1)} = \frac{1}{s}\frac{\Delta P_c\, r}{2GA}\left[(1-2\upsilon_u)(1-\upsilon)I_0\left(\sqrt{\frac{s}{\eta}}R\right) + 2(\upsilon_u-\upsilon)\frac{I_1\left(\sqrt{\frac{s}{\eta}}r\right)}{\sqrt{\frac{s}{\eta}}r}\right] \qquad \textit{Eq. 5-11}$$

Using **Eq. 5-10**, **Eq. 5-11**, and the constitutive equations (section **3.4.2**), the induced stresses (radial and tangential) can be developed. The corresponding derivations have been given in **Appendix-D.** For this mode, the final equations for the induced pore pressures are given in **Table 5-1**. The final equations for the induced radial stresses, denoted as $\widetilde{\sigma_{rr}}_{(r,s)}^{(hyd.1.1)}$ excluding mud cake effect, and $\widetilde{\sigma_{rr}}_{(r,s)}^{(hyd.1.2)}$ for only the mud cake effect, are presented in **Table 5-2**. The final equations for the induced hoop stresses, denoted as $\widetilde{\sigma_{\theta\theta}}_{(r,s)}^{(hyd.1.1)}$ excluding mud cake effect and $\widetilde{\sigma_{\theta\theta}}_{(r,s)}^{(hyd.1.2)}$ for only the mud cake effect, are presented in **Table 5-3**. Therefore, in the unloading mode I, collectively there are two effects on the induced stresses. Using the superposition principle, the total Laplace of the induced radial and hoop stresses are found as $\sum_{l=1}^{2}\widetilde{\Delta\sigma_{rr}}_{(r,s)}^{(hyd.2.l)}$ and $\sum_{l=1}^{2}\widetilde{\Delta\sigma_{\theta\theta}}_{(r,s)}^{(hyd.2.l)}$.

BVP II: Hydraulic, Pore Pressure Drop

Having combined (the Laplace transform of) the hydraulic diffusivity equation with the unloading mode II, the BVP corresponding to the pore pressure drop is made. Solving this BVP gives the corresponding Laplace of the pore pressure difference distribution $\widetilde{\Delta P_p}_{(r,s)}^{(hyd.1)}$ due to this effect as (*Wang, 2000; Detournay & Cheng, 1993*):

$$\widetilde{\Delta P_p}_{(r,s)}^{(hyd.2)} = -\frac{\Delta P_c}{sA}(1-f_{mc})\left[(1-\upsilon)I_0\left(\sqrt{\frac{s}{\eta}}r\right) - 2(\upsilon_u-\upsilon)\frac{I_1\left(\sqrt{\frac{s}{\eta}}R\right)}{\sqrt{\frac{s}{\eta}}R}\right] \qquad \textit{Eq. 5-12}$$

Where

$$A = (1-\upsilon)I_0\left(\sqrt{\frac{s}{\eta}}R\right) - 2(\upsilon_u-\upsilon)\frac{I_1\left(\sqrt{\frac{s}{\eta}}R\right)}{\sqrt{\frac{s}{\eta}}R}$$

The equation for the induced displacement within the sample due to unloading mode II has been given by Wang *(2000)* and *Detournay & Cheng (1993)* as:

$$\widetilde{\Delta U_{rr}}^{(hyd.2.1)}_{(r,s)} = -\frac{1}{s}a(1-2\upsilon)\left(\frac{\Delta P_c r}{2GA}\right)\left[\frac{I_1\left(\sqrt{\frac{s}{\eta}}r\right)}{\sqrt{\frac{s}{\eta}}r} + (1-2\upsilon_u)\frac{I_1\left(\sqrt{\frac{s}{\eta}}R\right)}{\sqrt{\frac{s}{\eta}}R}\right] \qquad \textit{Eq. 5-13}$$

Using **Eq. 5-12**, **Eq. 5-13**, and the constitutive equations (section **3.4.2**), the induced stresses (radial and tangential) can be developed. The corresponding derivations have been given in **Appendix-E.** The final equations for the induced radial stresses, denoted as $\widetilde{\sigma_{rr}}^{(hyd.2.1)}_{(r,s)}$ excluding mud cake effect, and $\widetilde{\sigma_{rr}}^{(hyd.2.2)}_{(r,s)}$ for only the mud cake effect in unloading mode II, are presented in **Table 5-2**. The final equations for the induced hoop stresses, denoted as $\widetilde{\sigma_{\theta\theta}}^{(hyd.2.1)}_{(r,s)}$ excluding the mud cake effect and $\widetilde{\sigma_{\theta\theta}}^{(hyd.2.2)}_{(r,s)}$ for only the mud cake effect, are presented in **Table 5-3**. Therefore, in the unloading mode II, collectively there are two effects on the induced stresses. Using the superposition principle, the total Laplace of the induced radial and hoop stresses are found as $\sum_{m=1}^{2}\widetilde{\Delta\sigma_{rr}}^{(hyd.2.m)}_{(r,s)}$ and $\sum_{l=1}^{2}\widetilde{\Delta\sigma_{\theta\theta}}^{(hyd.2.m)}_{(r,s)}$.

BVP III: Thermal, Temperature Drop

The thermal effect on the induced stresses is mainly due to the conduction heat transfer causing the expansion-contraction effect and thus induced stresses (denoted as *thermal-1*). The thermal effect indirectly causes also coupling effects on the pore pressure difference and stresses.

Having combined (the Laplace transform of) the thermal diffusivity equation (**Eq. 3-11**) with the unloading mode III, the BVP corresponding to the temperature drop is created. Solving this BVP gives the Laplace of the temperature difference distribution $\widetilde{\Delta T}$ due to this effect as (*Carslaw & Jaeger, 1959, p.327-329*):

$$\widetilde{\Delta T} = \frac{\Delta T_0}{s}\frac{I_0\left(\sqrt{\frac{s}{\eta_T}}r\right)}{I_0\left(\sqrt{\frac{s}{\eta_T}}R\right)} \qquad \textit{Eq. 5-14}$$

Taking inverse Laplace transformation from **Eq. 5-14** gives the temperature distribution within the core as shown in **Figure 5-5**.

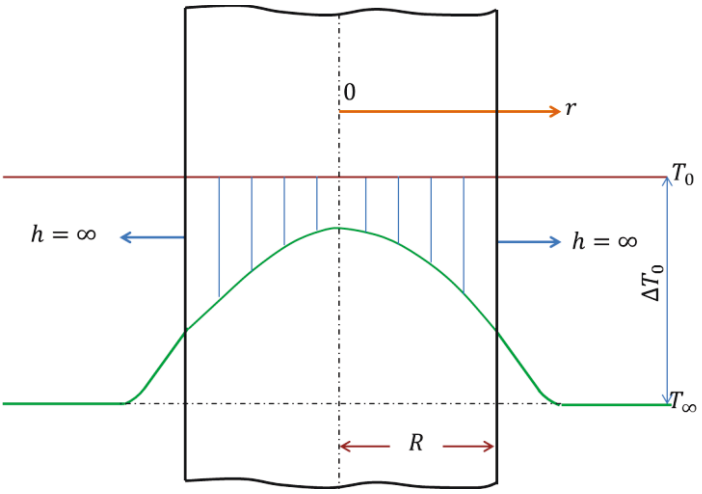

Figure 5-5: Thermal Distribution within the Cylindrical Sample while Tripping

The equation for the induced thermal displacement within the sample has been given by *Timoshenko, 1934, p. 407-412*:

$$\Delta U_{rr}{}^{(thermal)} = \frac{(1+\upsilon)}{(1-\upsilon)}\frac{\alpha_m}{3}\left[\frac{1}{R^2}\int_0^R \Delta T\, r\partial r + \frac{1}{r^2}\int_0^r \Delta T\, r\partial r - \Delta T\right] \qquad \textit{Eq. 5-15}$$

Using **Eq. 5-14**, **Eq. 5-15**, and the thermal constitutive equation (section **3.4.2**), the induced stresses (radial and tangential) can be developed**.** The corresponding derivations have been given in **Appendix-F.** The equations for the induced thermal radial stress, denoted as $\widetilde{\sigma_{rr}}_{(r,s)}^{(thermal).1}$ and the induced hoop stress, denoted as $\widetilde{\sigma_{\theta\theta}}_{(r,s)}^{(thermal.1)}$ are respectively presented in **Table 5-2** and **Table 5-3**.

Next, as we have considered coupling of thermal effect on the pore pressure and the induced stresses, we need to find these effects. This is also called thermally-induced coupling pore pressures and stresses. Cooling of the cores causes a reduction of the pore pressure particularly for tight cores. This is because the contained fluid has a larger thermal expansion coefficient than the solid part (inferred from *Perkins & Gonzales, 1984; Detournay & Cheng, 1988; Kurashige, 1989; Maurry & Guenot, 1995*; *Chen & Ewy, 2005*). However, for the induced stresses due to the thermal effect, there are two sources of stresses. First, the contraction of the inner part causes a relative compressive stress while the heat transfer from inside to outside and the expansion in the outer part exerts a tensile stress. Second, the reduction of the pore pressure by the temperature drop has a contribution for a compressive stress.

In this work, these thermally-coupled effects on the induced pore pressure and stresses are found using analogy with the equations developed by *Chen & Ewy (2005)*, as in **Appendix-F** (**Table 5-1** to **Table 5-3**). These effects on the induced radial stress, denoted as $\widetilde{\sigma_{rr}}_{(r,s)}^{(thermal.2)}$ and $\widetilde{\sigma_{rr}}_{(r,s)}^{(thermal.3)}$, are presented in **Table 5-2**. Similarly, these effects on the induced hoop stress, denoted as $\widetilde{\sigma_{\theta\theta}}_{(r,s)}^{(thermal.2)}$ and $\widetilde{\sigma_{\theta\theta}}_{(r,s)}^{(thermal.3)}$, are given in **Table 5-3**.

5.4.3 Summary of Equations

Having developed the equations for induced pore pressures and stresses in sections **5.4.1** and **5.4.2 (Appendix-D**, **E**, and **F)**, the lists of these equations have been summarized in **Table 5-1** to **Table 5-3**.

Table 5-1: Induced Pore Pressure (Difference) within the Core due to Tripping [coefficient A as in *]**
In this Research Convention, Tensile Stresses are Considered Positive.

a) Calculation of Pore Pressure Difference Induced due to:

a-1) Hydraulic, Confining Pressure Drop

$$\widetilde{\Delta P}_{p_{(r,s)}}^{(hyd.1)} = -\frac{2\Delta P_c}{3sA}(1-\upsilon)\upsilon_u B(1-f_{mc})\left[I_0\left(\sqrt{\frac{s}{\eta}}R\right) - I_0\left(\sqrt{\frac{s}{\eta}}r\right)\right]$$

a-2) Hydraulic, Pore-Pressure-Drop

$$\widetilde{\Delta P}_{p_{(r,s)}}^{(hyd.2)} = -\frac{\Delta P_c}{sA}(1-f_{mc})\left[(1-\upsilon)I_0\left(\sqrt{\frac{s}{\eta}}r\right) - 2(\upsilon_u-\upsilon)\frac{I_1\left(\sqrt{\frac{s}{\eta}}R\right)}{\sqrt{\frac{s}{\eta}}R}\right]$$

a-3) Thermal: Temperature Drop

$$\widetilde{\Delta P}_{p_{(r,s)}}^{(thermal)} = -\frac{\Delta T_0}{s}\frac{\eta_T}{1-\frac{\eta}{\eta_T}}\left[\frac{I_0\left(\sqrt{\frac{s}{\eta_T}}r\right)}{I_0\left(\sqrt{\frac{s}{\eta_T}}R\right)} - \frac{I_0\left(\sqrt{\frac{s}{\eta}}r\right)}{I_0\left(\sqrt{\frac{s}{\eta}}R\right)}\right]$$

b) Total Laplace of Pore Pressure Drop (by Applying Superposition):

$$\sum \widetilde{\Delta P}_p(r,s) = \widetilde{\Delta P}_{p_{(r,s)}}^{(hyd.1)} + \widetilde{\Delta P}_{p_{(r,s)}}^{(hyd.2)} + \widetilde{\Delta P}_{p_{(r,s)}}^{(thermal)}$$

c) Total Pore Pressure Drop (by Taking Laplace Inverse):

$$\Delta P_p(r,t) = L^{-1}\left(\sum \widetilde{\Delta P}_p(r,s)\right)$$

$$*** \mathrm{A} = (1-\upsilon)\mathrm{I}_0\left(\sqrt{\frac{s}{\eta}}R\right) - 2(\upsilon_u-\upsilon)\frac{\mathrm{I}_1\left(\sqrt{\frac{s}{\eta}}R\right)}{\sqrt{\frac{s}{\eta}}R}$$

Table 5-2: Induced Radial Stresses within the Core due to Tripping [coefficient A as in *]**

a) Calculation of Radial Stress Difference Induced due to:

a-1) Hydraulic, Confining Pressure Drop

$$\widetilde{\Delta\sigma_{rr}}^{(hyd.1.1)}_{(r,s)} = \frac{\Delta P_c}{sA}\left\{(1-\upsilon)I_0\left(\sqrt{\frac{s}{\eta}}R\right) - 2\,(\upsilon_u-\upsilon)\left[\frac{I_1\left(\sqrt{\frac{s}{\eta}}r\right)}{\sqrt{\frac{s}{\eta}}r}\right]\right\}$$

$$\widetilde{\Delta\sigma_{rr}}^{(hyd.1.2)}_{(r,s)} = 2\frac{\Delta P_c}{sA}\frac{(\upsilon_u-\upsilon)}{(1-2\upsilon)}(1-\upsilon)f_{mc}\left[I_0\left(\sqrt{\frac{s}{\eta}}R\right) - I_0\left(\sqrt{\frac{s}{\eta}}r\right)\right] \text{(due to mud cake effect)}$$

a-2) Hydraulic, Pore-Pressure-Drop

$$\widetilde{\Delta\sigma_{rr}}^{(hyd.2.1)}_{(r,s)} = -\frac{\Delta P_c}{sA}a(1-2\upsilon)\left[\frac{I_1\left(\sqrt{\frac{s}{\eta}}R\right)}{\sqrt{\frac{s}{\eta}}R} - \frac{I_1\left(\sqrt{\frac{s}{\eta}}r\right)}{\sqrt{\frac{s}{\eta}}r}\right]$$

$$\widetilde{\Delta\sigma_{rr}}^{(hyd.2.2)}_{(r,s)} = \frac{\Delta P_c}{sA}a(1-2\upsilon)f_{mc}\left[\frac{I_1\left(\sqrt{\frac{s}{\eta}}R\right)}{\sqrt{\frac{s}{\eta}}R} - \frac{I_1\left(\sqrt{\frac{s}{\eta}}r\right)}{\sqrt{\frac{s}{\eta}}r}\right] \text{(due to mud cake effect)}$$

a-3) Thermal: Temperature Drop

$$\widetilde{\Delta\sigma_{rr}}^{(thermal.1)}_{(r,s)} = -\frac{\Delta T_0}{s}\frac{E}{(1-\upsilon)}\frac{\alpha_m}{3}\times\frac{1}{I_0\left(\sqrt{\frac{s}{\eta_T}}R\right)\left(\sqrt{\frac{s}{\eta_T}}R\right)}\left[I_1\left(\sqrt{\frac{s}{\eta_T}}R\right) - \frac{R}{r}I_1\left(\sqrt{\frac{s}{\eta_T}}r\right)\right]$$

$$\widetilde{\Delta\sigma_{rr}}^{(thermal.2)}_{(r,s)} = \frac{\Delta T_0}{s}\left(\frac{\eta'}{1-\frac{\eta}{\eta_T}}\right)\frac{\alpha_m}{3}\frac{(1-2\upsilon)}{(1-\upsilon)I_0\left(\sqrt{\frac{s}{\eta}}R\right)\left(\sqrt{\frac{s}{\eta}}R\right)}\left[I_1\left(\sqrt{\frac{s}{\eta}}R\right) - \frac{R}{r}I_1\left(\sqrt{\frac{s}{\eta}}r\right)\right]$$

$$\widetilde{\Delta\sigma_{rr}}^{(thermal.3)}_{(r,s)} = -\frac{\Delta T_0}{s}\left(\frac{\eta'}{1-\frac{\eta}{\eta_T}}\right)\frac{\alpha_m}{3}\frac{a(1-2\upsilon)}{(1-\upsilon)I_0\left(\sqrt{\frac{s}{\eta_T}}R\right)\left(\sqrt{\frac{s}{\eta_T}}R\right)}\left[I_1\left(\sqrt{\frac{s}{\eta_T}}R\right) - \frac{R}{r}I_1\left(\sqrt{\frac{s}{\eta_T}}r\right)\right]$$

b) Total Laplace of Induced Radial Stress (by Applying Superposition):

$$\sum\widetilde{\Delta\sigma_{rr}}(r,s) = \sum_{l=1}^{2}\widetilde{\Delta\sigma_{rr}}^{(hyd.1.l)}_{(r,s)} + \sum_{m=1}^{2}\widetilde{\Delta\sigma_{rr}}^{(hyd.2.m)}_{(r,s)} + \sum_{n=1}^{3}\widetilde{\Delta\sigma_{rr}}^{(thermal.n)}_{(r,s)}$$

c) Total Induced Radial Stress (by Taking Laplace Inverse):

$$\Delta\sigma_{rr}(r,t) = L^{-1}\left(\sum\widetilde{\Delta\sigma_{rr}}(r,s)\right)$$

d) Effective Radial Stress::

$$\Delta\sigma'_{rr}(r,t) = \Delta\sigma_{rr}(r,t) + \Delta P_p$$

*** $\mathrm{A} = (1-\upsilon)\mathrm{I}_0\left(\sqrt{\frac{s}{\eta}}R\right) - 2(\upsilon_u-\upsilon)\frac{\mathrm{I}_1\left(\sqrt{\frac{s}{\eta}}R\right)}{\sqrt{\frac{s}{\eta}}R}$

Table 5-3: Induced Hoop Stresses within the Core due to Tripping [coefficient A as in *].**

a) Calculation of Hoop Stress Difference Induced due to:

a-1) Hydraulic, Confining Pressure Drop

$$\widetilde{\Delta\sigma_{\theta\theta}}^{(hyd.1.1)}_{(r,s)} = \frac{\Delta P_c}{sA}\left\{(1-\upsilon)I_0\left(\sqrt{\frac{s}{\eta}}R\right) - 2(\upsilon_u-\upsilon)\left[I_0\left(\sqrt{\frac{s}{\eta}}r\right) - \frac{I_1\left(\sqrt{\frac{s}{\eta}}r\right)}{\sqrt{\frac{s}{\eta}}r}\right]\right\}$$

$$\widetilde{\Delta\sigma_{\theta\theta}}^{(hyd.1.2)} = 2\frac{\Delta P_c}{sA}\frac{(\upsilon_u-\upsilon)}{(1-2\upsilon)}(1-\upsilon)f_{mc}\left[I_0\left(\sqrt{\frac{s}{\eta}}R\right) - I_0\left(\sqrt{\frac{s}{\eta}}r\right)\right](due\ to\ mud\ cake\ effect)$$

a-2) Hydraulic, Pore-Pressure-Drop

$$\widetilde{\Delta\sigma_{\theta\theta}}^{(hyd.2.1)}_{(r,s)} = -\frac{\Delta P_c}{sA}\alpha(1-2\upsilon)\left[\frac{I_1\left(\sqrt{\frac{s}{\eta}}r\right)}{\sqrt{\frac{s}{\eta}}r} + \frac{I_1\left(\sqrt{\frac{s}{\eta}}R\right)}{\sqrt{\frac{s}{\eta}}R} - I_0\left(\sqrt{\frac{s}{\eta}}r\right)\right]$$

$$\widetilde{\Delta\sigma_{\theta\theta}}^{(hyd.2.2)}_{(r,s)} = \frac{\Delta P_c}{sA}\alpha(1-2\upsilon)f_{mc}\left[\frac{I_1\left(\sqrt{\frac{s}{\eta}}r\right)}{\sqrt{\frac{s}{\eta}}r} + \frac{I_1\left(\sqrt{\frac{s}{\eta}}R\right)}{\sqrt{\frac{s}{\eta}}R} - I_0\left(\sqrt{\frac{s}{\eta}}r\right)\right](\text{due to mud cake effect})$$

a-3) Thermal: Temperature Drop

$$\widetilde{\Delta\sigma_{\theta\theta}}^{(thermal.1)}_{(r,s)} = -\frac{\Delta T_0}{s}\frac{E}{(1-\upsilon)}\frac{\alpha_m}{3}\times\frac{1}{I_0(\sqrt{\frac{s}{\eta_T}}R)\sqrt{\frac{s}{\eta_T}}R)}\left[I_1(\sqrt{\frac{s}{\eta_T}}R) + \frac{R}{r}I_1(\sqrt{\frac{s}{\eta_T}}r) - (\sqrt{\frac{s}{\eta}}R)I_0(\sqrt{\frac{s}{\eta_T}}r)\right]$$

$$\widetilde{\Delta\sigma_{\theta\theta}}^{(thermal.2)}_{(r,s)} = -\frac{\Delta T_0}{s}\left(\frac{\eta'}{1-\frac{\eta}{\eta_T}}\right)\frac{\alpha_m}{3}\frac{(1-2\upsilon)}{(1-\upsilon)I_0\left(\sqrt{\frac{s}{\eta_T}}R\right)\left(\sqrt{\frac{s}{\eta_T}}R\right)}\left[I_1(\sqrt{\frac{s}{\eta_T}}R) + \frac{R}{r}I_1(\sqrt{\frac{s}{\eta_T}}r) - (\sqrt{\frac{s}{\eta}}R)I_0(\sqrt{\frac{s}{\eta_T}}r)\right]$$

$$\widetilde{\Delta\sigma_{\theta\theta}}^{(thermal.3)}_{(r,s)} = \frac{\Delta T_0}{s}\left(\frac{\eta'}{1-\frac{\eta}{\eta_T}}\right)\frac{\alpha_m}{3}\frac{(1-2\upsilon)}{(1-\upsilon)I_0\left(\sqrt{\frac{s}{\eta}}R\right)\left(\sqrt{\frac{s}{\eta}}R\right)}\left[I_1(\sqrt{\frac{s}{\eta_T}}R) + \frac{R}{r}I_1(\sqrt{\frac{s}{\eta_T}}r) - (\sqrt{\frac{s}{\eta}}R)I_0(\sqrt{\frac{s}{\eta_T}}r)\right]$$

b) Total Laplace of Induced Radial Stress (by Applying Superposition):

$$\sum\widetilde{\Delta\sigma_{\theta\theta}}(r,s) = \sum_{l=1}^{2}\widetilde{\Delta\sigma_{\theta\theta}}^{(hyd.1.l)}_{(r,s)} + \sum_{m=1}^{2}\widetilde{\Delta\sigma_{\theta\theta}}^{(hyd.2.m)}_{(r,s)} + \sum_{n=1}^{3}\widetilde{\Delta\sigma_{\theta\theta}}^{(thermal.n)}_{(r,s)}$$

c) Total Induced Radial Stress (by Taking Laplace Inverse):

$$\Delta\sigma_{\theta\theta}(r,t) = L^{-1}\left(\sum\widetilde{\Delta\sigma_{\theta\theta}}(r,s)\right)$$

d) Effective Radial Stress::

$$\Delta\sigma'_{\theta\theta}(r,t) = \Delta\sigma_{\theta\theta}(r,t) + \Delta P_p$$

$$*** \text{ A} = (1-\upsilon)\text{I}_0\left(\sqrt{\frac{s}{\eta}}R\right) - 2(\upsilon_u-\upsilon)\frac{\text{I}_1\left(\sqrt{\frac{s}{\eta}}R\right)}{\sqrt{\frac{s}{\eta}}R}$$

5.5 Identifying Contributing Parameters

So far, the equations for the induced stresses during core tripping have been developed in section **5.4**. Having searched in these equations, the affecting coefficients or parameters can be identified. These constitute the input data required for thermoporoelastic modeling. Searching in these equations shows that: a) some of these parameters are general and appear in the equations for all the stresses and have effect in them (for all the unloading modes I to III), b) some appear and have effect only in equations for the hydraulically induced stresses (for unloading modes I and II), c) the rest appear only in equations for the induced thermal stresses (for unloading mode III). Therefore, these parameters can be classified into three classes based on their area of effect, as:

a) Hydraulically and thermally affecting (general parameters):

1) Bottomhole depth:
2) Tripping speed
3) Core diameter, R
4) Poisson's ratio υ

b) Hydraulic parameters:

1) Hydraulic diffusivity coefficient, η:
   It, in turn, depends on porosity, permeability, viscosity, and total compressibility.
2) Mud Properties:
   a. weight, ρ_m
   b. Mud cake pressure drop, $\Delta P\%$
3) Biot's coefficient a

c) Thermal parameters:

1) Thermal expansion coefficient a_m
2) Thermal diffusivity, η_T
3) Geothermal gradient
4) Young's modulus of elasticity, E

It is noted that core sample tensile strength depends on the Young's modulus (which is one of the parameters affecting the thermal induced stresses). It should also be noted that the lithology of the core sample has influence on the aforementioned listed parameters. Therefore, knowing the lithology can provide a general idea about the above parameters.

In **Chapter 6**, the effects of the above contributing parameters on the induced stresses within the sample and its failure will be investigated for a typical example.

5.6 Optimal Tripping Model

As the determination of the optimal tripping speed is one of the objectives of this research work, a proper procedure is required. This is because the tripping speed is the only contributing parameter that is selectable. Based on the developed procedure, given in **Figure 5-6**, the required input data is obtained including the selected highest possible tripping speed, i.e., wireline speed of $1.524\ m/s$. Next, the thermoporoelastic model is run using the input data and the possibility of failure is investigated. If failure does not occur with the given speed, tripping is possible with the wireline coring and the wireline speed is the optimum. If failure occurs with the given speed, a lower economical speed must be selected, and the model is rerun using the new speed. This speed should be in the economic limits of the operations. This process continues in an iterative manner until no failure occurs during tripping. The tripping speed by which no failure occurs is considered as the optimal one.

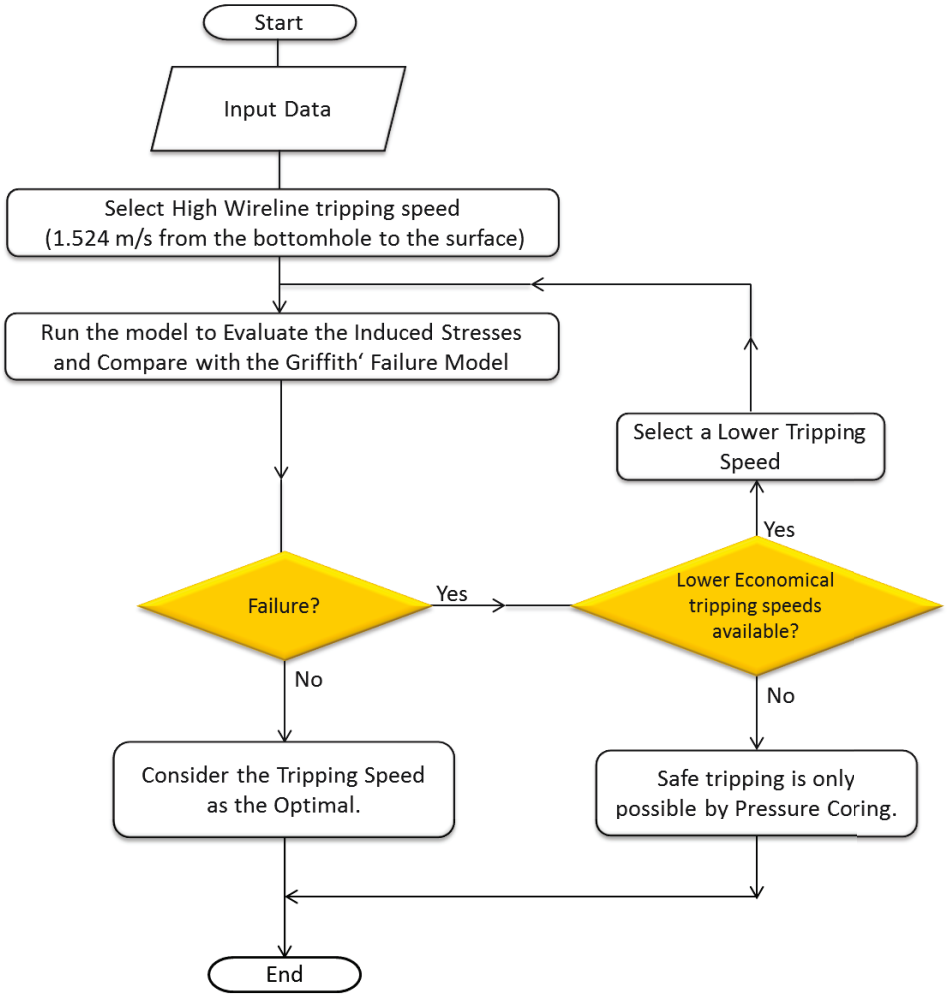

Figure 5-6: The Flowchart for Optimal Tripping Schedule

Chapter 6: Results and Discussion

6.1 Introduction

Based on **Chapter 4** and **5**, the thermoporoelastic model has been developed and coded in Matlab-2015. In this chapter, first this work's developed model is compared and checked with a literature's work, developed in *Ansys-Fluent* environment. The objective of this comparison is whether the thermoporoelastic model can give meaningful results. The parameters affecting the thermoporoelastic behavior were identified in the developed model in section **5.5**. As the investigation of the effects of these parameters is one of the objectives of this work, this is followed in this chapter using a typical investigation. To do this, a typical core sample with specified properties and conditions is considered. Following this investigation, the contributing parameters with the greatest or dominant effects are recognized and considered as the determinative factors. The determinative factors are important as they contribute to proper candidate selection for different core tripping and coring methods.

6.2 Matching

In this section, the results of the developed thermoporoelastic model are compared with *Zubizarreta et al.* (2013) in *Ansys-Fluent*. They assumed a 4-inch (10.16 cm) core sample with 2% porosity, and permeability of $2 \times 10^{-4} mD$, 0.02 cp gas viscosity, is retrieved from the depth of $1502.46\ m$ to the surface. The drilling mud weight in the wellbore is 12.5 ppg ($1259\ Kg/m3$) which gives $18.65\ Mpa$ as the initial bottomhole pressure. The initial sample pore pressure is assumed to be equal to the initial mud hydrostatic pressure. The surface and bottomhole temperatures are respectively 10 and 34 $^{\circ}C$. Based on the tripping schedule mentioned in their paper, the core is raised from 1502.46 to 914.5 m with $0.31\ m/s$ tripping speed; then from 914.5 to 198 m with the speed of $0.065\ m/s$; and finally from 198 m to the

surface with 0.05 m/s. Using this data, the hydraulic diffusivity coefficient η of $4 \times 10^6 \frac{m^2}{s}$ was obtained. This value will be used in the thermoporoelastic model.

In their work like the other works in the literature, as the role of the mechanical and thermal properties were neglected in the induced pore pressured and stresses. Just, the tensile strength is used for verifying possible failure. However, in the thermoporoelastic model of this work, the contribution of the mechanical properties has been considered and this requires the corresponding data as well. Therefore, we inserted the model some adjusted mechanical and thermal properties including the Poisson's ratio ($\upsilon = 0.18$), Undrained Poisson's ratio ($\upsilon_u = 0.28$), Biot's coefficient ($a = 0.7$), Young's modulus (10 GPa), thermal expansion coefficient ($10^{-5}\ \frac{1}{^\circ C}$), and thermal diffusivity coefficient of $8 \times 10^{-7} \frac{m^2}{s}$.

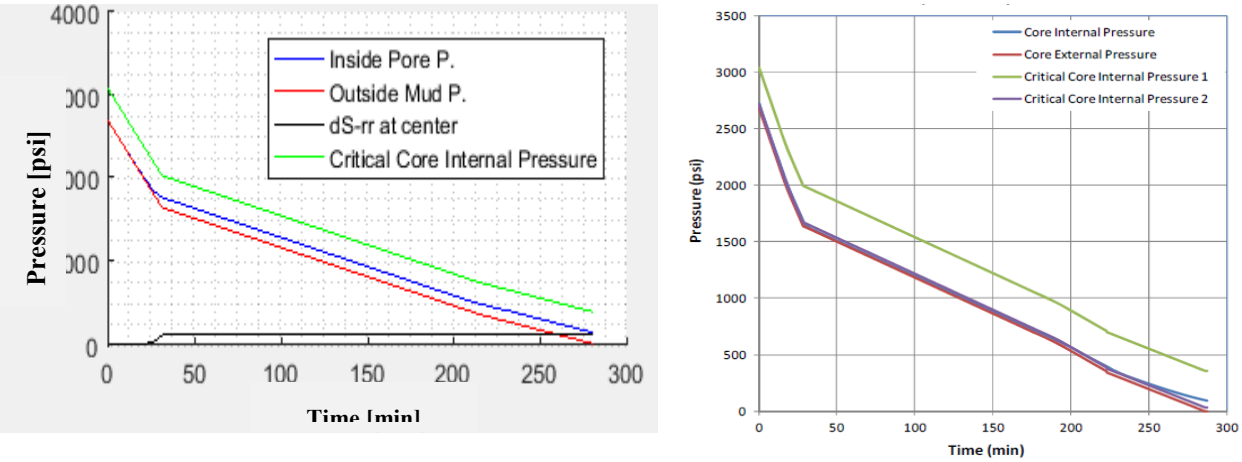

a) Result of the thermoporoelastic model of this work

b) Results of Ansys-Fluent Model by Zubizarreta et al. (2013), Case6, p.10

Figure 6-1: Comparison of the Results of the Thermoporoelastic Model with a Literature Work

As shown in **Figure 6-1 a** and **b**, the results of the two models look comparable, just the thermoporoelastic model has modeled greater pore pressure values than the *Fluent* model. This can be attributed to the different nature of the two models and the fact that the *Fluent* model had not considered the mechanical and thermal properties. The black color in **Figure 6-1-a** represents the induced radial stress in the center of the core. This induced stress in the center of the core is found as the difference between the inside pore pressure (blue) and the outside mud pressure (red). The critical core internal pressure (shown by the green color) is equal to the summation of the outside mud pressure with the equivalent tensile strength. As the purpose of this section is the comparison of results, we used the same terminology and

also color convention of *Zubizarreta et al (2013).* However, in the next section, for the investigation of the contributing parameters, this will be a little different.

6.3 Effects of Contributing Parameters

In section **5.5**, the affecting parameters were identified by searching the affecting coefficients through the developed equations for induced pore pressure and stresses. These are called *the contributing parameters*. Then, they were split into three classes: general (affecting both the hydraulically and thermally induced stresses within the sample), hydraulic (affecting only the hydraulically induced stresses) and thermal (affecting only the thermally induced stresses) classes. It was also noted that the tensile strength of the sample is affected by the Young's modulus (as one parameter which also affects the induced thermal stresses).

The investigation of the effects of the contributing parameters in the developed model is one of the objectives of this work. Therefore, this is accomplished in the following of this chapter, using the flowchart algorithm presented in section **5.3** and the equations presented in **Table 5-1** to **Table 5-3**. To do this, first, a typical set of input data representing the properties of a typical gas-bearing[1] tight core sample is required (as given in **Table 6-1**). This data is given in accordance to *Chen & Ewy (2005)*, *Hettema et al. (2002),* and also the typical industry's core analysis results. The input data is inserted into the model, the model is run, and the effective induced stresses are evaluated. Using the Griffith' criterion, the results of the induced stresses are compared with the tensile strength of the sample to investigate possible failure.

It is noted that as the effect of the first contributing parameter will be investigated, the corresponding graphs and the way of interpreting will be described in detail. The patterns of graphs for other parameters are similar. Using this, the results of the rest of the parameters can be similarly interpreted.

[1] For single phase fluids containing the sample, gas is the worst case as of being compressible.

Table 6-1: Initial Inputs (Except for the Tripping Speed) belonging to a Typical Tight Gas-Bearing Core Sample for Use in the Thermoporoelastic Model

Parameter	*Value*	*Evaluation Method*
Depth at bottomhole [m]	*Mostly* 500	
Diameter of core [in]	2 *(≈5 cm)*	
Porosity, ϕ [%]	40	*Estimated/Measurable*
Permeability of core, K [mD]	10^{-3}	*Estimated/Measurable*
Viscosity of gas, μ_g [cp]	0.02-0.04 *(surface)*	*Measured*
Viscosity of water, μ_g [cp]	1	
Molecular Weight of gas, M_g	16 *(Methane)*	*Depending on the gas*
Specific Gravity of gas (Surface)	0.65	*Depending on the gas*
Compressibility of rock, C_r [1/pa]	5×10^{-10}	*Estimated/Measurable*
Compressibility of gas (surface), C_g [1/Pa]	9.869×10^{-6}	*Estimated/Measurable*
Compressibility of water, C_w [1/pa]	5×10^{-10}	*Estimated/Measurable*
Interstitial Water Saturation, $S_{w,i}$	20 %	*Estimated/Measurable*
Total Compressibility, $C_{t,g}$ [1/Pa] (gas-bearing core)	7.89×10^{-6}	$C_t = C_r + S_w C_w + S_g C_g$ *[Ahmed & McKinney, 2005]*
Hydraulic-Diffusivity, η [m^2/s] (Gas-bearing at surface)	10^{-8}	$\eta = 9.869 \times 10^{-13} \frac{K}{\varphi \mu_g C_{t,g}}$ *[Ahmed & McKinney, 2005]*
Thermal Expansion Coefficient, α_m [1/°C]	10^{-5}	*Estimated/Measurable [Timoshenko, 1934)]*
Thermal Diffusivity, η_T [m^2/s]	8×10^{-7}	*Estimated*
Geothermal Gradient [°C/m]	0.025	*Estimated/Measurable*
Uniaxial Compressive Strength, UCS [Mpa]	20	*Measurable/Estimated*
Young's Modulus [GPa]	4.2	*Calculated/Estimated*
Tensile-Strength, T.S. [Mpa]	1.7–2	$T.S. = UCS/m$, m=7–15 *[Jaeger et al., 2007]*
Biot's coefficient, α	0.7	*0.6-0.7 (for shales)*
Poisson's Ratio, ν	0.3	*Estimated/Measurable*
Undrained Poisson's Ratio, ν	0.4	*Estimated/Measurable*
Mud Weight, ρ_m [kg/m3]	1078	$MW[ppg] \times 119.826 = MW\left[\frac{kg}{m3}\right]$
Coupling Coefficient, η' and η'_T	0.17–0.3	*Estimated*
Initial Bottomhole Pressure [Mpa]	5.4	
Initial Pore Pressure		*Equal to initial hydrostatic pressure*

6.4 General Parameters

General parameters affect both the hydraulically and thermally induced pore pressure and stresses. They consist of the initial bottomhole depth, tripping speed, core diameter, and the Poisson's ratio.

6.4.1 Bottomhole Depth

The initial bottomhole depth of the core sample is one of the parameters affecting the sample's thermoporoelastic behavior during its tripping. To simulate this effect using the thermoporoelastic model, first the input data corresponding to a typical very tight core sample with $\eta = 10^{-8} m^2/s$ (as given in **Table 6-1**) is considered. As the industry suggests using conventional coring for very tight samples, we first select this method and its tripping speed ($0.45\ m/s$) to notice how it works. Inserting the input data into the flowchart algorithm, as in section **5.3**, and using the equations presented in section **5.4.3**, the induced stresses are evaluated for different initial bottomhole depths. Next, to investigate the possible failure within the sample when it reaches the surface, the Griffith' failure criterion is applied for *a)* the induced radial stress, *b)* the induced hoop stress, and *c)* the induced radial stress in the center of the sample, evaluated by subtracting the mud pressure from the pore pressure in the center of the sample.

Therefore, in order to investigate the effect of different depths, first **Figure 6-2a** and **b** show the evaluated induced radial and hoop stresses along with the tensile strength, ranging from the core center to its boundary. Then, **Figure 6-2c** displays the central induced radial stresses along with the tensile strength, versus time (red flat line). Comparing the induced effective stresses with the strength determines whether the failure can occur or not. As can be seen in this figure, failure occurs for all the initial bottomhole depths, except for the initial bottomhole depth of 500 m. This proves that the industry suggestion regarding the conventional tripping speeds for very tight cores does not mostly help. To justify the results, the greater this depth is, the greater is the initial bottomhole confining pressure of the mud and the initial pore pressure of the sample. Therefore, the total confining and pore pressure differences that the sample has to experience during tripping, would be greater. As a result, with greater bottomhole depth, greater induced stresses are induced within the sample while the tensile strength remains constant. This means that the possibility of the failure becomes greater with greater bottomhole depth.

As the considered core sample with the initial bottomhole depth of 500 m can be retrieved safely to the surface, from now on the effects of the rest of the contributing parameters will be mainly concentrated on this sample.

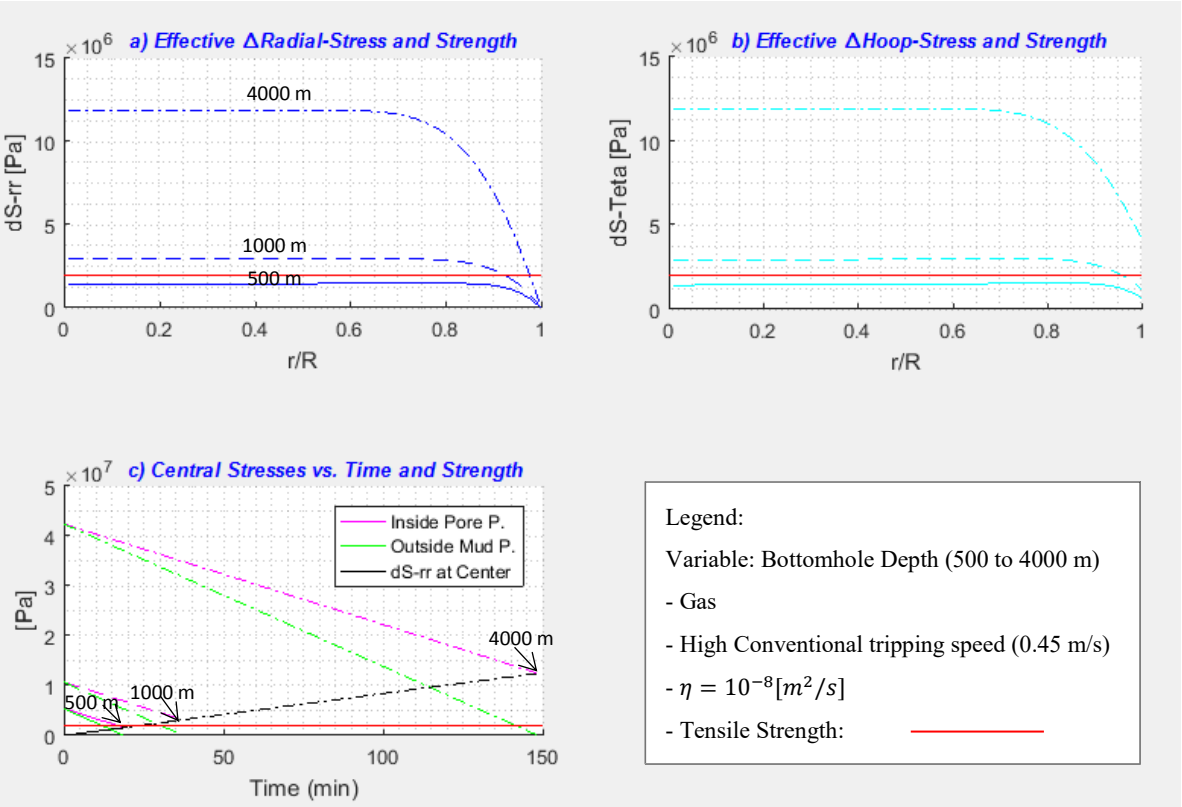

Figure 6-2: The Effect of the Bottomhole Depth (where the Sample is Initially Located) on the Induced Thermoporoelastic Stresses and Failure

6.4.2 Tripping Speed

The tripping speed of the core is considered as the only parameter that is controllable and we can select to modify the induced thermoporoelastic stresses. The other parameters are bound to the core and hole properties. In section **5.6**, a procedure was introduced for finding the optimal tripping speed. Following this procedure, the data given in **Table 6-1** is considered with the initial bottomhole depth of 500 m. Next, the wireline tripping speed (1.524 m/s) is considered and the modeling is performed. The simulation results in **Figure 6-3** (solid lines) indicate that the sample can be tripped almost safely. However, as there is an uncertainty for the tensile strength ranging from 1.7 to 2 Mpa, the induced stresses within the core almost reach its tensile strength (as seen in **Figure 6-3-b**). This makes wireline tripping probably a little risky for preserving the core.

Therefore, for comparison purposes, a lower tripping speed is selected, the high conventional tripping speed ($0.45\ m/s$) is selected and the modeling is again performed (the same figure, dashed lines). Using the conventional tripping speed compared with the wireline one, the induced stresses show a little decrease than with the wireline speed, except for a very slight increase in the inner part, and the core sample can be retrieved without any failure (as shown in the same figure). The result is attributed to the fact that using a lower tripping speed, there is greater time for the pore pressure difference in the sample to dissipate. In the considered case, the sample has very low hydraulic diffusivity coefficient and permeability. This is the reason that using lower conventional tripping speed than the wireline one, does not have considerable contribution to lowering the induced stresses and the induced stresses of about $1.5\ Mpa$ are still induced in the core (the same figure). Similarly, using lower tripping speeds, there is more time for the temperatures between the inside and outside of the sample to equalize. The temperature difference generally causes expansive thermal stress in the outer part and compressive stress in the inner part. Therefore, using conventional coring, less thermal stress is induced in the center and the outer part compared with the wireline method.

As another investigation of the effect of the tripping speed, the same core sample, but at the depth of 1000 m, is considered. Using the same thermoporoelastic approach, the modeling of the induced stresses and failure is performed using three tripping speeds (**Figure 6-4**). These are the speeds of high wireline ($\approx 1.524\ m/s$), high conventional ($\approx 0.45\ m/s$), and an imaginary $0.015\ m/s$. The results corresponding to the excessive low speed of $0.015\ m/s$ show that the sample can be safely retrieved without any failure. However, the time required is 18.5 hours which is far from economical. Therefore, there are no optimal tripping speeds for this core located at 1000 m.

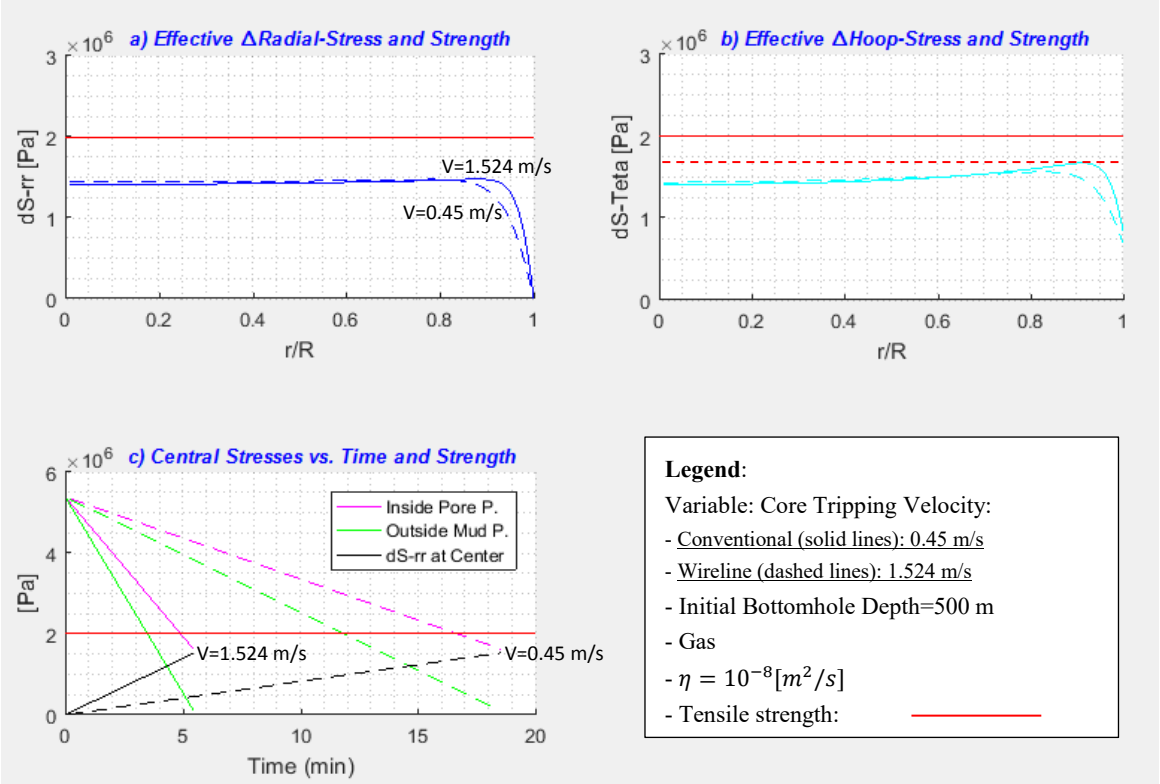

Figure 6-3: The Effect of Core Tripping Speed on the Induced Thermoporoelastic Stresses and Failure

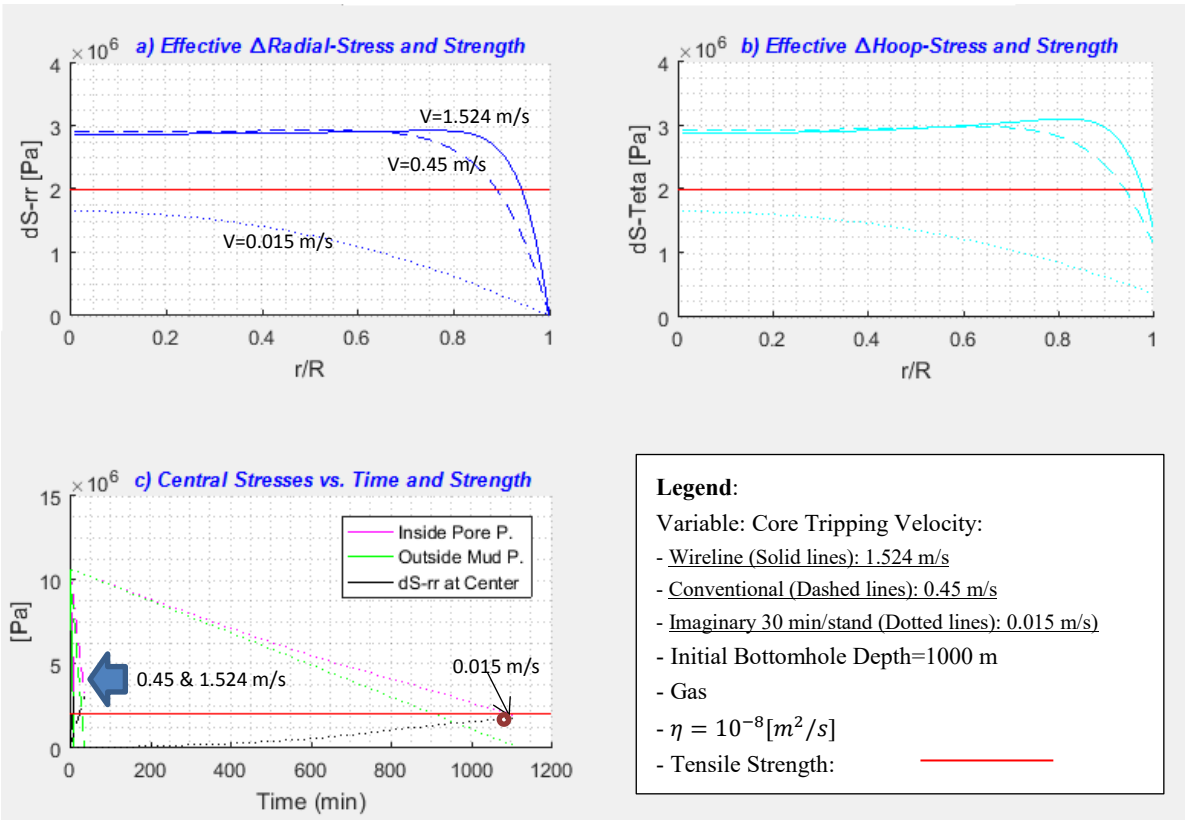

Figure 6-4: The Effect of Tripping Speed on the Induced Thermoporoelastic Stresses and Failure–Initial Bottomhole Depth of 1000 m

6.4.3 Core Diameter

The diameter of the sample is one of the parameters that generally affect the thermoporoelastic pore pressure and stresses. Two diameter values of 5 and 10 cm are considered for the assumed core sample located at 500 m. As shown in **Figure 6-5**, the *10 cm* sample shows to undergo greater induced stresses rather than the 5 *cm* one when it reaches the surface. However, this sample has not yet shown any failure. As another example of the investigation of the effect of core diameter, the same sample, but at the depth of 1000 m, has been considered with the two diameters of 1 *cm* and 5 *cm* (**Figure 6-6**). As the results show, the induced stresses significantly reduce and fall below the tensile strength. This means that for very small core diameter, e.g., *1-cm*, which is not realistic, the sample can be safely tripped to the surface without any failure.

To justify the results, the greater the core diameter becomes, the pore fluid diffusion and thermal diffusion out of the core slows down. This causes the core to have greater pore pressures and induced thermoporoelastic stresses when it reaches the surface.

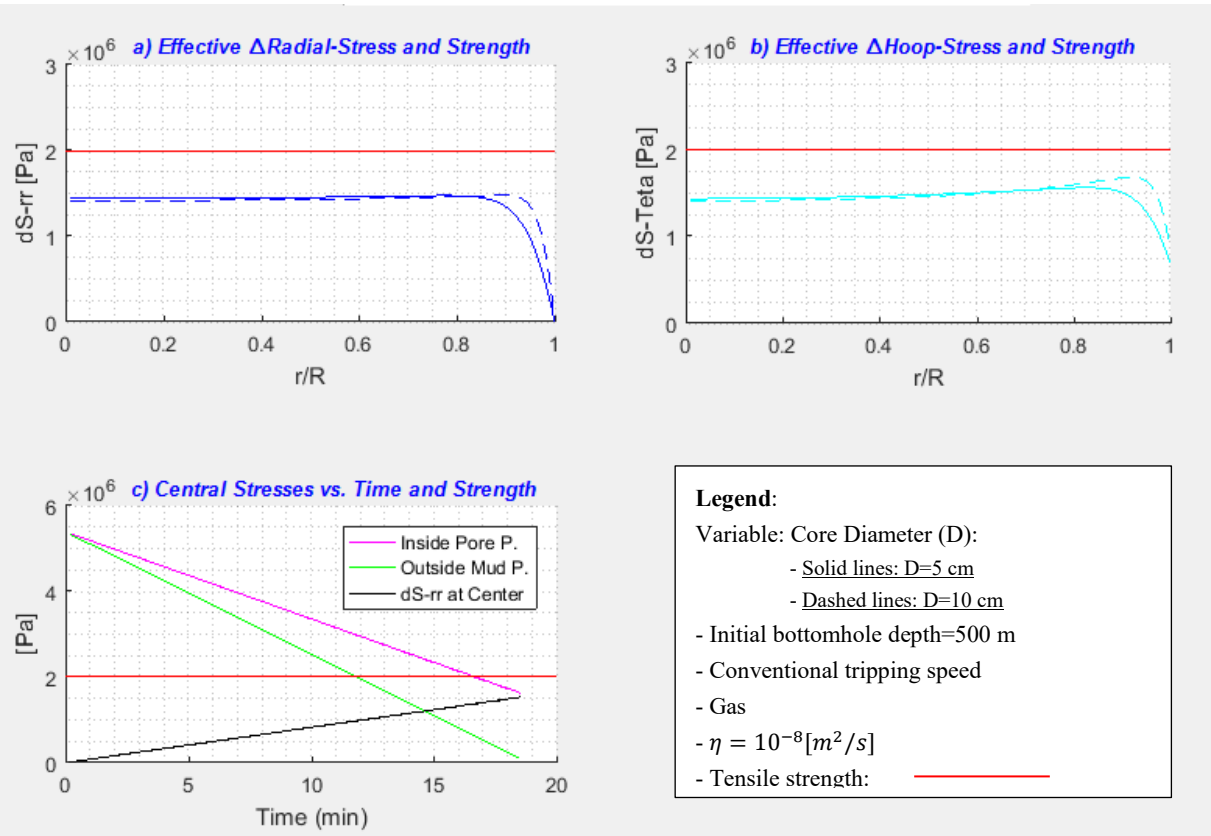

Figure 6-5: The Effect of Core Diameter on Induced Thermoporoelastic Stresses and Failure– Initial Bottomhole Depth of 500 m

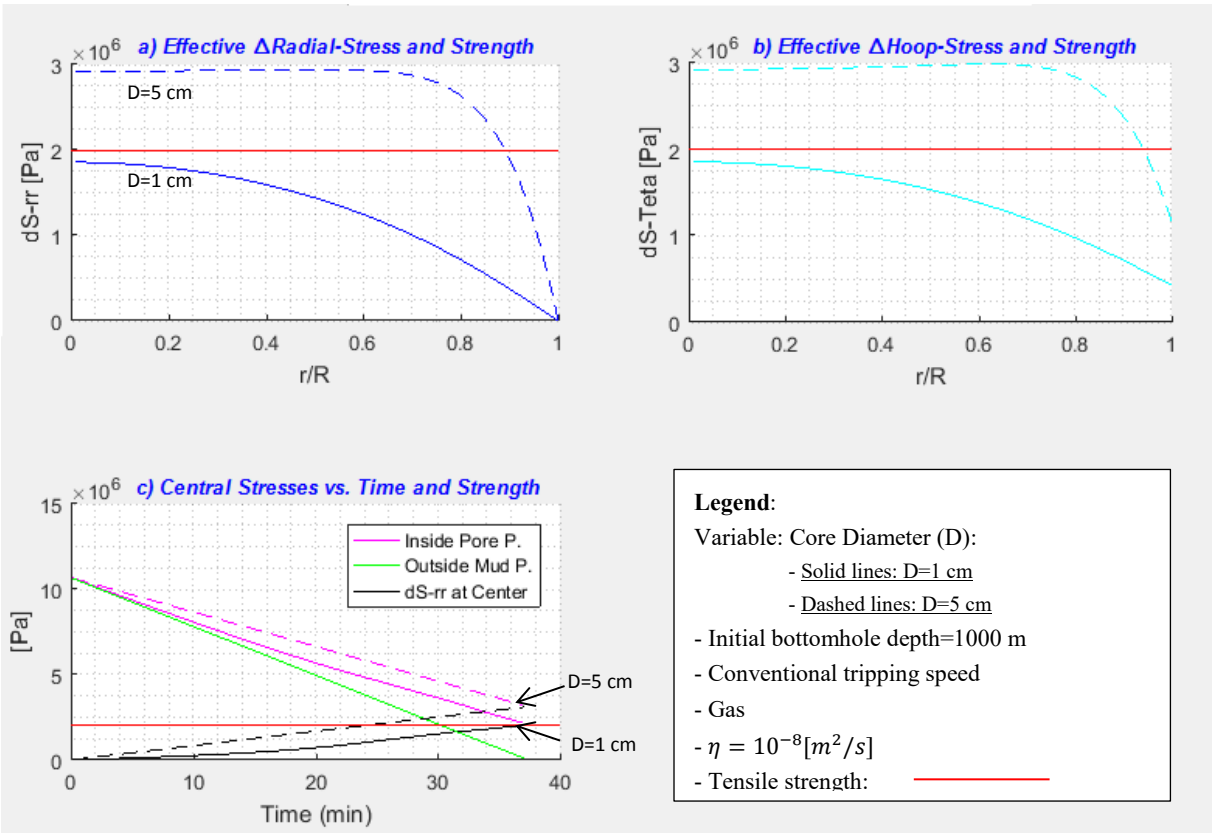

Figure 6-6: The Effect of Core Diameter on the Induced Stresses and Failure–Initial Bottomhole Depth of 1000 m. It is Noted that a 1-cm Core Diameter is Unrealistic in Bottom-Coring Operations

6.4.4 Poisson's Ratio

Poisson's ratio (ν) is one of the parameters that generally affect the hydraulically and thermally induced pore pressure and stresses. Two values of 0.2 and 0.3 are considered for the Poisson's ratio ν of the considered core sample, located at 500 m. As shown in **Figure 6-7**, the sample with $\nu = 0.2$ shows to experience significantly greater induced stresses rather than the sample with $\nu = 0.3$ ($\approx 1.8\ times$) such that it undergoes failure and microfractures.

To interpret the results, it must be known that the lower the Poisson's ratio becomes, the less is the ratio of the axial strain compared with the lateral strain. This means that the core becomes less flexible and thus greater induced stresses would be induced in the core (inferred from *Fjaer et al., 2008; Zoback, 2010; Kovacik, 2005*). In low-permeability or tight rocks, the reduction of Poisson's ratio causes a considerable increase in the induced stresses. In high-permeability rocks, the Poisson's ratio has negligible effect on the induced stresses. Because of the significant effect of ν on the induced stresses and possible failure, it is one significant

parameter factor for tight cores. Therefore, instead of using rules of thumb[1] (Zoback, 2010; *Kovacik, 2005*), it seems necessary either to measure or estimate it using dipole sonic well logs.

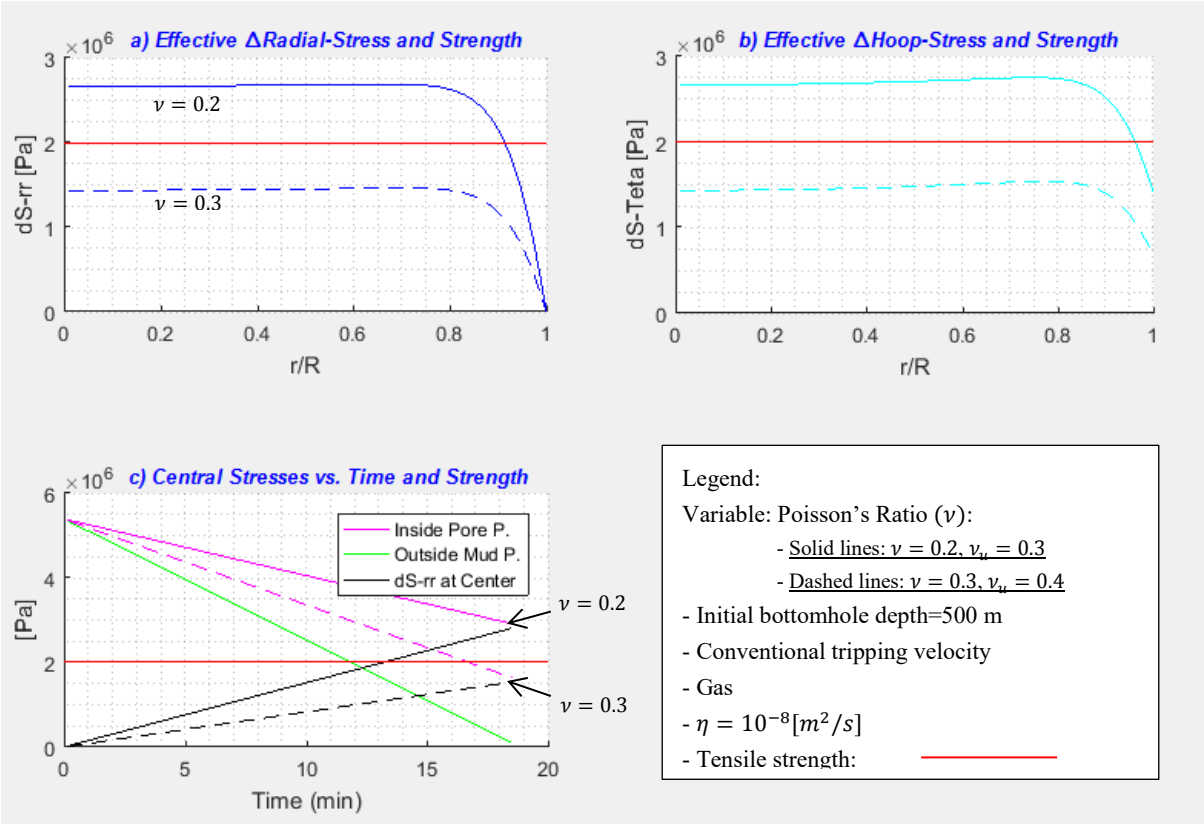

Figure 6-7: The Effect of Poisson's Ratio (ν) on the Induced Thermoporoelastic Stresses and Failure

[1] Rules of thumb consider that the Poisson's ratio ranges from 0.15-0.4, and that it increases with porosity.

6.5 Hydraulic Parameters

Hydraulic parameters affect only the hydraulically induced pore pressure and stresses. The hydraulically induced pore pressure and stresses were discussed in section **5.4.2-BVP I&II**. The corresponding equations were given in **Table 5-1** to **Table 5-3**. Searching in these equations for hydraulic parameters gives: the hydraulic diffusivity coefficient, mud properties (mud weight and mud cake fraction of pressure drop), and the Biot's coefficient.

6.5.1 Hydraulic Diffusivity Coefficient

The hydraulic diffusivity coefficient (η) is one of the hydraulic parameters. After considering the considered core sample properties as in **Table 6-1**, several values of the diffusivity coefficient ranging from 10^{-8} to $5 \times 10^{-6}\ m^2/s$, are considered with the initial bottomhole depth of 4000 m; the tripping speed is considered that of the wireline.

As shown in **Figure 6-8**, the induced stresses within the sample increase with decreasing η. For all the η values, except for $5 \times 10^{-6}\ m^2/s$, the induced stresses exceed the tensile strength and failure occurs. To account for this result, first it must be noted that the diffusivity coefficient is in turn, a function of permeability K, porosity $\emptyset$, viscosity μ, and total compressibility C_t (***Eq. 3-16***). As in this investigation the fluid properties of the core sample are unchanged (gas), larger values of η correspond to larger values of K. As a result, core samples with larger values of η provide higher rates of fluid diffusion out of the core. This contributes to the release of the induced pore pressure and lower induced stresses within the sample. This is the reason that in the sample with $\eta = 5 \times 10^{-6}\ m^2/s$, the smallest induced stress of maximum 0.12 Mpa has been induced. Therefore, samples with this value of η and higher can be safely tripped with maximum speed, even with low tensile strength as low as 0.15 Mpa.

As another investigation of the diffusivity coefficient, three samples are considered: 1) one sample contains gas and 2) the second one contains water (the rest of properties as in **Table 6-1**), 3) the third sample contains gas, but with $\eta = 10^{-6}\ m^2/s$ (at surface conditions). Their induced stresses and failure during tripping is investigated using the thermoporoelastic model as shown in **Figure 6-9**. The results show that the induced-stresses in the gas-bearing sample with $\eta = 10^{-8}\ m^2/s$, are (at minimum) 2.25 times those of the water-bearing one. In

addition, even in the gas-bearing sample with $\eta = 10^{-6}\ m^2/s$, the induced-stresses show to be greater than those of the water-bearing one.

To account for the above results, first the fluid changes from bottomhole to the surface should be investigated. For gas as a compressible fluid, during tripping from the bottomhole to the surface, the value of η is not constant. Rather, during tripping to the surface, C_g increases due to the pressure and temperature drop. This in turn, makes C_t increase which causes η to decrease during tripping. This signifies that the value of η of the gas-bearing sample reaches its minimum at the surface. Therefore, the fluid diffusion out of a gas-bearing sample is greater in its bottomhole than the surface. However, when the sample contains water as a rather incompressible fluid, η is constant from the bottomhole to the surface.

Second, to compare the first two samples, using the values given in **Table 6-1** for isothermal compressibility and viscosity shows that $\mu_g C_{t,g} \approx 100\mu_w C_{t,w}$ at surface conditions. Therefore, the value η for the gas-bearing core is at least 100 times that of the gas-bearing one at the surface (i.e., the value η of water-bearing core is $10^{-6}\ m^2/s$). Therefore, the diffusion out of the gas-bearing sample-1 is slower than the water-bearing sample-2, particularly near the surface. This is the reason why greater stresses are induced within gas-bearing cores. To compare the second and the third sample, the value of η for the water bearing sample is equal to $10^{-6}\ m^2/s$ during all its tripping time. Whereas, for the gas bearing sample it is greater than $10^{-6}\ m^2/s$, except at the surface where it reaches this value. That is the reason that the induced stresses in the water bearing sample-3 is lower than those of the gas-bearing sample-2.

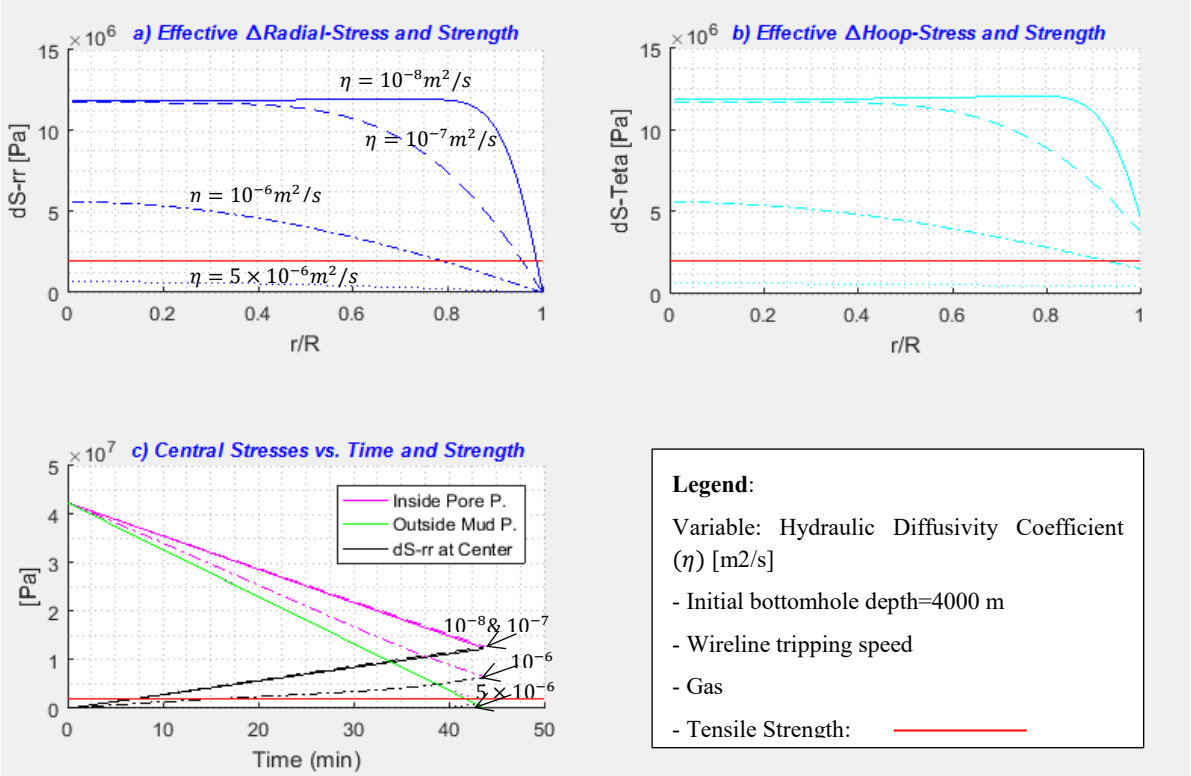

Figure 6-8: The Effect of the Hydraulic Diffusivity Coefficient (η) on the Induced Thermoporoelastic Stresses and Failure

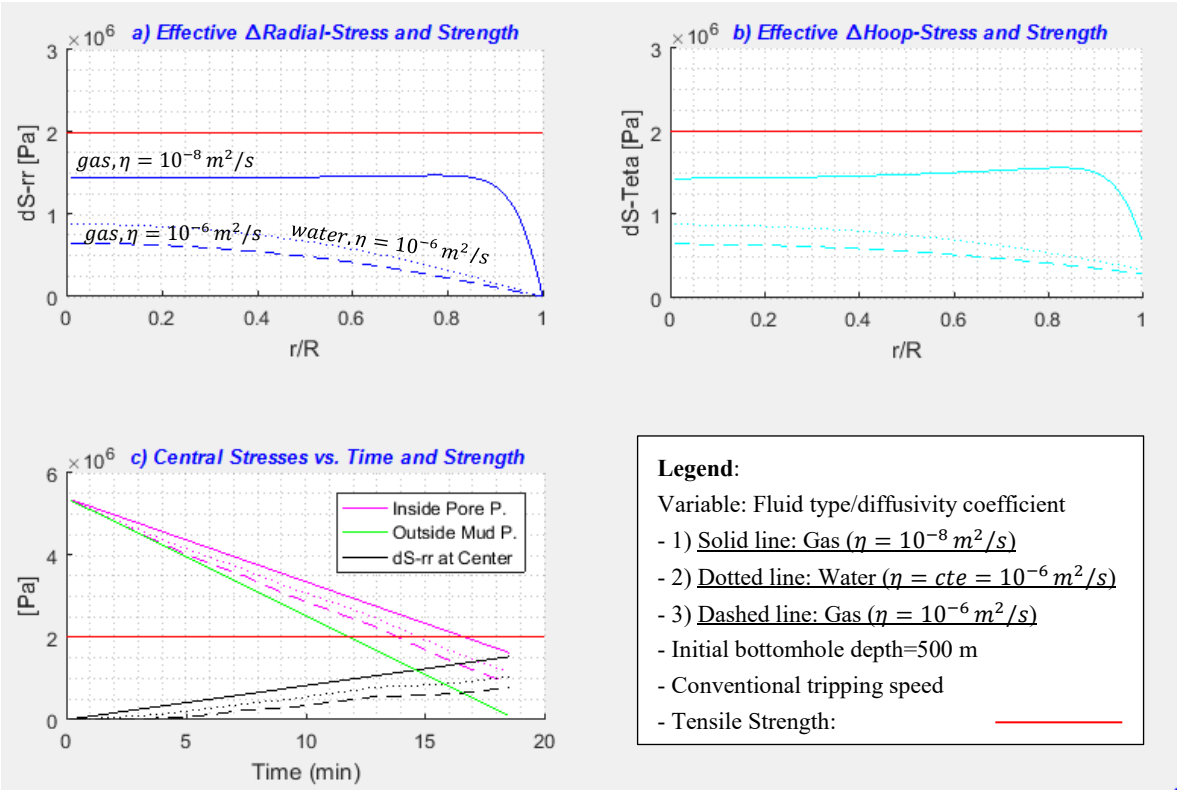

Figure 6-9: The Effect of the Fluid Type/Hydraulic Diffusivity Coefficient (η) on the Induced Thermoporoelastic Stresses and Failure

6.5.2 Mud Properties

The two mud properties affecting the hydraulically induced pore pressure and stresses are the mud weight and the mud cake pressure drop fraction.

Mud Weight

To investigate the effect of mud weight, two weight values of *9 ppg* (1078 kg/m^3) and *12.5 ppg* (1498 kg/m^3) are considered with the assumed core sample, located at 500 m. As shown in **Figure 6-10**, the sample experiences greater induced stresses with the heavier mud, around 1.3 times those of the lighter one. This causes the sample failure and the creation of microfracture within it. This is because the bottomhole hydrostatic mud pressure is directly proportional to the mud weight. Therefore, the higher the mud weight is, the greater is the initial confining pressure and the pore pressure that must be depleted during the core trip. This causes greater induced stresses for the case with the heavier mud weight.

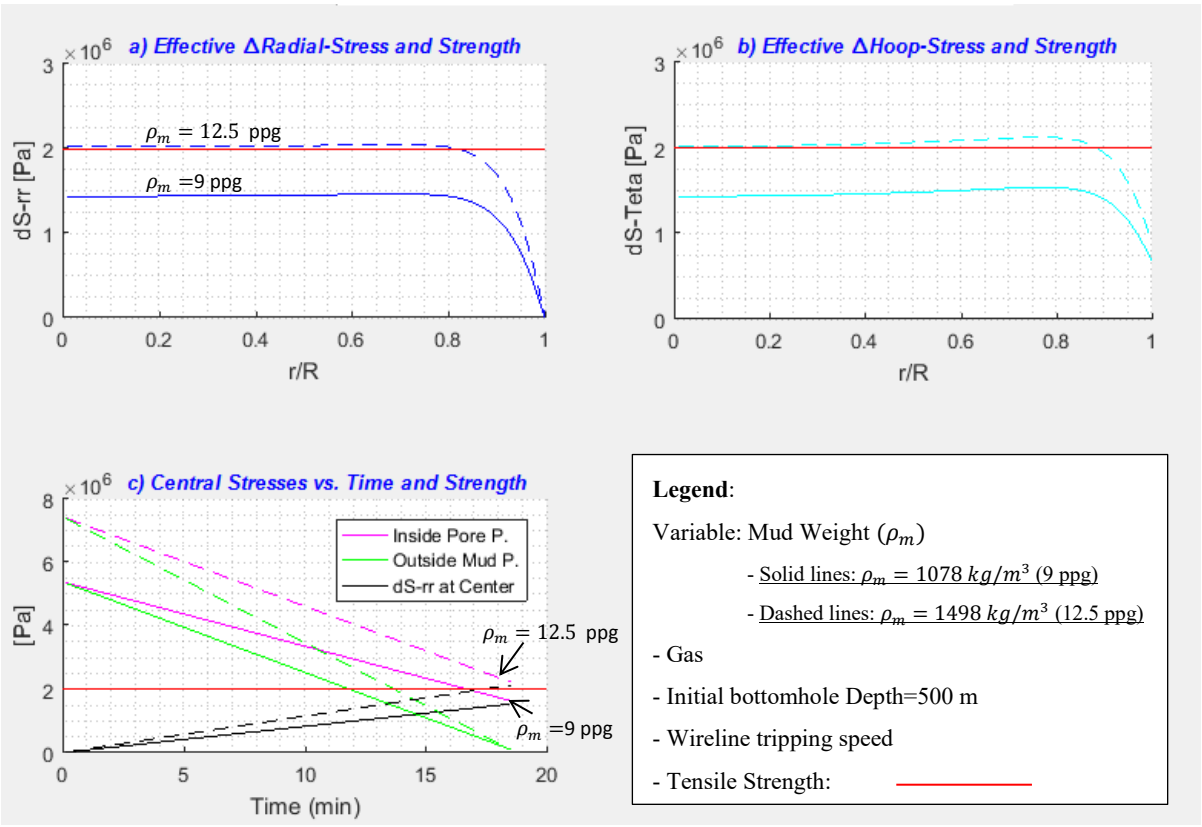

Figure 6-10: The Effect of Mud Weight (ρ_m) on the Induced Thermoporoelastic Stresses and Failure

Mud Cake Pressure Drop

Using water-based muds, the mud cake forms around the core sample and causes a pressure drop around the sample. In this work, its corresponding pressure drop ratio (f_{mc}) is considered as a fraction of the total pressure drop. This parameter is also one parameter affecting the hydraulically induced stresses during tripping.

To investigate the parameter effect, two different mud cake pressure drop values of $f_{mc} = 0$ (i.e. no mud cake) and $f_{mc} = 8\%$ are considered for the assumed core sample, located at 500 m. As shown in **Figure 6-11**, with $f_{mc} = 8\%$, the sample experiences severe induced stresses (≈37% increase) such that they exceed the strength. This means that the sample would undergo failure. This result is reasonable as the mud cake basically prevents dissipation of the fluid out of the sample. Therefore, it prevents the pore pressure release and thus causes increase in induced stresses within the sample (refer to **Table 5-2** and **Table 5-3**).

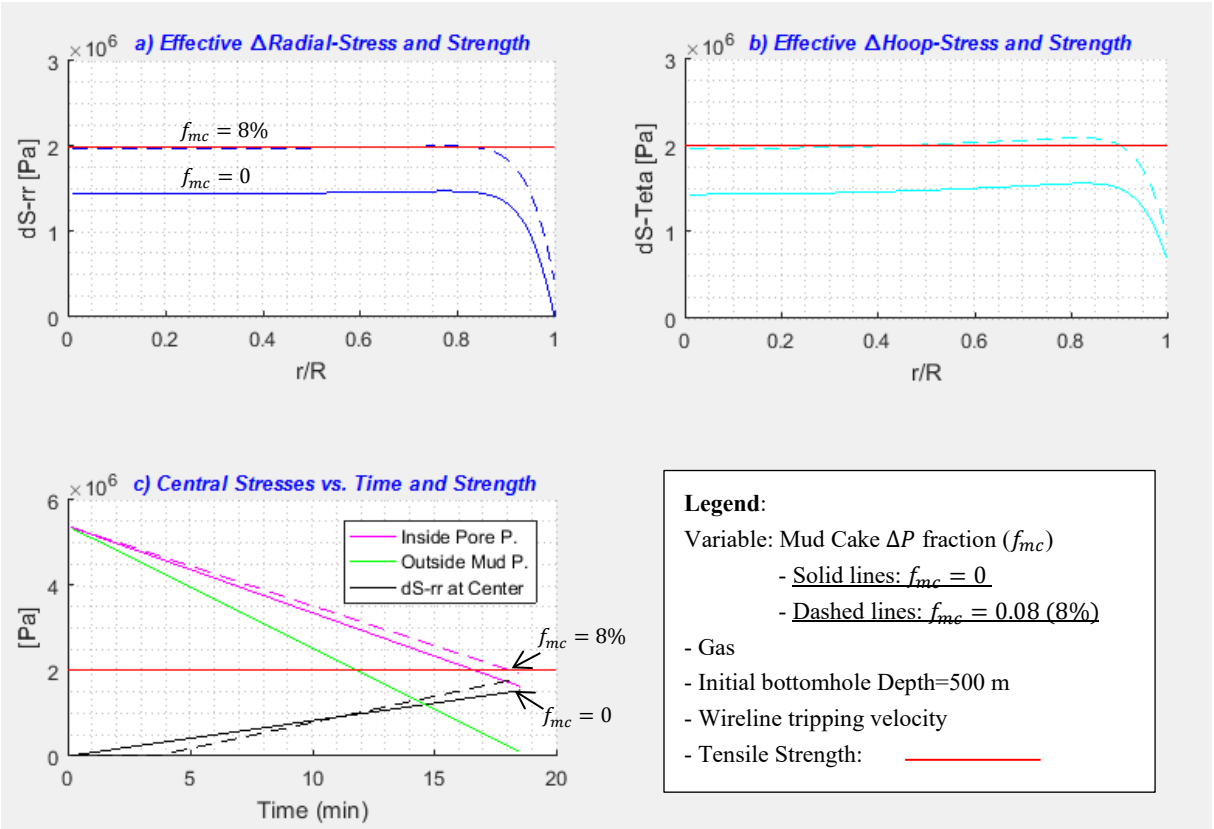

Figure 6-11: The Effect of Mud Cake ΔP% (f_{mc}) on the Induced Stresses and Failure

6.5.3 Biot's Coefficient

The Biot's coefficient (a) is also one of the parameters affecting the induced pore pressures and hydraulic stresses. Two values of 0.7 and 0.8 are considered for the Biot's coefficient a of the considered core sample (**Table 6-1**), located at 500 m. As shown in **Figure 6-12**, significantly greater stresses are induced with the larger a, i.e., around 1.4 times those with the smaller one. This causes the sample to undergo failure with $a = 0.8$. To account for this result, first it must be noted that the value of a depends on porosity and the difference between the bulk modulus (K_b) and the rock matrix modulus (K_r), as given by (*Geertsma, 1973)*:

$$a = 1 - (1 - \varphi)\frac{K_b}{K_r} \qquad \textit{Eq. 6-1}$$

A higher value of a means either greater difference between the moduli or a greater porosity. If the porosity is assumed fixed, the greater the difference between the bulk and the rock matrix means more interconnected pores (*Zobach, 2010*[1]*; Fjaer, 2008*). This means higher permeability. However, if we assume both porosity and permeability are fixed, a greater value of a indicates more captured pores within the sample. This causes greater captured pore pressure and induced stresses within the sample.

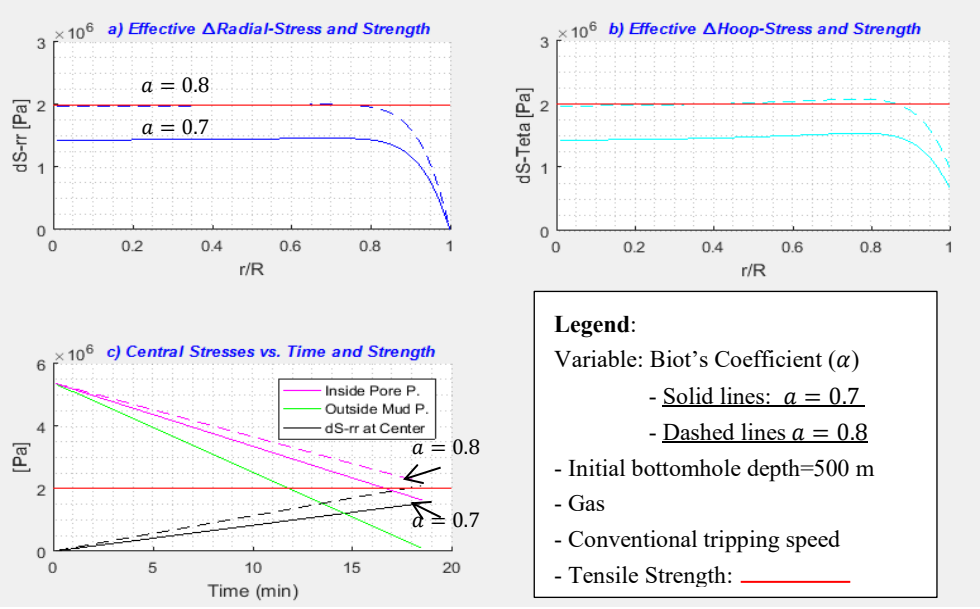

Figure 6-12: The Effect of Biot's Coefficient (a) on the Induced Thermoporoelastic Stresses and Failure

[1] As a rule of thumb, the Biot's coefficient for shales, carbonates, and sandstones can be 0.7, 0.7, and 0.9.

6.6 Thermal Parameters

The thermal effect was discussed in section **5.4.2-BVP III**. It was mentioned that the thermal stresses manifest itself as compressive stresses in the inner part and expansive stresses in the outer part of the sample. The corresponding equations for this effect have been given in **Table 5-1** to **Table 5-3**. Searching in these equations for thermal parameters gives: thermal expansion coefficient, thermal diffusivity, geothermal gradient, and Young's modulus.

6.6.1 Thermal Expansion Coefficient

The thermal expansion coefficient (α_m) is a parameter contributing to the thermally induced stresses. Two values of 10^{-5} and $5 \times 10^{-5} \frac{1}{°C}$ are considered for this coefficient of the considered core sample (**Table 6-1**), located at 500 m. As shown in **Figure 6-13**, with the larger α_m, the sample experiences lower induced stresses in the inner part (≈12% decrease) and higher ones in the outer part (≈18% reduction). To account for this result, first it must be noted that the greater the value of α_m is, the greater expansion and contraction occurs in the sample. Therefore, the thermally induced stresses increase with increasing α_m (refer to ***Eq. 3-6***). The thermal stresses act contractive in the inner part and expansive in the outer part (due to heat transfer from the center to the boundary). Therefore, the overall induced stress would decrease in the center and increase near the boundary.

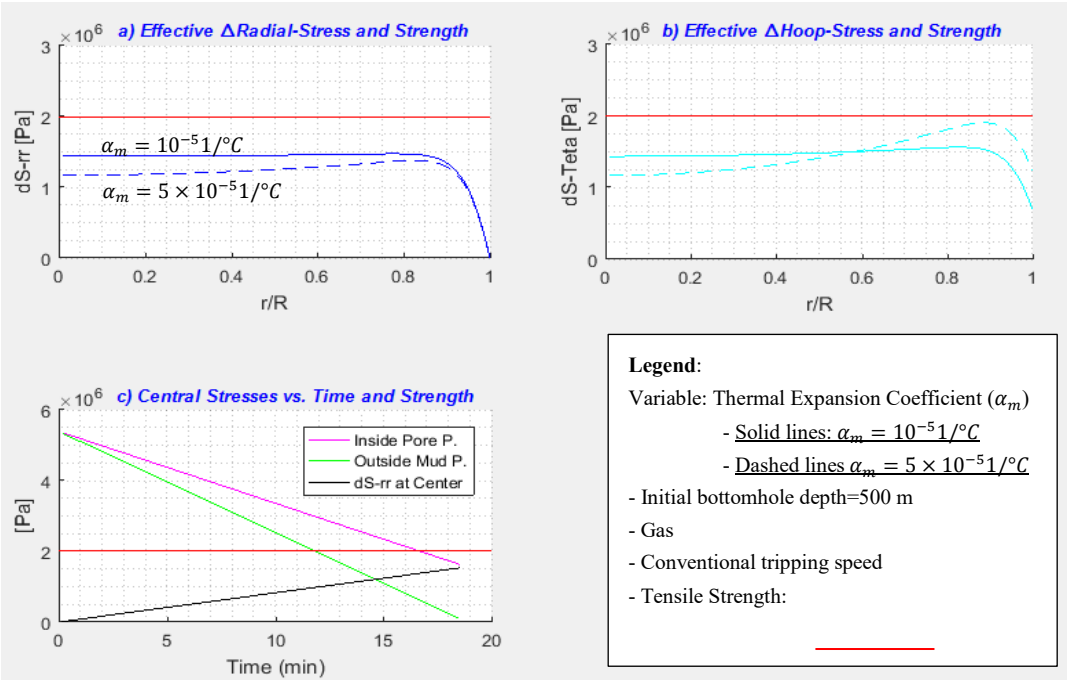

Figure 6-13: The Effect of Thermal Expansion Coefficient (α_m) on the Induced Stresses and Failure

6.6.2 Thermal Diffusivity Coefficient

Thermal diffusivity coefficient (η_T) is also one of the thermal parameters. Two values of 8×10^{-8} and $8 \times 10^{-7}\ \frac{1}{^\circ C}$ are considered for this coefficient of the considered core sample (**Table 6-1**), located at 500 m. As shown in **Figure 6-14**, with the lower η_T, the sample experiences a little greater thermally induced stresses. To account for this result, it must be mentioned that following relation for this coefficient:

$$\eta_T = \frac{\lambda_T}{\rho C_p} \qquad \textit{Eq. 6-2}$$

Where η_T is the thermal diffusivity coefficient $[m^2/s]$, $\boldsymbol{\lambda_T}$ is the thermal conductivity $[W/m/^\circ C]$, ρ is the density $[Kg/m^3]$; and C_p is the heat specific capacity $[J/Kg/^\circ C]$.

Therefore, with constant ρ and C_p, an decrease in η_T indicates smaller K_T. Therefore, the heat conduction from inside the sample to its outside would occur more slowly. Thus, the temperature difference would stay longer and would evade more slowly. This increases the thermal stresses. As the effect of thermal stresses are less significant than hydraulic, the effect of a decrease in $\boldsymbol{\eta_T}$ on the induced stresses is greatly smaller than that of $\boldsymbol{\eta}$.

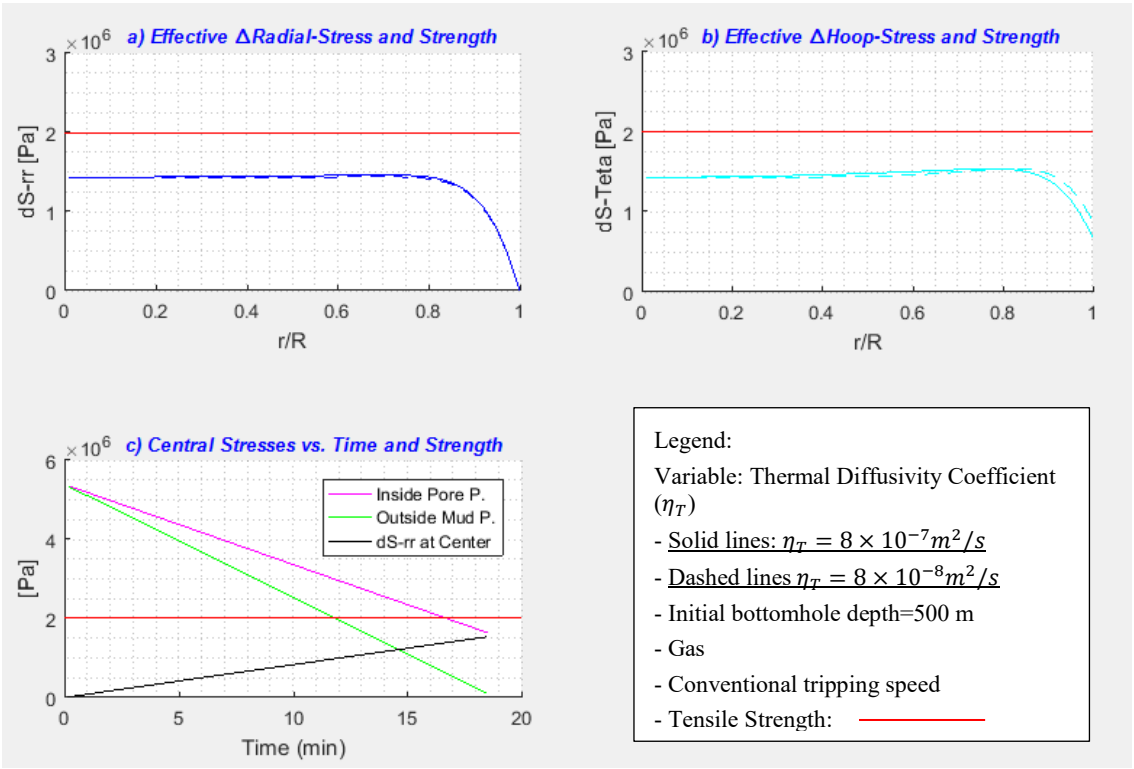

Figure 6-14: The Effect of Thermal Diffusivity Coefficient (η_T) on the Induced Thermoporoelastic Stresses and Failure

6.6.3 Geothermal Gradient

Geothermal gradient [$^{\circ}C/km$] is also one of the thermal parameters. Two values of 25 $^{\circ}C/km$ and 50 $^{\circ}C/km$ are considered with the considered core sample (**Table 6-1**), located at 500 m. As shown in **Figure 6-15**, with the higher gradient, the sample experiences a little greater thermal stresses (for ≈5.5%). To account for this result, higher geothermal gradients contribute to higher temperature differences from the bottom to the surface. This causes thus higher thermal stresses to be induced within the sample.

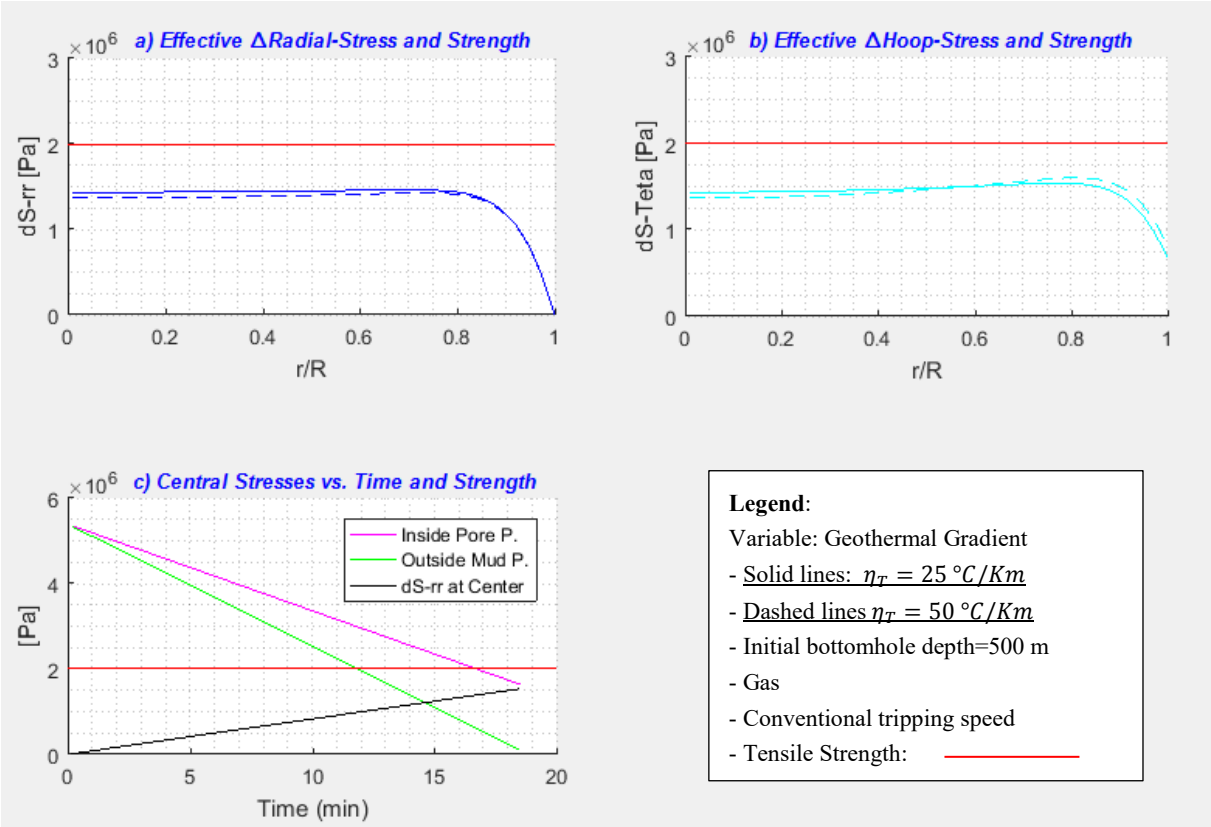

Figure 6-15: The Effect of Geothermal Gradient on the Induced Thermoporoelastic Stresses and Failure

6.6.4 Young's Modulus

Young's modulus (E) is also one of the contributing parameters that affect the thermal stresses. It also affects the tensile strength of the core. Two values of 4.2 Gpa and 11 Gpa are considered for the Young's modulus of the considered core sample (**Table 6-1**), located at 500 m. As shown in **Figure 6-16**, with the greater E, the sample experiences greater thermal stresses (for ≈13%). The tensile strength has shown increase from *2* to *4* Mpa. To account for this result, it should be noted that the thermal stresses are directly proportional to the

isothermal bulk modulus K_T (***Eq. 3-6***). This modulus is, in turn, directly proportional to the Young's modulus. Therefore, the thermal stresses are directly proportional to the E (as seen in **Table 5-2** and **Table 5-3**). Therefore, the increase in E from 4.2 to 11 Gpa makes the thermal stresses 2.6 times.

In addition, depending on the lithology, E, UCS are related (i.e., when E increases, UCS shows increase). UCS is, in turn, related to the tensile strength (i.e., when UCS increases, the tensile strength is increases). These relations have been shown in **Appendix-G**. Therefore, when the value of E is greater, the tensile strength becomes greater.

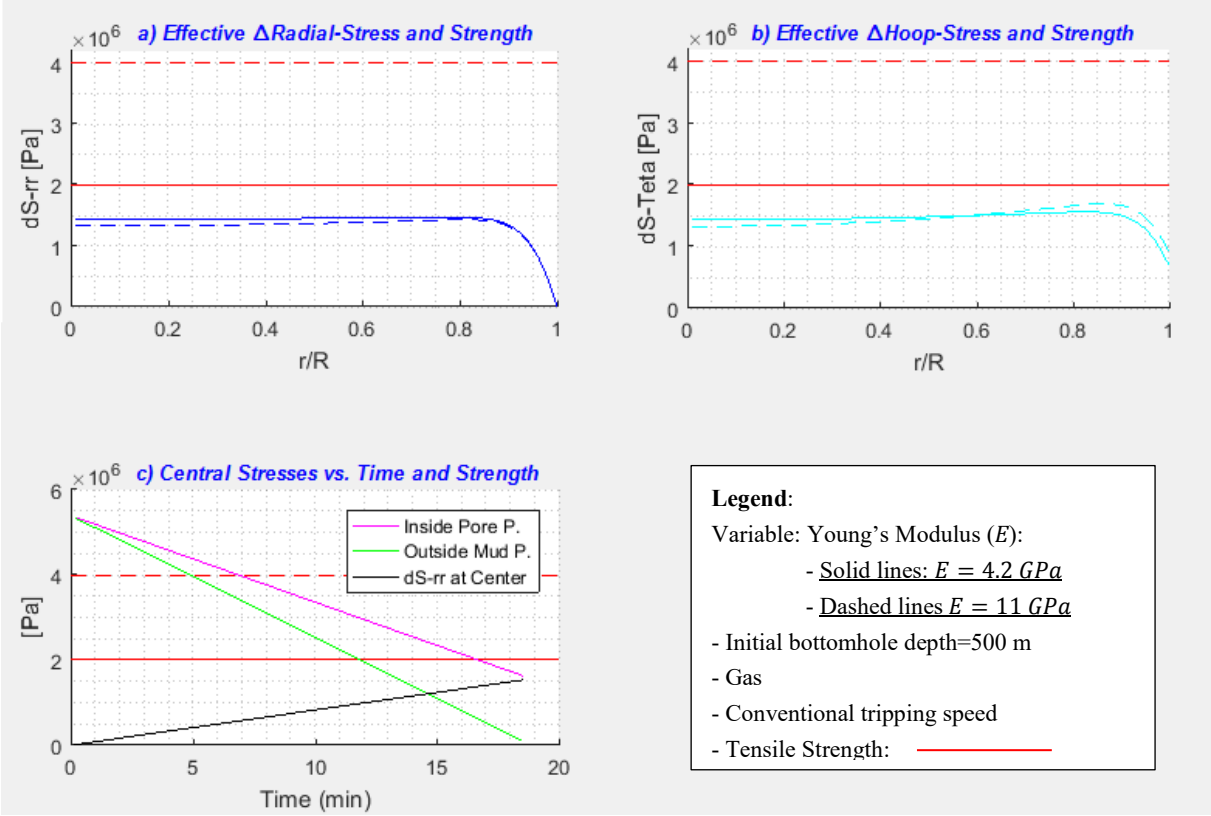

Figure 6-16: The Effect of Young's Modulus on the Induced Thermoporoelastic Stresses and Failure

6.7 Summary of Effects of Contributing Parameters

The summary of the effects of the contributing parameters on the induced hydraulic and thermal stresses (from sections **6.3** to **6.6**) have been listed in **Table 6-2**.

Table 6-2: Brief Summary of the Effects of the Contributing Parameters on the Induced Stresses

Parameter			Effect on Induced Stresses	Effect on Tensile Strength
General	**Initial Bottomhole Depth:**		Significant Increase in hydraulic stresses[1]	–
	Tripping speed:		Increase in hydraulic stresses	–
	Core Diameter:		Increase in hydraulic stresses	–
	Poisson's Ratio:		Significant Decrease in hydraulic stresses	–
Hydraulic	**Hydraulic Diffusivity Coefficient:**		Significant Decrease in hydraulic stresses	–
	Mud	**Weight:**	Significant Increase in hydraulic stresses	–
		Mud cake:		
	Biot's Coefficient:		Significant Increase in hydraulic stresses	–
Thermal	**Thermal Expansion Coefficient:**		Increase in thermal stresses[2]	–
	Thermal Diffusivity Coefficient:		Decrease in thermal stresses	–
	Geothermal Gradient:		Increase in thermal stresses	–
	Young's Modulus:		Significant Increase in thermal stresses	Significant Increase

[1] Hydraulic stresses cause induced stresses throughout the sample.

[2] Thermal stresses show as decrease in the central part and increase in the outer part.

6.8 Lithology

Lithology is not considered a contributing parameter. Instead, it is a qualitative factor that has influence on a number of quantitative contributing parameters already discussed. The lithology affects the hydraulic diffusivity coefficient η as it controls the rock properties, i.e., porosity and permeability. In addition, the lithology has influence on the mechanical properties including Poisson's ratio, Biot's coefficient, and Young's modulus. Some rough estimations of these parameters can be given using the lithology (**Appendix-G**).

Therefore, first, the typical properties of the tight gas-bearing core sample are considered as in **Table 6-1**, this sample can fall into tight shaly sandstone or shale. Next, a permeable sandstone sample is considered with typical properties as: $\emptyset = 30\%$, $K = 100\, mD$, $E = 12.5\, Mpa$, $Tensile\ Strength=3.6\ Mpa$, $\nu = 0.26$, and $\alpha = 0.9$. The thermoporoelastic model is run using the data for the sandstone and shale samples using the conventional and wireline speeds, for two initial bottomhole depths of 500 and 4000 m.

As shown in **Figure 6-17**, the sandstone sample shows to experience negligible induced stresses during its tipping, even using wireline speed and for the 4000 m initial depth. This means that sandstone samples can be generally tripped quickly while being preserved, without any failure. However, the shaly-sand sample undergoes significantly high induced stresses. For the initial depth of 500 m, the maximum induced stress is about 1.5 Mpa, and for the initial depth of 4000 m, the maximum induced stress is about 11.8 Mpa causing failure.

To account for the above results, the shaly-sand sample has the diffusivity of $\eta = 10^{-8}\mathrm{m}^2/\mathrm{s}$ whereas the sandstone sample has $\eta = 10^{-3}\mathrm{m}^2/\mathrm{s}$. Based on the discussion in section **6.5.1**, this signifies that the negligible induced stresses will occur to the sample due to its tripping to the surface. It should be noted that the considered sandstone sample has been generally selected very permeable with high diffusivity. Therefore, depending on the rock and fluid properties, not all sandstones will behave this way.

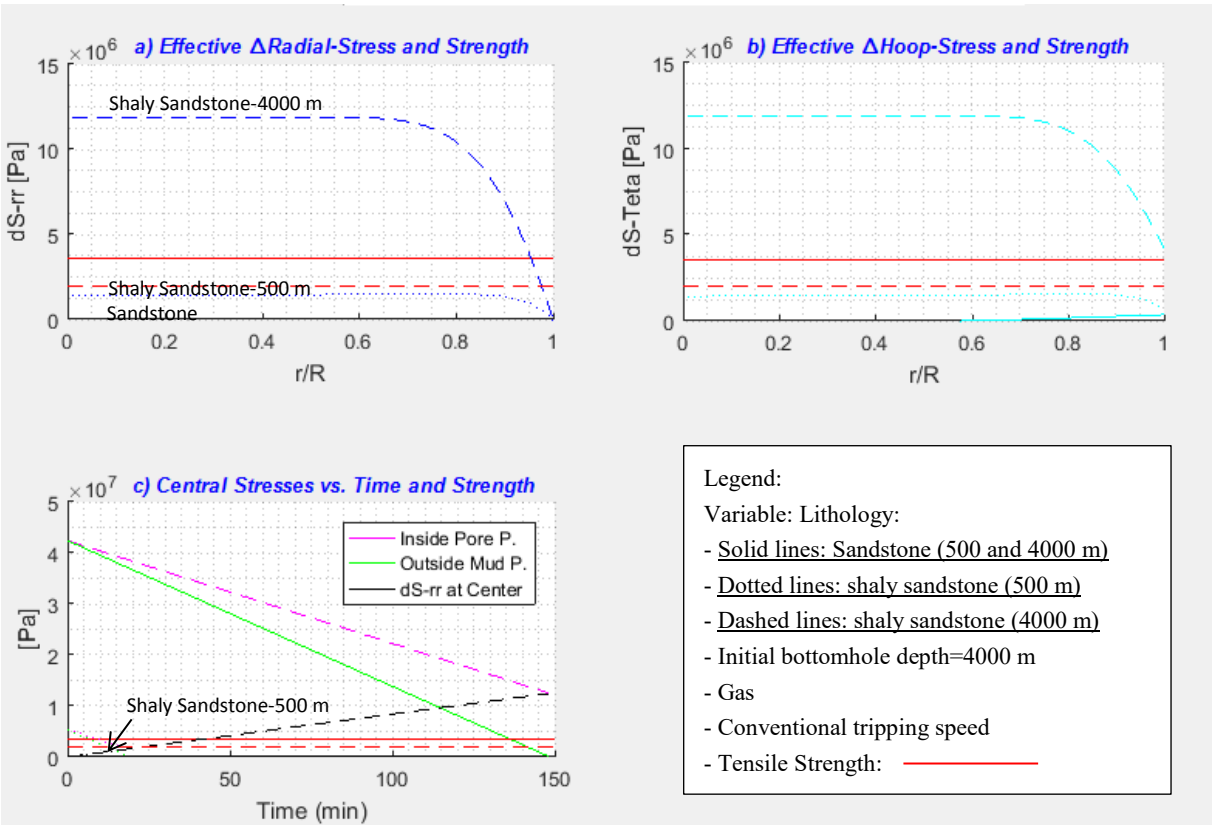

Figure 6-17: The Effect of Lithology on the Induced Thermoporoelastic Stresses and Failure

6.9 Thermal versus Hydraulic

In this section, the extent of thermal contribution to the whole induced stresses is evaluated as it is one of the objectives of this research. To do this, the data in **Table 6-1** is used. The results of this case, given in **Figure 6-18**, show that the thermal effect is only ≈6% of the total. However, as shown in section **6.6**, when both Young's modulus E and the thermal expansion coefficient β are large enough, i.e., $E > 4GPa$ and $\beta > 10^{-5}\frac{1}{^{\circ}C}$., the thermal effect is considered non-negligible.

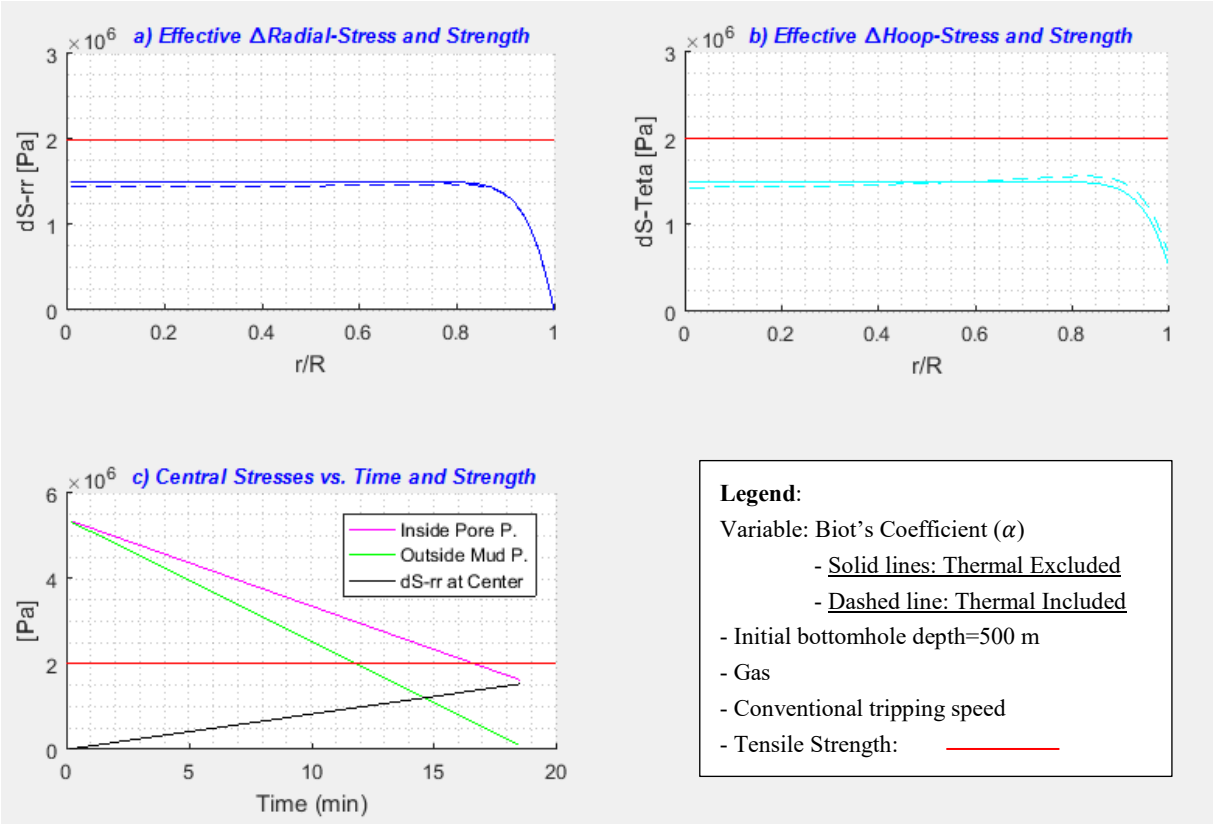

Figure 6-18: Thermal Effect Excluded and Included during Tripping

6.10 Determinative Factors

Based on **sections 6.4** to **6.6** and investigating into the effects of different contributing parameters, it is discovered that the hydraulic diffusivity coefficient η and the initial bottomhole depth have the greatest impact on the thermoporoelastic behavior during tripping. For very tight cores ($\eta < 10^{-8}\frac{m^2}{s}$), also the mechanical properties including Poisson's ratio ν, Biot's coefficient a, and Young's modulus E, have significant effects. Therefore, considering

these parameters, we can explain the sample's overall thermoporoelastic behavior during its tripping.

Based on the significance of the aforementioned mechanical parameters, their exact measurement is favorable and recommended particularly for tight cores. However, to make the model more practical, their rough estimated values can be used, as was the case with this work. This estimation is made using the correlations and estimations for each lithology using **Appendix–G** (as was done in **Table 6-1**). Using this methodology, the hydraulic diffusivity coefficient and the initial bottomhole depth can be used to: 1) determine whether the sample can be safely retrieved, 2) find the optimal tripping rates. For this reason, in this work, they are named *the determinative factors*. Using the results in section **6.5.1** signify that the core samples with $\eta > 5 \times 10^{-6} \frac{m^2}{s}$ can be retrieved with maximum possible tripping rate. However, samples with very low η values ($<10^{-8} \frac{m^2}{s}$) cannot be retrieved in a preserved manner.

Using the determinative factors for running the model, the only required input data would be those for the calculation of the determinative parameters (as seen in **Table 6-3**). Using average specific gravity of gas, its viscosity and the total compressibility can be found. Then, taking the estimated fluid properties, the porosity, and permeability, the hydraulic diffusivity coefficient can be found. Therefore using this coefficient and depth, it can be said if the sample can be safely retrieved. Next, the rest of the contributing parameters are estimated using **Appendix-G**. Then, the thermoporoelastic model can be run. This continues based on section **5.6** until the optimal speed is obtained.

Table 6-3: Practical Input Worksheet of the Core-Trip Schedule for the Developed Model

Trip Schedule Input Worksheet (Gas Reservoirs)			
Well:			
Field:			
Location:			
Date:			
A. Core Rock and Fluid:		**B. Bottomhole Depth and Temperature:**	
1. Core Diameter [in]		1. Depth [m]:	
2. Lithology:		2. Temperature (Average) [˚C]:	
3. ϕ (average) [%]:		**C. Drilling Mud**	
4. K (average) [mD]:		1. MW (ppg):	
5. Gas Specific Gravity:		2. Mud Cake thickness:	

Chapter 7: Summary and Conclusions

Optimized core tripping is essential to retrieve the samples in a preserved and economic manner. Although the drilling KPI for coring shows gradual changing towards measures of the core quality recovered rather than footage drilled, the industry has just sufficed to using only generic methods for core tripping. Recently, some research works in the literature have dealt with this problem. However, there are still some technical gaps including the inappropriate modeling of the thermal effect, mud cake effect, and considering mechanical properties. To fill these gaps, this research presents a state-of-the-art thermoporoelastic modeling approach to optimize the core tripping. This work consists of 1) providing the thermoporoelastic procedure for core tripping, 2) the derivation of the equations for the induced effective-stresses within the core sample due to the confining pressure drop, pore pressure drop, and temperature drop, 3) evaluation of induced effective stresses and comparing them with the failure criterion, 4) repeating this for different economic tripping rates, and 5) selecting the optimal rate. Using this approach, the following conclusions have been drawn:

- ✓ The development and application of the thermoporoelastic approach and model for core tripping optimization has been a state-of-the-art concept. Nevertheless, it has shown to be capable of evaluating the induced pore pressure and stresses within the core during its tripping, identifying whether failure occurs, and finding the optimal core tripping rates. The modeling procedure has considered almost all the effects involved including the thermal, mechanical and mud cake effects, which were neglected in the literature. Therefore, the resultant thermoporoelastic model is comprehensive enough. In addition, this model is also practical enough as it requires the minimum input data, then the rest of the required inputs can be estimated (in case not measured). This model has also shown

rather comparable results with a recent model in the literature, developed using *Fluent software* (*Zubizarreta et al., 2013*).

- ✓ The results signify, particularly for tight cores, that the Poisson's ratio ν, Biot's coefficient α, and Young's modulus E significantly affect the sample's thermoporoelastic behavior. Therefore, it is recommended to have them measured or at least carefully estimate them. This contributes to more accurate evaluation of the induced stresses and optimized tripping.
- ✓ The thermal effect has been evaluated about 6% of the overall induced stress. This effect cannot be ignored when both Young's modulus E and the thermal expansion coefficient α_m are large enough, i.e., $E > 4GPa$ and $\alpha_m > 10^{-5}\frac{1}{^\circ C}$.
- ✓ The mud cake pressure drop was considered proportional to the mud hydrostatic pressure drop (as it should be, but was considered a constant value in the literature). Its effect in the induced stresses and failure has been detected significant. Therefore, reducing this effect is recommended e.g. by using polymer muds instead of Bentonite-containing muds.
- ✓ Having considered the effects of the contributing parameters, hydraulic diffusivity coefficient η and the in-situ pressure state have been detected and introduced as the main determinative factors. Using these two factors, an engineered guideline has been presented for proper candidate selection for coring methods, as has been one main objective of this research.
- ✓ Therefore, the results show that the core samples with $\eta > 5 \times 10^{-6}\frac{m^2}{s}$, which typically fall into sandstones, can be retrieved with maximum possible tripping rate. This determines a proper core candidate selection for the application of wireline continuous coring. However, very tight samples with very low η values ($<10^{-8}\frac{m^2}{s}$) cannot be retrieved in a preserved manner unless 1) their initial bottomhole depth is lower than $500\ m$ and 2) the sample has rather considerable strength ($Tensile\ strength>2Mpa$). This constitutes a proper criterion for selecting pressure coring for such tight samples which fall into shaly sandstones or shales. This, in turn, shows that this notion of the industry, 'using the conventional tripping speed enables very tight cores to be retrieved preserved', does not apply, except for shallow depths.

Chapter 8: Future Work

The development of the state-of-the-art concept of thermoporoelastic approach for core tripping has presented a model that comprehensively considered almost all the involved effects. However, to complete the thermoporoelastic model and enhance the results, continued research is still required to consider the swabbing effect. In addition, because of the nature of thermoporoelasticity, the current model is not capable of dynamically modeling the induced stresses; instead, it can just predict the initiation of the microfractures. Therefore, further investigation work shall address methods using a mechanism to predict the microfractures. Such methods can be typically based on Discrete Element Modeling (DEM) in micro-scale.

Further investigation work and laboratory test designs are still required to prove the model. The test set-up should be able to detect the initiation of microfractures and failure within the sample. Finally, field tests would also be required to prove the model.

The procedure used in this current research work to find the optimal tripping speed is iterative. It is based on the calculation of the induced stresses within the sample, comparison with the failure criterion, identifying if the failure occurs with the current speed, repeating the process in an iterative manner until the optimal speed is found. Therefore, the process does not provide us with the ultimate critical tripping speed; therefore, further continued research is required to find a method to evaluate this speed.

Nomenclature

a:	Biot's coefficient
B:	Skempton's coefficient
C_r:	Rock/matrix compressibility [$1/Pa$]
C_g:	Gas compressibility [$1/Pa$]
C_w:	Water compressibility [$1/Pa$]
C_t:	Total compressibility [$1/Pa$]
C_p:	Heat specific capacity [$J/Kg/^{\circ}C$]
c_b:	Specific heat capacity of the bulk material
Cp:	Centipoise (the viscosity unit)
c':	Coupling coefficient between hydraulic and thermal effects
E:	Young's modulus of elasticity [GPa]
f_{mc}:	Mud cake fraction (of outside pressure)
G:	Shear modulus [GPa]
$h_{i,i}$	Heat flux
$\frac{1}{H}$:	*Poroelastic expansion coefficient*
I_0:	Hyperbolic Bessel functions of zero order of the first kind
K:	1) Permeability[mD], 2) Bulk modulus [MPa]
$\frac{1}{K}$:	Drained bulk compressibility [$1/Pa$]
K_u:	Undrained bulk modulus [MPa]

K_{fr}:	Bulk modulus at constant pore pressure [$1/pa$]
K_b:	Bulk modulus at constant confining pressure [$1/pa$]
K_r:	Rock matrix modulus
K_T:	Isothermal bulk modulus [$W/m/℃$]
$\frac{1}{K_t}$:	Thermal Isothermal Compressibility
L^{-1}:	The Laplace inverse operator
	1) Mass
m:	2) Coefficient of internal friction related to the Mohr-Coulomb part of the criterion
$\frac{1}{M}$ or S_ϵ:	Constrained storage coefficient
N:	Total number of thermoporelastic steps from the bottomhole to the surface
P_c:	The confining pressure around the core [Pa]
ΔP_c:	The confining pressure drop at the boundary (tensile: +) [Pa]
$\Delta P_{c,0}$:	The confining pressure drop around the core, for each step [Pa]
$\Delta P_{c,0,total}$:	The total confining pressure drop at the boundary, for each step [Pa]
P_p:	Pore pressure [Pa]
P_0:	Initial pore pressure [Pa]
ΔP_p:	Pore pressure drop [Pa]
ΔP_0:	The pore pressure drop at the boundary, for each step [Pa]
$\Delta P_{0,total}$:	The total pore pressure drop at the boundary, for each step [Pa]
pa:	Pascal
P_{pc}:	Pseudo-critical pressure [psi]
P_{pr}:	Pseudo-reduced pressure [psi]
q_i:	Fluid mass flux [kg/s]

r:	Radius [m]
R	Core radius at the boundary [m]
$\frac{r}{R}$:	Ratio of radius to the core radius
$\frac{1}{R}$ (S_σ):	*Unconstrained/Specific storage coefficient*
s:	The transformed dummy variable in Laplace form instead of t, for time
S_g:	Gas saturation
S_o:	Oil saturation
S_w:	Water saturation
$t=0^+$	All times after t=0 (t>0)
T_s:	Tensile strength of the rock [$^\circ C$]
T:	Temperature [$^\circ C$]
T_0:	The initial temperature [$^\circ C$]
T_∞:	The final temperature or medium mud temperature after each depth step [$^\circ C$] (lower than core temperature)
ΔT_0:	The temperature difference at the boundary, for each step [$^\circ C$]
$\Delta T_{0,total}$:	The total temperature difference at the boundary, for each step [$^\circ C$]
T_{pc}:	Pseudo-critical temperature [$^\circ C$]
T_{pr}:	Pseudo-reduced temperature
U_{rr}:	Radial displacement [mm]
ΔU_{rr}:	Radial displacement [mm]
UCS:	Uniaxial compressive strength [Mpa]
WCC	Wireline Continuous Coring
Z:	Gas compressibility or Z factor

Greek Letters:

σ:	Stress [Pa]
σ_{rr}:	Radial stress [Pa]
$\sigma_{\theta\theta}$:	Hoop stress (absolute) [Pa]
σ_{kk}:	Total stress [Pa]
$\Delta\sigma_{rr}$:	Induced radial Stress (difference) [Pa]
$\Delta\sigma_{\theta\theta}$:	Induced hoop Stress (difference) [Pa]
σ':	Effective stress [Pa]
σ_1':	Effective maximum principal stress [pa]
σ_3':	Effective minimum principal stress [pa]
σ'_{rr}:	Effective radial stress [Pa]
$\sigma'_{\theta\theta}$:	Effective hoop stress [Pa]
$\widetilde{\Delta\sigma}_{(r,s)}^{(hyd.1)}$:	Laplace of (radial or hoop) total induced hydraulic stress due to confining pressure drop (for unloading mode II) **Subscript 1** indicates the confining pressure drop.
$\widetilde{\Delta\sigma}_{(r,s)}^{(hyd.1.1)}$:	Laplace of (radial or hoop) induced hydraulic stress due to confining pressure drop (for unloading mode I) **Subscript 1.1**: 2 indicates due to confining pressure drop, 1: without mud cake
$\widetilde{\Delta\sigma}_{(r,s)}^{(hyd.1.2)}$:	Laplace of (radial or hoop) induced hydraulic stress due to mud cake effect (for unloading mode I: confining pressure drop) **[Subscript 1.2]**: 2 indicates due to confining pressure drop, 1: only for mud cake
$\widetilde{\Delta\sigma}_{(r,s)}^{(hyd.2)}$:	Laplace of (radial or hoop) total induced hydraulic stress due to pore pressure drop (for unloading mode II) **Subscript 2** indicates the pore pressure drop.
$\widetilde{\Delta\sigma}_{(r,s)}^{(hyd.2.1)}$:	Laplace of (radial or hoop) induced hydraulic stress due to pore pressure drop (for unloading mode II)

	Subscript 2.1: 2 indicates due to pore pressure drop, 1: without mud cake
$\widetilde{\Delta\sigma}_{(r,s)}^{(hyd.2.2)}$:	Laplace of (radial or hoop) induced hydraulic stress due to mud cake effect (for unloading mode II: pore pressure drop) **Subscript 2.2**: first 2 indicates due to pore pressure drop, second 2: only for mud cake
$\widetilde{\Delta\sigma}_{(r,s)}^{(thermal.1)}$:	Laplace of (radial or hoop) induced thermal stress (difference)
$\widetilde{\Delta\sigma}_{(r,s)}^{(thermal.2)}$ & $\widetilde{\Delta\sigma}_{(r,s)}^{(thermal.3)}$:	Laplace of (radial or hoop) induced thermal stresses due to the coupling effect of temperature drop
ϵ:	Strain
ϵ_{rr}:	Radial strain
$\epsilon_{\theta\theta}$:	Hoop strain
ϵ_{zz}:	Strain in vertical direction of the core
ϵ_{kk}:	Total strain
ϵ_T:	Thermal strain
ζ:	The increment of water content
$\tilde{\zeta}$:	Laplace form of the increment of water content
S_σ or $\frac{1}{R}$	Unconstrained/Specific storage coefficient
S_ϵ or $\frac{1}{M}$	Constrained storage coefficient
φ:	Porosity
ρ:	Density[$Kg/m3$]
ρ_f:	Fluid density [$Kg/m3$]
ρ_m:	Mud Weight [$Kg/m3$]
μ:	Fluid viscosity [cp]
μ_g:	Gas viscosity [cp]
μ_1:	Liquid viscosity obtained by Standing [cp]

γ_g:	Gas specific gravity
υ:	Poison's ratio
υ_u:	Undrained Poison's ratio
η:	Hydraulic diffusivity coefficient [m^2]
η_T:	Thermal diffusivity coefficient [m^2]
η' & η'_T:	Coupling coefficients for the hydraulic and thermal diffusivities
α_T:	(Linear) thermal expansion coefficient [$1/℃$]
α_m:	(Volumetric) thermal expansion coefficient [$1/℃$]
λ_T:	Thermal conductivity [$W/m/℃$]

Reference

Ahmed, T. & Mckinney, P. (2005) *Advanced Reservoir Engineering*, Elsevier Book Series, Published by Gulf Publishing.

Amyx, J.W., Bass, D.M. Jr., & Whiting, R.L. (1960) *Petroleum Reservoir Engineering*, New York City: McGraw-Hill Book Co.

American Petroleum Institute (1998) *Recommended Practices for Core Analysis, RP 40*.

Arpaci, V.S. (1966) *Conduction Heat Transfer*, Published by Addison Wesley Publishing Company, p.282-283.

Athy, L.F. (1930) *Density, Porosity and Compaction of Sedimentary Rocks*, American Association of petroleum Geologists Bulletin, 14, 1-24.

Baker Hughes (1999) *Coring Handbook, 503-001, Rev. B*, Technical Publication Group.

Baker Hughes Inteq (2012) *Introduction to Coring*, Technical Publication Group.

Baker Hughes Inteq (2013) *Coring Services Guide*, Technical Publication Group.

Bencic, A., Prohaska, M., De Sousa, J.T.V., Millheim, K.K. (1998) *Slimhole Drilling and Coring-A New Approach*, SPE 49261, Presented at SPE Annual Technical Conference and Exhibition, New Orleans, Louisiana, Sep. 27-30.

Berg, R.R. (1970) *Method for Determining Permeability from Reservoir Rock Properties*, Trans., Gulf Coast Association of Geological Societies 20: 303-335.

Biot, M. (1941a) *General Theory of Three Dimensional Consolidation*, Journal of Applied Physics.

Beloey B.A., & Weiner, J.H. (1985) *Theory of Thermal Stresses*, Wiley and Sons.

Bouteca, M.J., Bary, D., Piau, J.M., Kessler, N., Boisson, M., & Fourmaintraux, D. (1994) *Contribution of Poroelasticity to Reservoir Engineering: Lab Experiments, Application to Core Decompression and Implication in HP-HT Reservoirs Depletion*, Presented at the Eurock SPE/ISRM Rock Mechanics Conference.

Byrne, M., Zubizarreta, I., & Sorrentino, Y. (2015) *The Impact of Formation Damage on Core Quality*, SPE 174189-MS, Presented in SPE European Formation Damage Conference and Exhibition, 3-5 June, Budapest, Hungary.

Bjorum; M. (2013) *A New Coring Technology to Quantify Hydrocarbon Content and Saturation*, SPE 167228 MS, Presented at Unconventional Resources Conference, Calgary, Alberta, Canada, November 5-7.

Carman, P.C. (1956) *Flow of Gases through Porous Media*, New York City: Academic Press Inc.

Carslaw, H.S. & Jaeger, J.C. (1959) *Conduction of Heat in Solids*, 2nd edition, Oxford, Clarendon Press.

Chang, C., Zoback, M.D., & Khaksar, A. (2006) *Empirical Relations between Rock Strength and Physical Properties in Sedimentary Rocks*, Published in Journal of Petroleum Science and Engineering 51, 223 – 237.

Chen, G., & Ewy, R.T. (2005) *Thermoporoelastic Effect on Wellbore Stability*, SPE Journal, J. Eng. Material Technology 123(4), 409-416.

Chien, W.Y., Pan, J., & Tang, S.C. (2000) *Modified Anisotropic Gurson Yield Criterion for Porous Ductile Sheet Metals*, J. Eng. Mater. Technology 123(4), 409-416.

Dake, L.P. (1998) *Fundamentals of Reservoir Engineering*, Published by ELSEVIER Science B.V, Edition 17th.

Davis M., Williams, R., Willberg, D., Bjorum, M., Willberg, D.M., Akbarzadeh, K. (2013) *Novel Controlled Pressure Coring and Laboratory Methodologies Enable Quantitative Determination of Resource-in-Place and PVT Behavior of the Duvernay Shale*, SPE 167199, Presented at Unconventional Resources Conference, Calgary, Alberta, Canada, November 5-7.

Deliac, E.P., Messines, J.P., and Thierree, B.A. (1991) *Mining Technique Finds Applications in Oil Exploration*, Published in Oil and Gas Journal, May, 85.

Detournay, E., & Cheng, A. (1993) *Fundamentals of Poroelasticity*, Comprehensive Rock Engineering, Pergamon Press.

Dempsey, J.R. (1965) *Computer Routine Treats Gas as a Variable*, Oil and Gas Journal, p. 141-143.

Eppelbaum, L., Kutasov, I., & Pilchin, A. (2014) *Applied Geothermics*, Published by Springer.

Farese, T., Ahmed, H., Mohanna, A. (2013) *A New Standard in Wireline Coring: Recovering Larger Diameter Wireline Core Through Standard Drill Pipe and Custom Large Bore Jar*, SPE 163507, Presented at SPE/IADC Drilling Conference and Exhibition, Amsterdam, The Netherlands, March 5-7.

Fjaer, E., Holt, R.M., & Horsrud, P. (1992) *Petroleum Related Rock Mechanics*, 2nd edition, p.59.

Geertsma, J. (1973) *A Basic Theory of Subsidence due to Reservoir Compaction: The Homogeneous Case*, Trans. Royal Dutch Society of Geologists and Mining Eng., 28, 43-62.

Gelfgat, M. (1994) *Complete System for Continuous Coring With Retrievable Tools in Deep Water*, SPE 27521 MS, Presented at SPE/IADC Drilling Conference, Dallas, Texas, Feb. 15-18.

Gillian, T.M., & Morgan, I.L. (1987) *Shale: Measurement of Thermal Properties*, by Oak Ridge National Laboratory, p. 30.

Griffith, A.A. (1921) *The Phenomena of Rupture and Flow in Solids*, The Philosophical Transactions of the Royal Society London (Series A), 221 (1921), pp. 163–198.

Harrigan, J.J., Cole, F.W. (2011) *Advances in Engineering and Technology of Oil Well Drilling*, Chapter 16, *Coring*, pages 359-370.

Hettema, M.H.H., Hanssen, T.H., & Jones, B.L. (2002) *Minimizing Coring-Induced Damage in Consolidated Rock*, SPE 78156 MS, Presented at SPE/ISRM Rock Mechanics Conference, Irving, Texas, Oct. 20-23.

Hoeink, T., Van Der Zee, W., & Arndt, S. (2015) *Optimal Core Retrieval Time for Minimizing Core Decompression Damage*, Presented at SPE Pacific Unconventional Resources Conference and Exhibition, 9-11 Nov., Brisbane, Australia.

Holt, R.M. (1994) *Effects of Coring on Petrophysical Measurements*, SCA-9407, SCA International Symposium Proceedings, SPWLA, Chapter-at-Large, p. 77-86.

Huotori, T., & Kukkonen, I. (2004) *Thermal Expansion Properties of Rocks*, Working Report 2004-04, p. 37.

Hyland, C.R. (1983) *Pressure Coring-An Oilfield Tool*, Presented at SPE Annual Technical Conference and Exhibition, San Francisco, SPE 12093, California, US, October 5-8.

Jacquot, R. G., Steadman, J. W. & Rhodine, C. N. (1983) *The Gaver-Stehfest Algorithm for Approximate Inversion of Laplace Transforms*, Circuits Systems Magazine, 5. Pp.4-8.

Jaeger, J.C., Cook, N.G.W., & Zimmerman, R.W. (2007) *Fundamentals of Rock Mechanics*, 4th Edition, P. 221-228.

Kovacik, J. (2005) *Correlation between Poisson's Ratio and Porosity in Porous Materials*, Published by Springer Science.

Kreyszig, E. (2006) *Advanced Engineering Mathematics*, Published by John Wiley and Sons, 9th International Edition.

Kurashige, M. (1989) *A Thermoelastic Theory of Fluid-Filled Porous Materials*, International Journal of Solids Structures, 25, No. 9, 1039.

Lama, R., & Vutukuri, V. (1978) *Handbook on Mechanical Properties of Rock*, Trans Tech Publications.

Li, X., Cui, L., and Roegiers, J.C. (1998) *Thermoporoelastic Modeling of Wellbore Stability in Non-hydrostatic Stress Field*, Journal of Rock Mechanics Science.

Malvern, L.E. (1969) *Introduction to the Mechanics of a Continuous Medium*, Prentice Hall.

Maury, V. & Guenot (1995) *A. Practical Advantages of Mud Cooling Systems for Drilling*, SPE Drillings & Completion, vol. 10, no. 1, pp. 42–48.

McCain, W. (1990) *The Properties of Petroleum Fluids*, 2nd Edition, PennWell Publishing Corp.

McPhee, C., Reed, J., & Zubizarreta, I. (2015) *Core Analysis: A Best Practice Guide*, Published by Elsevier, p.52-57. ISBN: 9780444635334.

Perkins, T.K., and Gonzalez, J.A. (1985) *The Effect of Thermoelastic Stresses on Injection Well Fracturing*, SPE Journal, Sept., p.937-949.

Randolf, S.B., and Jourdan, A.P. (1991) *Slim-hole Continuous Coring and Drilling in Tertiary Sediments*, SPE 21906, Presented at SPE/IADC Drilling Conference, Amsterdam, The Netherlands, March 11-14.

Rzhevsky, V., & Novick, G. (1971) *The Physics of Rocks*, MIR Publ. pp. 320.

Rosen, R., Mickelson, B., Fry, J., Hill, G., Knabe, B., & Sharf-Aldin, M. (2007) *Recent Experience with Unconsolidated Core Analysis*, SCA 2007, 41.

Standing, M.B. (1977) *Volumetric and Phase Behavior of Oil Field Hydrocarbon Systems*, Published by SPE of AIME.

Shinmoto, Y., Miyazaki, E., Wada, K., Yamao, M. (2012) *Development of a Continuous Directional Coring System for Deep-Sea Drilling*, SPE 140913-PA, Published in SPE Journal of Drilling and Completion, March.

Sutton, R.P. (1985) *Compressibility Factors for High-Molecular-Weight Reservoir Gases*, Presented at the SPE Annual Technical Conference and Exhibition, Las Vegas, Nevada, USA, 22-26 September. SPE-14265-MS.

Terzaghi, K. (1925) *Erdbaumechanik auf Bodenphysikalischer Grundlage*, Published by Leipzig u. Wien, F. Deuticke.

Timoshenko, S. (1934) *Theory of Elasticity*, Published by McGraw-Hill Book Company.

Von Mises, R. (1913) *Mechanik der festen Körper im plastisch deformablen Zustand,* Nachr Math. Phys., vol. 1, pp. 582–592.

Wang, H. (2000) *Theory of Linear Poroelasticity with Applications to Geomechanics and Hydrogeology*, Princeton University Press.

Walker, S.H., and Millheim, K.K. (1990) *An Innovative Approach to Exploration Exploitation Drilling: The Slim-Hole High-Speed Drilling System*, Published in JPT, Sep., 1184, Trans., AIME, 289.

Warren, T., Powers, J., Bode, D., Carre, E., Smith, L. (1998) *Development of a Commercial Wireline Retrievable Coring System*, Published in SPE Reservoir Evaluation and Engineering, Dec.

Worthington, A.E., Gidman, J., & Newman, G.H. (1987) *Reservoir Petrophysics of Poorly Consolidated Rocks. I. Well Site Procedures and Laboratory Methods*, SCA 8704.

Zoback, M. (2010) *Reservoir Geomechanics*, Cambridge University Press.

Zubizarreta, I., Byrne, M., Sorrentino, Y., & Rojas, E. (2013) *Pore Pressure Evolution, Core Damage and Tripping Out Schedules: A Computational Fluid Dynamics Approach*, SPE-163527-MS, SPE/IADC Drilling Conference, 5-7 March, Amsterdam, The Netherlands.

Appendix

Appendix A:

Relationships between Poroelastic Coefficients (*Wang, 2000*)

$$\eta = \frac{a(1-2\upsilon)}{2(1-\upsilon)} \qquad \textit{Eq. A-1}$$

$$\gamma = \frac{B(1+\nu_u)}{3(1-\nu_u)} = \frac{\eta}{GS} \qquad \textit{Eq. A-2}$$

$$B = \frac{3(\nu_u-\nu)}{a(1-2\nu)(1+\nu_u)} = \frac{3(\nu_u-\nu)}{2\eta(1-\upsilon)(1+\nu_u)} \qquad \textit{Eq. A-3}$$

$$M = \frac{BK_u}{a} = \frac{2G(\nu_u-\nu)}{a^2(1-2\nu_u)(1-2\nu)} \qquad \textit{Eq. A-4}$$

$$S = \frac{(1-\nu_u)(1-2\nu)}{M(1-\nu)(1-2\nu_u)} \qquad \textit{Eq. A-5}$$

$$S_\sigma = \frac{1}{R} = \frac{a}{KB} \qquad \textit{Eq. A-6}$$

$$S_\epsilon = \frac{1}{M} = \frac{a}{K_u B} \qquad \textit{Eq. A-7}$$

Appendix B:

Gaver-Stehfest Algorithm for Inversion of Laplace Transforms

Stehfest provided an algorithm to numerically invert Laplace transforms *F* from *P* as follows (*Jacquot et al., 1983*):

$$F = \frac{ln(2)}{t}\sum_{i=1}^{N} V_i P(\frac{ln(2)}{t} i)$$

Where V_i is found as*:*

$$V_i = (-1)^{(\frac{N}{2}+i)} \sum_{k=\lfloor\frac{i+1}{2}\rfloor}^{min(i,\frac{N}{2})} \frac{K^{\frac{N}{2}}(2k)!}{\left(\frac{N}{2}-k!\right)k!\,(k-1)!\,(i-k)!\,(2k-i)!}$$

Where N is an even integer, e.g., 8, 10, 12, so on.

Appendix C:

Tensile Stresses Induced in a Solid Elastic Cylinder

In the following, using mechanics of solid elastic cylinders, the induced stress propagation throughout the sample is investigated. This approach cannot be used for porous cylinders. As a solid mechanics work, *Jaeger et al. (2007, p. 225-228)* have investigated the compression over two symmetrical arcs of a cylindrical solid (**Figure-C, below**) to reach the stress distribution throughout the solid cylinder. Assuming that the tensile stress ΔT_0 is applied instead of compression, we have:

$$\sigma_{rr} = \frac{2\Delta T_0}{\pi}\left\{\frac{(1-\left(\frac{r}{R}\right)^2 sin(2\theta_0)}{1-2\left(\frac{r}{R}\right)^2 cos(2\theta_0)+\left(\frac{r}{R}\right)^4} + Arctan\left[\frac{1+\left(\frac{r}{R}\right)^2}{1-\left(\frac{r}{R}\right)^2}tan(\theta_0)\right]\right\} \qquad \textit{Eq. C-1}$$

$$\sigma_{\theta\theta} = \frac{2\Delta T_0}{\pi}\left\{-\frac{(1-\left(\frac{r}{R}\right)^2 sin(2\theta_0))}{1-2\left(\frac{r}{R}\right)^2 cos(2\theta_0)+\left(\frac{r}{R}\right)^4} + Arctan\left[\frac{1+\left(\frac{r}{R}\right)^2}{1-\left(\frac{r}{R}\right)^2}tan(\theta_0)\right]\right\} \qquad \textit{Eq. C-2}$$

In order to translate the Jaeger's method for the decompression of imaginary solid elastic samples, the tensile stress ΔT_0 which represents the mud hydrostatic pressure drop during tripping, is applied around the sample boundary. Therefore, the θ_0 must be considered equal to 90˚ in Eq.C-1 and Eq.C-2 (as shown in **Figure C-a**). This results in the following equations for the induced stresses radially and tangentially within the sample. These induced stresses are equal to ΔT_0 as illustrated in **Figure C-b.**

$$\sigma_{rr} = \frac{2\Delta T_0}{\pi}\, Arctan\left[\frac{1+\left(\frac{r}{R}\right)^2}{1-\left(\frac{r}{R}\right)^2}tan(\frac{\pi}{2})\right] = \Delta T_0 \qquad \textit{Eq. C-3}$$

$$\sigma_{\theta\theta} = \frac{2\Delta T_0}{\pi}\, Arctan\left[\frac{1+\left(\frac{r}{R}\right)^2}{1-\left(\frac{r}{R}\right)^2}tan(\frac{\pi}{2})\right] = \Delta T_0 \qquad \textit{Eq. C-4}$$

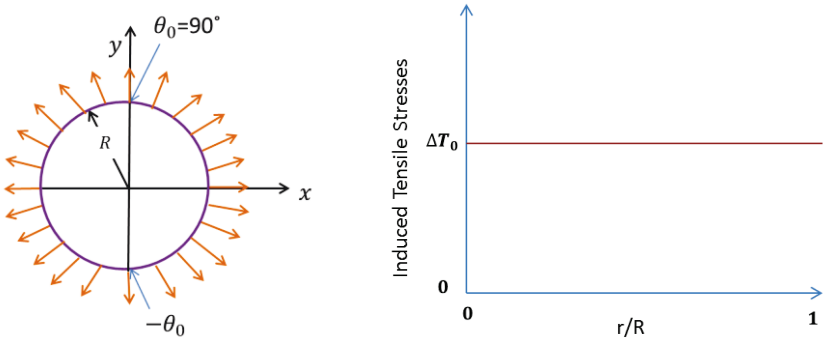

a) **b)**

Figure C: Induced Tensile Stresses for a Solid Elastic Cylinder, a) Initially Applied Tensile Stress around the Boundary of the Solid Elastic Cylinder, b) the Propagation of the Induced Stresses within the sample

Appendix D:

Deriving and Developing Induced Stresses (Unloading Mode–I)

D.1: Deriving the Equation for $\widetilde{\Delta\sigma_{rr}}_{(r,s)}^{(hyd.1)}$

In order to find the induced radial stress (or radial stress difference) $\Delta\sigma_{rr}$, first the following constitutive relation is considered (*Wang, 2000 & Detournay & Cheng, 1993*):

$$\Delta\sigma_{rr} = 2G\epsilon_{rr} + 2G\frac{\upsilon}{1-2\upsilon}\epsilon_{kk} - a\Delta P_p \qquad \textit{(Eq. D.1–1)}$$

Where G is the shear modulus; ϵ_{rr} is the radial strain; υ is the Poisson's ratio; ϵ_{kk} is the bulk strain ($\epsilon_{rr} + \epsilon_{\theta\theta}$); and ΔP_p is the pore pressure drop.

The following relation exists between the radial strain ϵ_{rr} and the radial displacement ΔU_{rr} (*Wang, 2000 & Detournay & Cheng, 1993*):

$$\epsilon_{rr} = \frac{\partial \Delta U_{rr}}{\partial r} \qquad \textit{(Eq. D.1–2)}$$

The following relation exists between the total strain ϵ_{kk} and the radial displacement ΔU_{rr} (*Wang, 2000 & Detournay & Cheng, 1993*):

$$\epsilon_{kk} = \frac{1}{r}\frac{\partial (r\Delta U_{rr})}{\partial r} \qquad \textit{(Eq. D.1–3)}$$

Taking Laplace transforms from both sides of Eq. D.1–1, we have:

$$\widetilde{\Delta\sigma_{rr}} = 2G\widetilde{\epsilon_{rr}} + 2G\frac{\upsilon}{1-2\upsilon}\widetilde{\epsilon_{kk}} - a\widetilde{\Delta P_p} \qquad \textit{(Eq. D.1–4)}$$

Taking Laplace transforms of Eq. D.1–2 and Eq. D.1–3 and replacing into Eq. D.1–4, we have:

$$\widetilde{\Delta\sigma_{rr}}_{(r,s)}^{(hyd.1)} = 2G\left(\frac{\partial \widetilde{\Delta U}_{rr}^{(hyd.1)}}{\partial r}\right) + 2G\frac{\upsilon}{1-2\upsilon}\left(\frac{1}{r}\frac{\partial\left(r\widetilde{\Delta U}_{rr}^{(hyd.1)}\right)}{\partial r}\right) - a\widetilde{\Delta P_p}^{(hyd.1)} \qquad \textit{(Eq. D.1–5)}$$

To find the equation for $\widetilde{\Delta\sigma_{rr}}_{(r,s)}^{(hyd.1)}$, we need to have $\frac{\partial \widetilde{\Delta U}_{rr}^{(hyd.1)}}{\partial r}$, $\frac{1}{r}\frac{\partial (r\widetilde{\Delta U}_{rr}^{(hyd.1)})}{\partial r}$ and $\widetilde{\Delta P_p}_{(r,s)}^{(hyd.1)}$. The induced pore pressure difference for unloading mode-I ($\widetilde{\Delta P_p}^{(hyd.1)}$) has been already equated in the literature (*Wang, 2000; Detournay & Cheng, 1993*):

$$\widetilde{\Delta P}_{p_{(r,s)}}^{(hyd.1)} = -\frac{2}{3s}(1+\upsilon_u)\Delta P_c B(1-f_{mc})\left[\frac{I_0\left(\sqrt{\frac{s}{\eta}}R\right) - I_0\left(\sqrt{\frac{s}{\eta}}r\right)}{I_0\left(\sqrt{\frac{s}{\eta}}R\right) - 2\frac{(\upsilon_u-\upsilon)}{(1-\upsilon)}\frac{I_1\left(\sqrt{\frac{s}{\eta}}R\right)}{\sqrt{\frac{s}{\eta}}R}}\right] \quad \textit{(Eq. D.1–6)}$$

Where f_{mc} is the mud cake fraction of total pressure drop across the core sample; υ_u is the undrained Poisson's ratio, B is the Skempton's coefficient; R is the core radius; η is the hydraulic diffusivity coefficient; I_0 and I_1 are respectively the hyperbolic Bessel functions of zero and first order of the first kind.

For simplicity, we take a coefficient A for the following expression:

$$A = (1-\upsilon)I_0\left(\sqrt{\frac{s}{\eta}}R\right) - 2(\upsilon_u-\upsilon)\frac{I_1\left(\sqrt{\frac{s}{\eta}}R\right)}{\sqrt{\frac{s}{\eta}}R} \quad \textit{(Eq. D.1–7)}$$

Therefore, Eq. D.1–6 becomes:

$$\widetilde{\Delta P}_{p_{(r,s)}}^{(hyd.1)} = -\frac{2\Delta P_c}{3s}\frac{(1+\upsilon_u)(1-\upsilon)B}{A}(1-f_{mc})\left[I_0\left(\sqrt{\frac{s}{\eta}}R\right) - I_0\left(\sqrt{\frac{s}{\eta}}r\right)\right] \quad \textit{(Eq. D.1–8)}$$

We have the following relation between poroelastic coefficients (using **Appendix A.1**):

$$a \times B = \frac{3(\upsilon_u-\upsilon)}{(1-2\upsilon)(1+\upsilon_u)} \quad \textit{(Eq. D.1–9)}$$

Where a and B are respectively the Biot's and Skempton's coefficients.

Assuming zero mud cake effect ($f_{mc} = 0$) and using Eq. D.1–9, converts Eq. D.1–8 to:

$$\widetilde{\Delta P}_{p_{(r,s)}}^{(hyd.1.1)} = \frac{2\Delta P_c}{s}\frac{(\upsilon_u-\upsilon)}{(1-2\upsilon)A}(1-\upsilon)\left[I_0\left(\sqrt{\frac{s}{\eta}}R\right) - I_0\left(\sqrt{\frac{s}{\eta}}r\right)\right] \quad \textit{(Eq. D.1–10)}$$

We still need to find the equations for $\frac{\partial \widetilde{\Delta U}_{rr}^{(hyd.1)}}{\partial r}$ and $\frac{1}{r}\frac{\partial (r\widetilde{\Delta U}_{rr}^{(hyd.1)})}{\partial r}$ [15] in order to find $\widetilde{\Delta\sigma_{rr}}_{(r,s)}^{(hyd.1.1)}$. *Wang* (*2000*) has presented the following relation for the Laplace transform of the radial displacement $\widetilde{\Delta U}_{rr}^{(hyd.1)}$:

$$\widetilde{\Delta U_{rr}}_{(r,s)}^{(hyd.1)} = \frac{1}{s}\frac{\Delta P_c\, r}{2GA}\left[(1-2\upsilon_u)(1-\upsilon)I_0\left(\sqrt{\frac{s}{\eta}}R\right) + 2(\upsilon_u-\upsilon)\frac{I_1\left(\sqrt{\frac{s}{\eta}}r\right)}{\sqrt{\frac{s}{\eta}}r}\right] \qquad \textit{(Eq. D.1–11)}$$

At this step, we first need to know how to take derivatives from hyperbolic Bessel functions. Thus, the following derivation rules for the hyperbolic Bessel functions will be used (*Kreyszig, 2006*):

$$\frac{d(zI_1(z))}{dz} = zI_0(z) \qquad \textit{(Eq. D.1–12)}$$

$$\frac{dI_1(z)}{dz} = I_0(z) - \frac{1}{z}I_1(z) \qquad \textit{(Eq. D.1–13)}$$

Thus, using Eq. D.1–12 and Eq. D.1–13 to take derivatives from Eq. D.1–11, we have:

$$\frac{\partial \widetilde{\Delta U}_{rr}^{(hyd.1)}}{\partial r} = \frac{1}{s}\frac{\Delta P_c}{2GA}\left\{(1-2\upsilon_u)(1-\upsilon)I_0\left(\sqrt{\frac{s}{\eta}}R\right) + 2(\upsilon_u-\upsilon)\left[I_0\left(\sqrt{\frac{s}{\eta}}r\right) - \frac{I_1\left(\sqrt{\frac{s}{\eta}}r\right)}{\sqrt{\frac{s}{\eta}}r}\right]\right\} \qquad \textit{(Eq. D.1–14)}$$

Similarly, using derivation rules of Eq. D.1–12 and Eq. D.1–13, we can equate $\frac{1}{r}\frac{\partial (r\widetilde{\Delta U}_r^{(hyd.1)})}{\partial r}$ as:

$$\frac{1}{r}\frac{\partial (r\widetilde{\Delta U}_{rr}^{(hyd.1)})}{\partial r} = \frac{1}{s}\frac{\Delta P_c}{2GA}\left[2(1-2\upsilon_u)(1-\upsilon)I_0\left(\sqrt{\frac{s}{\eta}}R\right) + 2(\upsilon_u-\upsilon)I_0\left(\sqrt{\frac{s}{\eta}}r\right)\right] \qquad \textit{(Eq. D.1–15)}$$

Now, we have all the terms required to evaluate $\widetilde{\Delta\sigma_{rr}}_{(r,s)}^{(hyd.1)}$. Therefore, using Eq. D.1–10, Eq. D.1–14, and Eq. D.1–15 and replacing them into Eq. D.1–5, we have:

[15] In the unloading mode I (i.e. confining pressure drop), only the pore pressure term ΔP_p depends on the mud cake effect, the displacement ΔU_{rr} is independent of the mud cake effect.

$$\widetilde{\Delta\sigma_{rr}}^{(hyd.1.1)}_{(r,s)} = \frac{1}{s}\frac{\Delta P_c}{A}\left\{(1-2\upsilon_u)(1-\upsilon)I_0\left(\sqrt{\frac{s}{\eta}}R\right) + 2(\upsilon_u-\upsilon)\left[I_0\left(\sqrt{\frac{s}{\eta}}r\right) - \frac{I_1\left(\sqrt{\frac{s}{\eta}}r\right)}{\sqrt{\frac{s}{\eta}}r}\right]\right.$$
$$+\frac{\upsilon}{1-2\upsilon}\left[2(1-2\upsilon_u)(1-\upsilon)I_0\left(\sqrt{\frac{s}{\eta}}R\right) + 2(\upsilon_u-\upsilon)I_0\left(\sqrt{\frac{s}{\eta}}r\right)\right] \qquad \textit{(Eq. D.1–16)}$$
$$\left.+\frac{2(\upsilon_u-\upsilon)}{1-2\upsilon}(1-\upsilon)\left[I_0\left(\sqrt{\frac{s}{\eta}}R\right) - I_0\left(\sqrt{\frac{s}{\eta}}r\right)\right]\right\}$$

In order to rearrange Eq. D.1–16, we classify the coefficients as follows:

Coefficient of $I_0\left(\sqrt{\frac{s}{\eta}}R\right)$: $\frac{1}{s}\frac{\Delta P_c}{A}\left\{(1-2\upsilon_u)(1-\upsilon) + \frac{\upsilon}{1-2\upsilon}\times 2(1-2\upsilon_u)(1-\upsilon) + \frac{2(\upsilon_u-\upsilon)}{1-2\upsilon}(1-\upsilon)\right\}$

$$= \frac{1}{s}\frac{\Delta P_c}{A}\frac{(1-\upsilon)}{1-2\upsilon}\{(1-2\upsilon_u) + 2(\upsilon_u-\upsilon)\} = \frac{1}{s}\frac{\Delta P_c}{A}(1-\upsilon)$$

Coefficient of $I_0\left(\sqrt{\frac{s}{\eta}}r\right)$: $\frac{1}{s}\frac{\Delta P_c}{A}\left\{2(\upsilon_u-\upsilon) + \frac{\upsilon}{1-2\upsilon}\times 2(\upsilon_u-\upsilon) - \frac{2(\upsilon_u-\upsilon)}{1-2\upsilon}(1-\upsilon)\right\} = 0$

Coefficient of $\frac{I_1\left(\sqrt{\frac{s}{\eta}}r\right)}{\sqrt{\frac{s}{\eta}}r}$: $-\frac{1}{s}\frac{\Delta P_c}{A}2(\upsilon_u-\upsilon)$

Using the above rearrangement method, we have:

$$\widetilde{\Delta\sigma_{rr}}^{(hyd.1.1)} = \frac{\Delta P_c}{sA}\left\{(1-\upsilon)I_0\left(\sqrt{\frac{s}{\eta}}R\right) - 2\,(\upsilon_u-\upsilon)\left[\frac{I_1\left(\sqrt{\frac{s}{\eta}}r\right)}{\sqrt{\frac{s}{\eta}}r}\right]\right\} \qquad \textit{(Eq. D.1–17)}$$

If the mud cake pressure drop fraction is assumed non-zero ($f_{mc} \neq 0$) in Eq. D.1–8 and using the same procedure, we have $\widetilde{\Delta\sigma_{rr}}^{(hyd.1)}$ as follows:

$$\widetilde{\Delta\sigma_{rr}}^{(hyd.1)} = \frac{\Delta P_c}{sA}\left\{(1-\upsilon)I_0\left(\sqrt{\frac{s}{\eta}}R\right) - 2\,(\upsilon_u-\upsilon)\left[-\frac{I_1\left(\sqrt{\frac{s}{\eta}}r\right)}{\sqrt{\frac{s}{\eta}}r}\right]\right.$$
$$\left.+2f_{mc}\frac{(\upsilon_u-\upsilon)}{(1-2\upsilon)}(1-\upsilon)\left[I_0\left(\sqrt{\frac{s}{\eta}}R\right) - I_0\left(\sqrt{\frac{s}{\eta}}r\right)\right]\right\} \qquad \textit{(Eq. D.1–18)}$$

Comparing Eq. D.1–17 and Eq. D.1–18, the mud cake effect $\widetilde{\Delta\sigma_{rr}}^{(hyd.1.2)}$ can be found as follows:

$$\widetilde{\Delta\sigma_{rr}}^{(hyd.1.2)} = 2\frac{\Delta P_c}{sA}\frac{(\upsilon_u - \upsilon)}{(1-2\upsilon)}(1-\upsilon)f_{mc}\left[I_0\left(\sqrt{\frac{s}{\eta}}R\right) - I_0\left(\sqrt{\frac{s}{\eta}}r\right)\right] \qquad \textit{(Eq. D.1–19)}$$

Finally, the total induced radial stress for the unloading mode-I, $\widetilde{\Delta\sigma_{rr}}^{(hyd.1)}$ is found by:

$$\widetilde{\Delta\sigma_{rr}}^{(hyd.1)} = \sum_{\boldsymbol{l}=1}^{2} \widetilde{\Delta\sigma_{rr}}_{(r,s)}^{(hyd.2.\boldsymbol{l})} \qquad \textit{(Eq. D.1–20)}$$

D.2: Deriving $\widetilde{\Delta\sigma_{\theta\theta}}_{(r,s)}^{(hyd.1)}$

In order to find the induced radial stress (or radial stress difference) $\Delta\sigma_{\theta\theta}$, first the following constitutive relation is considered (*Wang, 2000 & Detournay & Cheng, 1993*):

$$\Delta\sigma_{\theta\theta} = 2G\epsilon_{\theta\theta} + 2G\frac{\upsilon}{1-2\upsilon}\epsilon_{kk} - a\Delta P_p \qquad \textit{(Eq. D.2–1)}$$

Where G is the shear modulus; $\epsilon_{\theta\theta}$ is the hoop strain; υ is the Poisson's ratio; ϵ_{kk} is the bulk strain ($\epsilon_{rr} + \epsilon_{\theta\theta}$); and ΔP_p is the pore pressure drop.

The following relation exists between the hoop strain $\epsilon_{\theta\theta}$ and the radial displacement ΔU_{rr} (*Wang, 2000 & Detournay & Cheng, 1993*):

$$\epsilon_{\theta\theta} = \frac{\Delta U_{rr}}{r} \qquad \textit{(Eq. D.2–2)}$$

The following relation exists between the total strain ϵ_{kk} and the radial displacement ΔU_{rr} (*Wang, 2000 & Detournay & Cheng, 1993*):

$$\epsilon_{kk} = \frac{1}{r}\frac{\partial(r\Delta U_{rr})}{\partial r} \qquad \textit{(Eq. D.2–3)}$$

Taking Laplace transforms from both sides of Eq. D.2–1, we have:

$$\widetilde{\Delta\sigma_{\theta\theta}} = 2G\widetilde{\epsilon_{\theta\theta}} + 2G\frac{\upsilon}{1-2\upsilon}\widetilde{\epsilon_{kk}} - a\widetilde{\Delta P_p} \qquad \textit{(Eq. D.2–4)}$$

Taking Laplace transforms from both sides of Eq. D.2–2 and Eq. D.2–3 and replacing into Eq. D.2–4, we have:

$$\widetilde{\Delta\sigma_{\theta\theta}}_{(r,s)}^{(hyd.1)} = 2G\left(\frac{\widetilde{\Delta U}_{rr}^{(hyd.1)}}{r}\right) + 2G\frac{\upsilon}{1-2\upsilon}\left(\frac{1}{r}\frac{\partial\left(r\widetilde{\Delta U}_{rr}^{(hyd.1)}\right)}{\partial r}\right) - a\widetilde{\Delta P_p}^{(hyd.1)} \qquad \textit{(Eq. D.2–5)}$$

To find the equation for $\widetilde{\Delta\sigma_{\theta\theta}}_{(r,s)}^{(hyd.1)}$, we need to have $\frac{\widetilde{\Delta U}_{rr}^{(hyd.1)}}{r}$, $\frac{1}{r}\frac{\partial(r\widetilde{\Delta U}_{rr}^{(hyd.1)})}{\partial r}$ and $\widetilde{\Delta P_p}_{(r,s)}^{(hyd.1)}$. The induced pore pressure difference for unloading mode-I ($\widetilde{\Delta P_p}^{(hyd.1)}$) has been already equated in the literature (*Wang, 2000; Detournay & Cheng, 1993*):

$$\widetilde{\Delta P_p}_{(r,s)}^{(hyd.1)} = -\frac{2}{3s}(1+\upsilon_u)\Delta P_c B(1-f_{mc})\left[\frac{I_0\left(\sqrt{\frac{s}{\eta}}R\right) - I_0\left(\sqrt{\frac{s}{\eta}}r\right)}{I_0\left(\sqrt{\frac{s}{\eta}}R\right) - 2\frac{(\upsilon_u-\upsilon)}{(1-\upsilon)}\frac{I_1\left(\sqrt{\frac{s}{\eta}}R\right)}{\sqrt{\frac{s}{\eta}}R}}\right] \qquad \textit{(Eq. D.2–6)}$$

Where f_{mc} is the mud cake fraction of total pressure drop across the core sample; υ_u is the undrained Poisson's ratio, B is the Skempton's coefficient; R is the core radius; η is the hydraulic diffusivity coefficient; I_0 and I_1 are respectively the hyperbolic Bessel functions of zero and first order of the first kind.

For simplicity, we take a coefficient A for the following expression:

$$A = (1-\upsilon) I_0\left(\sqrt{\frac{s}{\eta}}R\right) - 2(\upsilon_u - \upsilon)\frac{I_1\left(\sqrt{\frac{s}{\eta}}R\right)}{\sqrt{\frac{s}{\eta}}R} \qquad \textit{(Eq. D.2–7)}$$

Therefore, Eq. D.2–6 becomes:

$$\widetilde{\Delta P}_{p_{(r,s)}}^{(hyd.1)} = -\frac{2\Delta P_c}{3s}\frac{(1+\upsilon_u)(1-\upsilon)B}{A}(1-f_{mc})\left[I_0\left(\sqrt{\frac{s}{\eta}}R\right) - I_0\left(\sqrt{\frac{s}{\eta}}r\right)\right] \qquad \textit{(Eq. D.2–8)}$$

We have the following relation between poroelastic coefficients (using **Appendix A.1**):

$$a \times B = \frac{3(\upsilon_u - \upsilon)}{(1-2\upsilon)(1+\upsilon_u)} \qquad \textit{(Eq. D.2–9)}$$

Where a and B are respectively the Biot's and Skempton's coefficients.

Assuming zero mud cake effect ($f_{mc} = 0$) and using Eq. D.2–9 converts Eq. D.2–8 to:

$$\widetilde{\Delta P}_{p_{(r,s)}}^{(hyd.1.1)} = -\frac{2\Delta P_c}{s}\frac{(\upsilon_u - \upsilon)}{(1-2\upsilon)A}(1-\upsilon)\left[I_0\left(\sqrt{\frac{s}{\eta}}R\right) - I_0\left(\sqrt{\frac{s}{\eta}}r\right)\right] \qquad \textit{(Eq. D.2–10)}$$

We still need to find the equations for $\frac{\widetilde{\Delta U}_{rr}^{(hyd.1)}}{r}$ and $\frac{1}{r}\frac{\partial(r\widetilde{\Delta U}_{rr}^{(hyd.1)})}{\partial r}$ in order to find $\widetilde{\Delta\sigma_{\theta\theta}}_{(r,s)}^{(hyd.1)}$. *Wang* (*2000*) has presented the following relation for the Laplace transform of the radial displacement $\widetilde{\Delta U}_{rr}^{(hyd.1)}$:

$$\widetilde{\Delta U_{rr}}_{(r,s)}^{(hyd.1)} = \frac{1}{s}\frac{\Delta P_c\, r}{2GA}\left[(1-2\upsilon_u)(1-\upsilon)I_0\left(\sqrt{\frac{s}{\eta}}R\right) + 2(\upsilon_u - \upsilon)\frac{I_1\left(\sqrt{\frac{s}{\eta}}r\right)}{\sqrt{\frac{s}{\eta}}r}\right] \qquad \textit{(Eq. D.2–11)}$$

Therefore, using Eq. D.2–2, $\epsilon_{\theta\theta}$ is found as:

$$\epsilon_{\theta\theta} = \frac{\Delta U_{rr}}{r} = \frac{1}{s}\frac{\Delta P_c}{2GA}\left[(1-2\upsilon_u)(1-\upsilon)I_0\left(\sqrt{\frac{s}{\eta}}R\right) + 2(\upsilon_u - \upsilon)\frac{I_1\left(\sqrt{\frac{s}{\eta}}r\right)}{\sqrt{\frac{s}{\eta}}r}\right] \qquad \textit{(Eq. D.2–12)}$$

We have already found the equation for $\frac{1}{r}\frac{\partial(r\widetilde{\Delta U_r}^{(hyd.1)})}{\partial r}$ in Eq. D.1–15.

Now, we have all the terms required to evaluate $\widetilde{\Delta\sigma_{\theta\theta}}^{(hyd.1.1)}_{(r,s)}$. Therefore, using Eq. D.2–10, Eq. D.2–12, and Eq. D.1–15 and replacing them into Eq. D.2–5, we have:

$$\widetilde{\Delta\sigma_{\theta\theta}}^{(hyd.1.1)} = \frac{1}{s}\frac{\Delta P_c}{A}\left\{(1-2\upsilon_u)(1-\upsilon)I_0\left(\sqrt{\frac{s}{\eta}}R\right) + 2(\upsilon_u-\upsilon)\frac{I_1\left(\sqrt{\frac{s}{\eta}}r\right)}{\sqrt{\frac{s}{\eta}}r}\right.$$
$$+\frac{\upsilon}{1-2\upsilon}\left[2(1-2\upsilon_u)(1-\upsilon)I_0\left(\sqrt{\frac{s}{\eta}}R\right) + 2(\upsilon_u-\upsilon)I_0\left(\sqrt{\frac{s}{\eta}}r\right)\right] \qquad \textit{(Eq. D.2–13)}$$
$$\left.+\frac{2(\upsilon_u-\upsilon)}{1-2\upsilon}(1-\upsilon)\left[I_0\left(\sqrt{\frac{s}{\eta}}R\right) - I_0\left(\sqrt{\frac{s}{\eta}}r\right)\right]\right\}$$

In order to rearrange Eq. D.2–13, we classify the coefficients as follows:

Coefficient of $I_0\left(\sqrt{\frac{s}{\eta}}R\right) = (1-2\upsilon_u)(1-\upsilon) + \frac{\upsilon}{1-2\upsilon}\times 2(1-2\upsilon_u)(1-\upsilon) + \frac{2(\upsilon_u-\upsilon)}{1-2\upsilon}(1-\upsilon)$

$$= \frac{(1-\upsilon)}{1-2\upsilon}\{(1-2\upsilon_u)(1-2\upsilon) + 2[\upsilon(1-2\upsilon_u) + (\upsilon_u-\upsilon)]\} = (1-\upsilon)$$

Coefficient of $I_0\left(\sqrt{\frac{s}{\eta}}r\right) = \upsilon\left(\frac{2(\upsilon_u-\upsilon)}{1-2\upsilon}\right) - \frac{(1-\upsilon)\times 2(\upsilon_u-\upsilon)}{1-2\upsilon} = -2(\upsilon_u-\upsilon)$

Coefficient of $\frac{I_1\left(\sqrt{\frac{s}{\eta}}r\right)}{\sqrt{\frac{s}{\eta}}r} = 2(\upsilon_u-\upsilon)$

Using the above rearrangement method, we have:

$$\widetilde{\Delta\sigma_{\theta\theta}}^{(hyd.1.1)}_{(r,s)} = \frac{\Delta P_c}{sA}\left\{(1-\upsilon)I_0\left(\sqrt{\frac{s}{\eta}}R\right) - 2(\upsilon_u-\upsilon)\left[I_0\left(\sqrt{\frac{s}{\eta}}r\right) - \frac{I_1\left(\sqrt{\frac{s}{\eta}}r\right)}{\sqrt{\frac{s}{\eta}}r}\right]\right\} \qquad \textit{(Eq. D.2–14)}$$

If the mud cake pressure drop fraction is assumed non-zero ($f_{mc} \neq 0$) in Eq. D.2–8 and using the same procedure from Eq. D.2–8 to Eq. D.2–12, we have $\widetilde{\Delta\sigma_{\theta\theta}}^{(hyd.1)}_{(r,s)}$ as follows:

$$\widetilde{\sigma_{\theta\theta}}_{(r,s)}^{(hyd.1)} = \frac{\Delta P_c}{sA}\left\{\left[(1-\upsilon)I_0\left(\sqrt{\frac{s}{\eta}}R\right) - 2(\upsilon_u-\upsilon)\left(I_0\left(\sqrt{\frac{s}{\eta}}r\right) - \frac{I_1\left(\sqrt{\frac{s}{\eta}}r\right)}{\sqrt{\frac{s}{\eta}}r}\right)\right]\right.$$
$$\left. + 2f_{mc}\frac{(\upsilon_u-\upsilon)}{(1-2\upsilon)}(1-\upsilon)\left[I_0\left(\sqrt{\frac{s}{\eta}}R\right) - I_0\left(\sqrt{\frac{s}{\eta}}r\right)\right]\right\} \qquad \textit{(Eq. D.2–15)}$$

Comparing Eq. D.2–14 and Eq. D.2–15, the mud cake effect $\widetilde{\Delta\sigma_{\theta\theta}}^{(hyd.1.2)}$ can be found as follows:

$$\widetilde{\Delta\sigma_{\theta\theta}}^{(hyd.1.2)} = 2\frac{\Delta P_c}{sA}\frac{(\upsilon_u-\upsilon)}{(1-2\upsilon)}(1-\upsilon)f_{mc}\left[I_0\left(\sqrt{\frac{s}{\eta}}R\right) - I_0\left(\sqrt{\frac{s}{\eta}}r\right)\right] \qquad \textit{(Eq. D.2–16)}$$

Finally, the total induced radial stress for the unloading mode-I, $\widetilde{\Delta\sigma_{\theta\theta}}^{(hyd.1)}$ is found by:

$$\widetilde{\Delta\sigma_{\theta\theta}}^{(hyd.1)} = \sum_{l=1}^{2}\widetilde{\Delta\sigma_{\theta\theta}}_{(r,s)}^{(hyd.2.l)} \qquad \textit{(Eq. D.2–17)}$$

Appendix E:

Deriving and Developing Induced Stresses (Unloading Mode–II)

E.1: Deriving the Equation for $\widetilde{\Delta\sigma_{rr}}^{(hyd.2)}_{(r,s)}$

In order to find the induced radial stress (or radial stress difference) $\Delta\sigma_{rr}$, first the following constitutive relation is considered (*Wang, 2000 & Detournay & Cheng, 1993*):

$$\Delta\sigma_{rr} = 2G\epsilon_{rr} + 2G\frac{\upsilon}{1-2\upsilon}\epsilon_{kk} - a\Delta P_p \qquad \textit{(Eq. E.1–1)}$$

Where G is the shear modulus; ϵ_{rr} is the radial strain; υ is the Poisson's ratio; ϵ_{kk} is the bulk strain ($\epsilon_{rr} + \epsilon_{\theta\theta}$); and ΔP_p is the pore pressure drop.

The following relation exists between the radial strain ϵ_{rr} and the radial displacement ΔU_{rr} (*Wang, 2000 & Detournay & Cheng, 1993*):

$$\epsilon_{rr} = \frac{\partial \Delta U_{rr}}{\partial r} \qquad \textit{(Eq. E.1–2)}$$

The following relation exists between the total strain ϵ_{kk} and the radial displacement ΔU_{rr} (*Wang, 2000 & Detournay & Cheng, 1993*):

$$\epsilon_{kk} = \frac{1}{r}\frac{\partial (r\Delta U_{rr})}{\partial r} \qquad \textit{(Eq. E.1–3)}$$

Taking Laplace transforms from both sides of Eq. D.1–1, we have:

$$\widetilde{\Delta\sigma_{rr}} = 2G\widetilde{\epsilon_{rr}} + 2G\frac{\upsilon}{1-2\upsilon}\widetilde{\epsilon_{kk}} - a\widetilde{\Delta P_p} \qquad \textit{(Eq. E.1–4)}$$

Taking Laplace transforms of Eq. E.1–2 and Eq. E.1–3 and replacing into Eq. E.1–4, we have:

$$\widetilde{\Delta\sigma_{rr}}^{(hyd.2)}_{(r,s)} = 2G\left(\frac{\partial \widetilde{\Delta U}_{rr}^{(hyd.2)}}{\partial r}\right) + 2G\frac{\upsilon}{1-2\upsilon}\left(\frac{1}{r}\frac{\partial\left(r\widetilde{\Delta U}_{rr}^{(hyd.2)}\right)}{\partial r}\right) - a\widetilde{\Delta P_p}^{(hyd.2)} \qquad \textit{(Eq. E.1–5)}$$

To find the equation for $\widetilde{\Delta\sigma_{rr}}^{(hyd.2)}_{(r,s)}$, we need to have $\frac{\partial \widetilde{\Delta U}_{rr}^{(hyd.2)}}{\partial r}$, $\frac{1}{r}\frac{\partial (r\widetilde{\Delta U}_{rr}^{(hyd.2)})}{\partial r}$ and $\widetilde{\Delta P_p}^{(hyd.2)}_{(r,s)}$. The induced pore pressure difference for unloading mode-II ($\widetilde{\Delta P_p}^{(hyd.2)}$) has been already equated in the literature (*Wang, 2000; Detournay & Cheng, 1993*):

$$\widetilde{\Delta P}_{p_{(r,s)}}^{(hyd.2)} = -\frac{\Delta P_c}{s}(1-f_{mc})\left[\frac{(1-\upsilon)I_0\left(\sqrt{\frac{s}{\eta}}r\right) - 2(\upsilon_u-\upsilon)\dfrac{I_1\left(\sqrt{\frac{s}{\eta}}R\right)}{\sqrt{\frac{s}{\eta}}R_c}}{(1-\upsilon)I_0\left(\sqrt{\frac{s}{\eta}}R_c\right) - 2(\upsilon_u-\upsilon)\dfrac{I_1\left(\sqrt{\frac{s}{\eta}}R\right)}{\sqrt{\frac{s}{\eta}}R}}\right] \qquad \textit{(Eq. E.1-6)}$$

Where f_{mc} is the mud cake fraction of total pressure drop across the core sample; υ_u is the undrained Poisson's ratio, B is the Skempton's coefficient; R is the core radius; η is the hydraulic diffusivity coefficient; I_0 and I_1 are respectively the hyperbolic Bessel functions of zero and first order of the first kind.

For simplicity, we take a coefficient A for the following expression:

$$A = (1-\upsilon)I_0\left(\sqrt{\frac{s}{\eta}}R\right) - 2(\upsilon_u-\upsilon)\frac{I_1\left(\sqrt{\frac{s}{\eta}}R\right)}{\sqrt{\frac{s}{\eta}}R} \qquad \textit{(Eq. E.1-7)}$$

Therefore, Eq. E.1–6 becomes:

$$\widetilde{\Delta P}_{p_{(r,s)}}^{(hyd.2)} = -\frac{1}{s}\frac{\Delta P_c}{A}(1-f_{mc})\left[(1-\upsilon)I_0\left(\sqrt{\frac{s}{\eta}}r\right) - 2(\upsilon_u-\upsilon)\frac{I_1\left(\sqrt{\frac{s}{\eta}}R\right)}{\sqrt{\frac{s}{\eta}}R}\right] \qquad \textit{(Eq. E.1-8)}$$

Assuming zero mud cake effect ($f_{mc} = 0$), Eq. E.1–8 becomes:

$$\widetilde{\Delta P}_{p_{(r,s)}}^{(hyd.2.1)} = -\frac{1}{s}\frac{\Delta P_c}{A}\left[(1-\upsilon)I_0\left(\sqrt{\frac{s}{\eta}}r\right) - 2(\upsilon_u-\upsilon)\frac{I_1\left(\sqrt{\frac{s}{\eta}}R\right)}{\sqrt{\frac{s}{\eta}}R}\right] \qquad \textit{(Eq. E.1-9)}$$

We still need to find the equations for $\frac{\partial \widetilde{\Delta U}_{rr}^{(hyd.2.1)}}{\partial r}$ and $\frac{1}{r}\frac{\partial (r\widetilde{\Delta U}_{rr}^{(hyd.2.1)})}{\partial r}$ [16] in order to find $\widetilde{\Delta\sigma_{rr}}_{(r,s)}^{(hyd.2.1)}$.

Wang (*2000*) has presented the following relation for the Laplace transform of the radial displacement, $\widetilde{\Delta U}_{rr}^{(hyd.2.1)}$ (excluding the mud cake effect):

[16] The notation 2.1 indicates excluding the mud cake effect. In the unloading mode II (i.e. pore pressure drop), both the displacement ΔU_{rr} and the pore pressure ΔP_p depends on the mud cake effect. However, in the unloading mode I (i.e. confining pressure drop), only the pore pressure depends on the mud cake effect.

$$\widetilde{\Delta U_{rr}}_{(r,s)}^{(hyd.2.1)} = -\frac{1}{s}a(1-2v)\left(\frac{\Delta P_c r}{2GA}\right)\left[\frac{I_1\left(\sqrt{\frac{s}{\eta}}r\right)}{\sqrt{\frac{s}{\eta}}r} + (1-2v_u)\frac{I_1\left(\sqrt{\frac{s}{\eta}}R\right)}{\sqrt{\frac{s}{\eta}}R}\right] \quad \textit{(Eq. E.1–10)}$$

At this step, we first need to know how to take derivatives from hyperbolic Bessel functions. Thus, the following derivation rules for the hyperbolic Bessel functions will be used (*Kreyszig, 2006*):

$$\frac{d(zI_1(z))}{dz} = zI_0(z) \quad \textit{(Eq. E.1–11)}$$

$$\frac{dI_1(z)}{dz} = I_0(z) - \frac{1}{z}I_1(z) \quad \textit{(Eq. E.1–12)}$$

Thus, using Eq. E.1–11 and Eq. E.1–12 to take derivatives from Eq. E.1–10, we have:

$$\frac{\partial \widetilde{\Delta U_{rr}}^{(hyd.2.1)}}{\partial r} = -\frac{1}{s}\frac{\Delta P_c}{2GA}a(1-2v)\left\{I_0\left(\sqrt{\frac{s}{\eta}}r\right) - \frac{I_1\left(\sqrt{\frac{s}{\eta}}r\right)}{\sqrt{\frac{s}{\eta}}r} + (1-2v_u)\frac{I_1\left(\sqrt{\frac{s}{\eta}}R\right)}{\sqrt{\frac{s}{\eta}}R}\right\} \quad \textit{(Eq. E.1–13)}$$

Similarly, using the derivation rules of Eq. E.1–11 and Eq. E.1–12, we can equate $\frac{1}{r}\frac{\partial(r\widetilde{\Delta U_r}^{(hyd.2.1)})}{\partial r}$ as:

$$\frac{1}{r}\frac{\partial(r\widetilde{\Delta U_{rr}}^{(hyd.2.1)})}{\partial r} = -\frac{1}{s}\frac{\Delta P_c}{2GA}a(1-2v)\left\{I_0\left(\sqrt{\frac{s}{\eta}}r\right) + 2(1-2v_u)\frac{I_1\left(\sqrt{\frac{s}{\eta}}R\right)}{\sqrt{\frac{s}{\eta}}R}\right\} \quad \textit{(Eq. E.1–14)}$$

Now, we have all the terms required to evaluate $\widetilde{\Delta\sigma_{rr}}_{(r,s)}^{(hyd.2.1)}$. Therefore, using Eq. E.1–9, Eq. E.1–13, and Eq. E.1–14 and replacing them into Eq. E.1–5, we have:

$$\begin{aligned}\widetilde{\Delta\sigma_{rr}}_{(r,s)}^{(hyd.2.1)} = &-\frac{1}{s}\frac{\Delta P_c}{A}a(1-2v)\left\{I_0\left(\sqrt{\frac{s}{\eta}}r\right) - \frac{I_1\left(\sqrt{\frac{s}{\eta}}r\right)}{\sqrt{\frac{s}{\eta}}r} + (1-2v_u)\frac{I_1\left(\sqrt{\frac{s}{\eta}}R\right)}{\sqrt{\frac{s}{\eta}}R}\right\}) \\ &-\frac{1}{s}\frac{\Delta P_c}{A}a(1-2v)\frac{v}{1-2v}\left\{I_0\left(\sqrt{\frac{s}{\eta}}r\right) + 2(1-2v_u)\frac{I_1\left(\sqrt{\frac{s}{\eta}}R\right)}{\sqrt{\frac{s}{\eta}}R}\right\} \\ &+\frac{a}{s}\frac{\Delta P_c}{A}\left[(1-v)I_0\left(\sqrt{\frac{s}{\eta}}r\right) - 2(v_u - v)\frac{I_1\left(\sqrt{\frac{s}{\eta}}R\right)}{\sqrt{\frac{s}{\eta}}R}\right]\end{aligned} \quad \textit{(Eq. E.1–15)}$$

In order to rearrange Eq. E.1–15, we classify the coefficients as follows:

Coefficient $\frac{I_1\left(\sqrt{\frac{s}{\eta}}R\right)}{\sqrt{\frac{s}{\eta}}R}$: $\frac{1}{s}\frac{P_R}{A}a[-(1-2v)(1-2v_u)-2v(1-2v_u)-2(v_u-v)] = -\frac{1}{s}\frac{P_R}{A}a(1-2v)$

Coefficient of $I_0\left(\sqrt{\frac{s}{\eta}}r\right)$: $\frac{1}{s}\frac{P_R}{A}a[-(1-2v)-v+(1-v)] = \frac{1}{s}\frac{P_R}{A}a(1-2v)2v = 0$

Coefficient of $\frac{I_1\left(\sqrt{\frac{s}{\eta}}r\right)}{\sqrt{\frac{s}{\eta}}r}$: $\frac{1}{s}\frac{P_R}{A}a(1-2v)$

Using the above rearrangement method, we have:

$$\widetilde{\Delta\sigma_{rr}}^{(hyd.2.1)}_{(r,s)} = -\frac{\Delta P_c}{sA}a(1-2v)\left[\frac{I_1\left(\sqrt{\frac{s}{\eta}}R\right)}{\sqrt{\frac{s}{\eta}}R} - \frac{I_1\left(\sqrt{\frac{s}{\eta}}r\right)}{\sqrt{\frac{s}{\eta}}r}\right] \qquad \textit{(Eq. E.1–16)}$$

If the mud cake pressure drop fraction is assumed non-zero ($f_{mc} \neq 0$), it affects Eq. D.1–8. For the unloading mode II (i.e. the pore pressure drop) unlike the first unloading mode (i.e. the confining pressure drop), the mud cake effect also affects the core displacement ($\widetilde{\Delta U_{rr}}^{(hyd.2)}_{(r,s)}$) as follows:

$$\widetilde{\Delta U_{rr}}^{(hyd.2)}_{(r,s)} = -\frac{1}{s}a(1-2v)\left(\frac{\Delta P_c r}{2GA}\right)(1-f_{mc})\left[\frac{I_1\left(\sqrt{\frac{s}{\eta}}r\right)}{\sqrt{\frac{s}{\eta}}r} + (1-2v_u)\frac{I_1\left(\sqrt{\frac{s}{\eta}}R\right)}{\sqrt{\frac{s}{\eta}}R}\right] \qquad \textit{(Eq. E.1–17)}$$

Therefore, a coefficient of $(1-f_{mc})$ will be created on the right hand side of Eq. E.1–5. This means that following the same procedure, we find $\widetilde{\Delta\sigma_{rr}}^{(hyd.2)}$ as follows:

$$\widetilde{\Delta\sigma_{rr}}^{(hyd.2)}_{(r,s)} = -\frac{\Delta P_c}{sA}a(1-2v)(1-f_{mc})\left[\frac{I_1\left(\sqrt{\frac{s}{\eta}}R\right)}{\sqrt{\frac{s}{\eta}}R} - \frac{I_1\left(\sqrt{\frac{s}{\eta}}r\right)}{\sqrt{\frac{s}{\eta}}r}\right] \qquad \textit{(Eq. E.1–18)}$$

Comparing Eq.E.1–16 and Eq. E.1–18, the mud cake effect $\widetilde{\Delta\sigma_{rr}}^{(hyd.2.2)}_{(r,s)}$ can be found as follows:

$$\widetilde{\Delta\sigma_{rr}}^{(hyd.2.2)}_{(r,s)} = \frac{\Delta P_c}{sA}a(1-2v)f_{mc}\left[\frac{I_1\left(\sqrt{\frac{s}{\eta}}R\right)}{\sqrt{\frac{s}{\eta}}R} - \frac{I_1\left(\sqrt{\frac{s}{\eta}}r\right)}{\sqrt{\frac{s}{\eta}}r}\right] \qquad \textit{(Eq. E.1–19)}$$

Finally, the total $\widetilde{\sigma_{rr}}^{(hyd.2)}_{(r,s)}$ is found as the summation of:

$$\widetilde{\Delta\sigma_{rr}}_{(r,s)}^{(hyd.2)} = \sum_{m=1}^{2} \widetilde{\Delta\sigma_{rr}}_{(r,s)}^{(hyd.2.m)} \qquad \textit{(Eq. E.1–20)}$$

E.2: Deriving $\widetilde{\Delta\sigma_{\theta\theta}}_{(r,s)}^{(hyd.2)}$

In order to find the induced radial stress (or radial stress difference) $\Delta\sigma_{\theta\theta}$, first the following constitutive equation is considered (*Wang, 2000 & Detournay & Cheng, 1993*):

$$\Delta\sigma_{\theta\theta} = 2G\epsilon_{\theta\theta} + 2G\frac{\upsilon}{1-2\upsilon}\epsilon_{kk} - a\Delta P_p \qquad \textit{(Eq. E.2–1)}$$

Where G is the shear modulus; $\epsilon_{\theta\theta}$ is the hoop strain; υ is the Poisson's ratio; ϵ_{kk} is the bulk strain ($\epsilon_{rr} + \epsilon_{\theta\theta}$); and ΔP_p is the pore pressure drop.

The following relation exists between the hoop strain $\epsilon_{\theta\theta}$ and the radial displacement ΔU_{rr} (*Wang, 2000; Detournay & Cheng, 1993*):

$$\epsilon_{\theta\theta} = \frac{\Delta U_{rr}}{r} \qquad \textit{(Eq. E.2–2)}$$

The following relation exists between the total strain ϵ_{kk} and the radial displacement ΔU_{rr} (*Wang, 2000 & Detournay & Cheng, 1993*):

$$\epsilon_{kk} = \frac{1}{r}\frac{\partial(r\Delta U_{rr})}{\partial r} \qquad \textit{(Eq. E.2–3)}$$

Taking Laplace transforms from both sides of Eq. E.2–1, we have:

$$\widetilde{\Delta\sigma_{\theta\theta}} = 2G\widetilde{\epsilon_{\theta\theta}} + 2G\frac{\upsilon}{1-2\upsilon}\widetilde{\epsilon_{kk}} - a\widetilde{\Delta P_p} \qquad \textit{(Eq. E.2–4)}$$

Taking Laplace transforms from both sides of Eq. E.2–2 and Eq. E.2–3 and replacing into Eq. E.2–4, we have:

$$\widetilde{\Delta\sigma_{\theta\theta}}_{(r,s)}^{(hyd.1)} = 2G\left(\frac{\widetilde{\Delta U}_{rr}^{(hyd.2)}}{r}\right) + 2G\frac{\upsilon}{1-2\upsilon}\left(\frac{1}{r}\frac{\partial\left(r\widetilde{\Delta U}_{rr}^{(hyd.2)}\right)}{\partial r}\right) - a\widetilde{\Delta P_p}^{(hyd.2)} \qquad \textit{(Eq. E.2–5)}$$

To find the equation for $\widetilde{\Delta\sigma_{\theta\theta}}_{(r,s)}^{(hyd.2)}$, we need to have $\frac{\widetilde{\Delta U}_{rr}^{(hyd.2)}}{r}$, $\frac{1}{r}\frac{\partial(r\widetilde{\Delta U}_{rr}^{(hyd.2)})}{\partial r}$ and $\widetilde{\Delta P_p}_{(r,s)}^{(hyd.2)}$. The induced pore pressure difference for the unloading mode-II ($\widetilde{\Delta P_p}^{(hyd.2)}$) has been already equated in the literature (*Wang, 2000; Detournay & Cheng, 1993*):

$$\widetilde{\Delta P_p}_{(r,s)}^{(hyd.2)} = -\frac{\Delta P_c}{sA}(1-f_{mc})\left[\frac{(1-\upsilon)I_0\left(\sqrt{\frac{s}{\eta}}r\right) - 2(\upsilon_u-\upsilon)\dfrac{I_1\left(\sqrt{\frac{s}{\eta}}R\right)}{\sqrt{\frac{s}{\eta}}R}}{(1-\upsilon)I_0\left(\sqrt{\frac{s}{\eta}}R\right) - 2(\upsilon_u-\upsilon)\dfrac{I_1\left(\sqrt{\frac{s}{\eta}}R\right)}{\sqrt{\frac{s}{\eta}}R}}\right] \qquad \textit{(Eq. E.2–6)}$$

Where f_{mc} is the mud cake fraction of total pressure drop across the core sample; υ_u is the undrained Poisson's ratio, B is the Skempton's coefficient; R is the core radius; η is the hydraulic diffusivity coefficient; I_0 and I_1 are respectively the hyperbolic Bessel functions of zero and first order of the first kind.

For simplicity, we take a coefficient A for the following expression:

$$A = (1-\upsilon) I_0\left(\sqrt{\frac{s}{\eta}}R\right) - 2(\upsilon_u - \upsilon)\frac{I_1\left(\sqrt{\frac{s}{\eta}}R\right)}{\sqrt{\frac{s}{\eta}}R} \qquad \textit{(Eq. E.2–7)}$$

Therefore, Eq. E.2–6 becomes:

$$\widetilde{\Delta P_p}_{(r,s)}^{(hyd.2)} = -\frac{1}{s}\frac{\Delta P_c}{A}(1-f_{mc})\left[(1-\upsilon) I_0\left(\sqrt{\frac{s}{\eta}}r\right) - 2(\upsilon_u - \upsilon)\frac{I_1\left(\sqrt{\frac{s}{\eta}}R\right)}{\sqrt{\frac{s}{\eta}}R}\right] \qquad \textit{(Eq. E.2–8)}$$

Assuming zero mud cake effect ($f_{mc} = 0$), Eq. E.2–8 becomes:

$$\widetilde{\Delta P_p}_{(r,s)}^{(hyd.2.1)} = -\frac{1}{s}\frac{\Delta P_c}{A}\left[(1-\upsilon) I_0\left(\sqrt{\frac{s}{\eta}}r\right) - 2(\upsilon_u - \upsilon)\frac{I_1\left(\sqrt{\frac{s}{\eta}}R\right)}{\sqrt{\frac{s}{\eta}}R}\right] \qquad \textit{(Eq. E.2–9)}$$

We still need to find the equations for $\frac{\widetilde{\Delta U}_{rr}^{(hyd.2.1)}}{r}$ and $\frac{1}{r}\frac{\partial(r\widetilde{\Delta U}_{rr}^{(hyd.2.1)})}{\partial r}$ in order to find $\widetilde{\Delta\sigma_{\theta\theta}}_{(r,s)}^{(hyd.2)}$. *Wang* (*2000*) has presented the following relation for the Laplace transform of the radial displacement $\widetilde{\Delta U}_{rr}^{(hyd.2.1)}$:

$$\widetilde{\Delta U_{rr}}_{(r,s)}^{(hyd.2.1)} = -\frac{1}{s}a(1-2\upsilon)\left(\frac{\Delta P_c r}{2GA}\right)\left[\frac{I_1\left(\sqrt{\frac{s}{\eta}}r\right)}{\sqrt{\frac{s}{\eta}}r} + (1-2\upsilon_u)\frac{I_1\left(\sqrt{\frac{s}{\eta}}R\right)}{\sqrt{\frac{s}{\eta}}R}\right] \qquad \textit{(Eq. E.2–10)}$$

Therefore, using Eq. E.2–2, $\epsilon_{\theta\theta}$ is found as:

$$\epsilon_{\theta\theta} = \frac{\Delta U_{rr}}{r} = -\frac{1}{s}a(1-2\upsilon)\left(\frac{\Delta P_c}{2GA}\right)\left[\frac{I_1\left(\sqrt{\frac{s}{\eta}}r\right)}{\sqrt{\frac{s}{\eta}}r} + (1-2\upsilon_u)\frac{I_1\left(\sqrt{\frac{s}{\eta}}R\right)}{\sqrt{\frac{s}{\eta}}R}\right] \qquad \textit{(Eq. E.2–11)}$$

We have already found the equation for $\frac{1}{r}\frac{\partial(r\widetilde{\Delta U}_r{}^{(hyd.2.1)})}{\partial r}$ in Eq. E.1–14.

Now, we have all the terms required to evaluate $\widetilde{\Delta\sigma_{\theta\theta}}_{(r,s)}^{(hyd.2.1)}$. Therefore, using Eq. E.2–9, Eq. E.2–11, and Eq. E.1–14 and replacing them into Eq. E.2–5, we have:

$$\widetilde{\Delta\sigma_{\theta\theta}}^{(hyd.1)} = \frac{1}{s}\frac{\Delta P_c}{A}a\left\{-(1-2\upsilon)\left[\frac{I_1\left(\sqrt{\frac{s}{\eta}}r\right)}{\sqrt{\frac{s}{\eta}}r}+(1-2\upsilon_u)\frac{I_1\left(\sqrt{\frac{s}{\eta}}R\right)}{\sqrt{\frac{s}{\eta}}R}\right]\right.$$
$$-\upsilon\left[I_0\left(\sqrt{\frac{s}{\eta}}r\right)+2(1-2\upsilon_u)\frac{I_1\left(\sqrt{\frac{s}{\eta}}R\right)}{\sqrt{\frac{s}{\eta}}R}\right] \qquad \textit{(Eq. E.2–12)}$$
$$\left.+\left[(1-\upsilon)I_0\left(\sqrt{\frac{s}{\eta}}r\right)-2(\upsilon_u-\upsilon)\frac{I_1\left(\sqrt{\frac{s}{\eta}}R\right)}{\sqrt{\frac{s}{\eta}}R}\right]\right\}$$

In order to rearrange Eq. E.2–12, we classify the coefficients as follows:

Coefficient of $\frac{I_1\left(\sqrt{\frac{s}{\eta}}R\right)}{\sqrt{\frac{s}{\eta}}R} = \frac{1}{s}\frac{\Delta P_c}{A}a(1+f_{mc})[-(1-2\upsilon)(1-2\upsilon_u)-2\upsilon(1-2\upsilon_u)-2(\upsilon_u-\upsilon)] = -(1-2\upsilon)$

Coefficient of $I_0\left(\sqrt{\frac{s}{\eta}}r\right) = -\upsilon+(1-\upsilon) = (1-2\upsilon)$

Coefficient of $\frac{I_1\left(\sqrt{\frac{s}{\eta}}r\right)}{\sqrt{\frac{s}{\eta}}r} = -(1-2\upsilon)$

Using the above rearrangement method, we have:

$$\widetilde{\Delta\sigma_{\theta\theta}}^{(hyd.2.1)}_{(r,s)} = -\frac{1}{sA}\Delta P_c\alpha(1-2\upsilon)\left[\frac{I_1\left(\sqrt{\frac{s}{\eta}}r\right)}{\sqrt{\frac{s}{\eta}}r}+\frac{I_1\left(\sqrt{\frac{s}{\eta}}R\right)}{\sqrt{\frac{s}{\eta}}R}-I_0\left(\sqrt{\frac{s}{\eta}}r\right)\right] \qquad \textit{(Eq. E.2–13)}$$

If the mud cake pressure drop fraction is assumed non-zero ($f_{mc} \neq 0$), it affects Eq. E.2–8. For the unloading mode II (i.e. the pore pressure drop) unlike the first unloading mode (i.e. the confining pressure drop), the mud cake effect also affects the core displacement ($\widetilde{\Delta U_{rr}}^{(hyd.2)}_{(r,s)}$) as follows:

$$\widetilde{\Delta U_{rr}}^{(hyd.2)}_{(r,s)} = -\frac{1}{s}a(1-2\upsilon)\left(\frac{\Delta P_c r}{2GA}\right)(1-f_{mc})\left[\frac{I_1\left(\sqrt{\frac{s}{\eta}}r\right)}{\sqrt{\frac{s}{\eta}}r}+(1-2\upsilon_u)\frac{I_1\left(\sqrt{\frac{s}{\eta}}R\right)}{\sqrt{\frac{s}{\eta}}R}\right] \qquad \textit{(Eq. E.2–14)}$$

Therefore, a coefficient of $(1-f_{mc})$ will be created on the right hand side of Eq. E.2–5. Therefore, we have $\widetilde{\Delta\sigma_{\theta\theta}}^{(hyd.2)}_{(r,s)}$ as follows:

$$\widetilde{\Delta\sigma_{\theta\theta}}^{(hyd.2)}_{(r,s)} = -\frac{\Delta P_c}{sA}\alpha(1-2v)(1-f_{mc})\left[\frac{I_1\left(\sqrt{\frac{s}{\eta}}r\right)}{\sqrt{\frac{s}{\eta}}r} + \frac{I_1\left(\sqrt{\frac{s}{\eta}}R\right)}{\sqrt{\frac{s}{\eta}}R} - I_0\left(\sqrt{\frac{s}{\eta}}r\right)\right] \quad \textit{(Eq. E.2–15)}$$

Comparing Eq. E.2–13 and Eq. E.2–15, the mud cake effect $\widetilde{\Delta\sigma_{\theta\theta}}^{(hyd.2.2)}$ can be found as follows:

$$\widetilde{\Delta\sigma_{\theta\theta}}^{(hyd.2.2)} = \frac{\Delta P_c}{sA}\alpha(1-2v)f_{mc}\left[\frac{I_1\left(\sqrt{\frac{s}{\eta}}r\right)}{\sqrt{\frac{s}{\eta}}r} + \frac{I_1\left(\sqrt{\frac{s}{\eta}}R\right)}{\sqrt{\frac{s}{\eta}}R} - I_0\left(\sqrt{\frac{s}{\eta}}r\right)\right] \quad \textit{(Eq. E.2–16)}$$

Finally, the total $\widetilde{\sigma_{\theta\theta}}^{(hyd.2)}_{(r,s)}$ is found as the summation of:

$$\widetilde{\Delta\sigma_{\theta\theta}}^{(hyd.2)}_{(r,s)} = \sum_{m=1}^{2}\widetilde{\Delta\sigma_{\theta\theta}}^{(hyd.2.m)}_{(r,s)} \quad \textit{(Eq. E.2–17)}$$

Appendix F:

Deriving and Developing Induced Stresses (Unloading Mode–III)

The main thermal effect on the induced stresses is due to conduction heat transfer which causes the expansion-contraction effect. We denote it as thermal-1. The relation between the induced thermal radial and hoop stresses and the thermal displacement is given as (*Timoshenko, 1934, p. 407–412*):

$$\Delta\sigma_{rr}{}^{(thermal.1)} = \frac{E}{1-\nu^2}[\epsilon_{rr}{}^{(thermal)} + \nu\epsilon_{\theta\theta}{}^{(thermal)} - (1+\nu)\frac{\alpha_m}{3}\Delta T] \quad \textit{(Eq. F–1)}$$

$$\Delta\sigma_{\theta\theta}{}^{(thermal.1)} = \frac{E}{1-\nu^2}[\epsilon_{\theta\theta}{}^{(thermal)} + \nu\epsilon_{rr}{}^{(thermal)} - (1+\nu)\frac{\alpha_m}{3}\Delta T] \quad \textit{(Eq. F–2)}$$

Where E is the Young's modulus; ν is the Poisson's ratio; $\frac{\alpha_m}{3}$ is the one-dimensional bulk thermal expansion coefficient.

The following relation exists between the thermally-induced radial strain $\epsilon_{rr}{}^{(thermal)}$ and the radial displacement $\Delta U_{rr}{}^{(thermal)}$ (*Wang, 2000; Detournay & Cheng, 1993*):

$$\epsilon_{rr}{}^{(thermal)} = \frac{\partial(\Delta U_{rr}{}^{(thermal)})}{\partial r} \quad \textit{(Eq. F–3)}$$

The following relation exists between the thermally-induced hoop strain $\epsilon_{\theta\theta}$ and the radial displacement ΔU_{rr} (*Wang, 2000 & Detournay & Cheng, 1993*):

$$\epsilon_{\theta\theta}{}^{(thermal)} = \frac{\Delta U_{rr}{}^{(thermal)}}{r} \quad \textit{(Eq. F–4)}$$

The equation for $\Delta U_{rr}{}^{(thermal)}$ is needed to find the strains. The thermally-induced radial displacement is given by (*Timoshenko, 1934*):

$$\Delta U_{rr}{}^{(thermal)} = \frac{(1+\upsilon)}{(1-\upsilon)}\frac{\alpha_m}{3}\left[\frac{1}{R^2}\int_0^R \Delta T\, r\partial r + \frac{1}{r^2}\int_0^r \Delta T\, r\partial r - \Delta T\right] \quad \textit{(Eq. F–5)}$$

Therefore, using Eq. F–1, to F–5, we can find the thermally induced stresses as:

$$\Delta\sigma_{rr}{}^{(thermal.1)} = \frac{E}{(1-\upsilon)}\frac{\alpha_m}{3}\left[\frac{1}{R^2}\int_0^R \Delta T\, r\partial r - \frac{1}{r^2}\int_0^r \Delta T\, r\partial r\right] \quad \textit{(Eq. F–6)}$$

$$\Delta\sigma_{\theta\theta}{}^{(thermal.1)} = \frac{E}{(1-\upsilon)}\frac{\alpha_m}{3}\left[\frac{1}{{R_c}^2}\int_0^R \Delta T\, r\partial r + \frac{1}{r^2}\int_0^r \Delta T\, r\partial r - \Delta T\right] \quad \textit{(Eq. F–7)}$$

In order to facilitate making the integrations, we turn the equations to Laplace transforms. Taking Laplace transforms from both sides of Eq. F–6 and Eq. F–7, gives:

$$\widetilde{\Delta\sigma_{rr}}^{(thermal.1)} = \frac{E}{(1-\upsilon)}\frac{\alpha_m}{3}\left[\frac{1}{R^2}\int_0^R \widetilde{\Delta T}\, r\partial r - \frac{1}{r^2}\int_0^r \widetilde{\Delta T}\, r\partial r\right] \qquad \textit{(Eq. F–8)}$$

$$\widetilde{\Delta\sigma_{\theta\theta}}^{(thermal.1)} = \frac{E}{(1-\upsilon)}\frac{\alpha_m}{3}\left[\frac{1}{R^2}\int_0^R \widetilde{\Delta T}\, r\partial r + \frac{1}{r^2}\int_0^r \widetilde{\Delta T}\, r\partial r - \widetilde{\Delta T}\right] \qquad \textit{(Eq. F–9)}$$

To find the integrations, first we need the Laplace transform of the temperature difference across the sample ($\widetilde{\Delta T}$). This is found as (*Carslaw and Jaeger, 1959, p. 327 and 328*):

$$\widetilde{\Delta T} = \frac{\Delta T_0}{s}\frac{I_0(\sqrt{\frac{s}{\eta_T}}r)}{I_0(\sqrt{\frac{s}{\eta_T}}R)} \qquad \textit{(Eq. F–10)}$$

Where ΔT_0 is the initial temperature difference around the sample boundary during tripping.

The following integration rule holds for the hyperbolic Bessel function I_0 (*Kreyszig, 2006*):

$$\frac{d(z^v I_v(z))}{dz} = r^v I_{v-1}(z)$$

Thus:

$$\int zI_0(z)dz = zI_1(z) \qquad \textit{(Eq. F–11)}$$

Using the above rule and Eq. F–10, $\int_0^R \widetilde{\Delta T}\, \mathrm{r}\, \partial \mathrm{r}$ is found by:

$$\int_0^R \widetilde{\Delta T}\, r\partial r = -\int_0^R \frac{\Delta T_0}{s}\frac{I_0\left(\sqrt{\frac{s}{\eta_T}}r\right)}{I_0\left(\sqrt{\frac{s}{\eta_T}}R\right)} r\partial r = \frac{T_0}{s}\frac{1}{I_0\left(\sqrt{\frac{s}{\eta_T}}R\right)}\int_0^R I_0\left(\sqrt{\frac{s}{\eta_T}}r\right) r\partial r$$
$$= -\frac{\Delta T_0}{s}\frac{(R)I_1(\sqrt{\frac{s}{\eta_T}}R)}{(\sqrt{\frac{s}{\eta_T}})I_0(\sqrt{\frac{s}{\eta_T}}R)} \qquad \textit{(Eq. F–12)}$$

Thus, using Eq. F–8 and Eq. F–12, the final equation for the Laplace of the thermally-induced radial stress is:

$$\widetilde{\Delta\sigma_{rr}}^{(thermal.1)} = -\frac{\Delta T_0}{s}\frac{E}{(1-\upsilon)}\frac{\alpha_m}{3} \times \frac{1}{I_0(\sqrt{\frac{s}{\eta_T}}R)(\sqrt{\frac{s}{\eta_T}}R)}\left[I_1(\sqrt{\frac{s}{\eta_T}}R) - \frac{R}{r}I_1(\sqrt{\frac{s}{\eta_T}}r)\right] \qquad \textit{(Eq. F–13)}$$

Thus, using Eq. F–9, Eq. F–10, and Eq. F–12, the final equation for the Laplace of the thermally-induced hoop stress is:

$$\widetilde{\Delta\sigma_{\theta\theta}}^{(thermal.1)} = -\frac{\Delta T_0}{s}\frac{E}{(1-\upsilon)}\frac{\alpha_m}{3} \times \frac{1}{I_0(\sqrt{\frac{s}{\eta_T}}R)\sqrt{\frac{s}{\eta_T}}R)}\left[I_1(\sqrt{\frac{s}{\eta_T}}R) + \frac{R}{r}I_1(\sqrt{\frac{s}{\eta_T}}r) - (\sqrt{\frac{s}{\eta_T}}R)I_0(\sqrt{\frac{s}{\eta_T}}r)\right] \quad \textit{(Eq. F–14)}$$

Next, as we have considered the coupling the thermal effect on the pore pressure effect and the induced stresses, we need to find the induced coupling effect of the temperature drop. This is also called thermally-induced coupling stress. These effects on the induced radial stress, denoted as $\widetilde{\sigma_{rr}}_{(r,s)}^{(thermal.2)}$ and $\widetilde{\sigma_{rr}}_{(r,s)}^{(thermal.3)}$, are found using the analogy with the equations developed by *Chen & Ewy (2005)*:

$$\widetilde{\sigma_{rr}}_{(r,s)}^{(thermal.2)} = \frac{\Delta T_0}{s}\left(\frac{\eta'}{1-\frac{\eta}{\eta'}}\right)\frac{\alpha_m}{3}\frac{(1-2\upsilon)}{(1-\upsilon)I_0(\sqrt{\frac{s}{\eta}}R)(\sqrt{\frac{s}{\eta}}R)} \times \left[I_1\left(\sqrt{\frac{s}{\eta}}R\right) - \frac{R}{r}I_1(\sqrt{\frac{s}{\eta}}r)\right] \quad \textit{(Eq. F–15)}$$

$$\widetilde{\sigma_{rr}}_{(r,s)}^{(thermal.3)} = -\frac{\Delta T_0}{s}\left(\frac{\eta'}{1-\frac{\eta}{\eta'}}\right)\frac{\alpha_m}{3}\frac{(1-2\upsilon)}{(1-\upsilon)I_0(\sqrt{\frac{s}{\eta_T}}R)(\sqrt{\frac{s}{\eta_T}}R)} \times \left[I_1\left(\sqrt{\frac{s}{\eta_T}}R\right) - \frac{R}{r}I_1(\sqrt{\frac{s}{\eta_T}}r)\right] \quad \textit{(Eq. F–16)}$$

These effects on the induced hoop stress, denoted as $\widetilde{\sigma_{\theta\theta}}_{(r,s)}^{(thermal.2)}$ and $\widetilde{\sigma_{\theta\theta}}_{(r,s)}^{(thermal.3)}$, are found using the analogy with the equations developed by *Chen & Ewy (2005)*:

$$\widetilde{\sigma_{\theta\theta}}_{(r,s)}^{(thermal.2)} = -\frac{\Delta T_0}{s}\left(\frac{\eta'}{1-\frac{\eta}{\eta'}}\right)\frac{\alpha_m}{3}\frac{(1-2\upsilon)}{(1-\upsilon)I_0(\sqrt{\frac{s}{\eta}}R)(\sqrt{\frac{s}{\eta}}R)} \times \left[I_1(\sqrt{\frac{s}{\eta}}R) + \frac{R}{r}I_1(\sqrt{\frac{s}{\eta}}r) - RI_0(\sqrt{\frac{s}{\eta}}r)\right] \quad \textit{(Eq. F–17)}$$

$$\widetilde{\sigma_{\theta\theta}}_{(r,s)}^{(thermal.3)} = \frac{\Delta T_0}{s}\left(\frac{\eta'}{1-\frac{\eta}{\eta'}}\right)\frac{\alpha_m}{3}\frac{(1-2\upsilon)}{(1-\upsilon)I_0(\sqrt{\frac{s}{\eta_T}}R)(\sqrt{\frac{s}{\eta_T}}R)} \times \left[I_1(\sqrt{\frac{s}{\eta_T}}R) + \frac{R}{r}I_1(\sqrt{\frac{s}{\eta_T}}r) - (\sqrt{\frac{s}{\eta_T}}R)I_0(\sqrt{\frac{s}{\eta_T}}r)\right] \quad \textit{(Eq. F–18)}$$

Finally, the total $\widetilde{\sigma_{rr}}_{(r,s)}^{(thermal)}$ is found as the summation of:

$$\widetilde{\Delta\sigma_{rr}}^{(thermal)}_{(r,s)} = \sum_{n=1}^{3} \widetilde{\Delta\sigma_{rr}}^{(thermal.n)}_{(r,s)} \qquad \textit{(Eq. F–19)}$$

Finally, the total $\widetilde{\sigma_{\theta\theta}}^{(hyd.2)}_{(r,s)}$ is found as the summation of:

$$\widetilde{\Delta\sigma_{\theta\theta}}^{(thermal)}_{(r,s)} = \sum_{n=1}^{3} \widetilde{\Delta\sigma_{\theta\theta}}^{(thermal.n)}_{(r,s)} \qquad \textit{(Eq. F–20)}$$

Appendix G:

Correlations for Rock Mechanical and Thermal Properties-Based on Lithology:

Poisson's Ratio ν:

Table G-1: Typical Values of the Poisson's Ratio for Different Types of Rocks (*Zoback, 2010; Lama and Vutukuri, 1978*)

Type of Rock	ν
Shales	e.g. 0.3
Sandstones	0.125 ($\varphi = 5\%$) – 0.35 ($\varphi = 35\%$)
Carbonates	e.g. 0.25

Biot's Coefficient a:

Table G-2: Typical Values of the Biot's Coefficient for Different Types of Rocks (*Zoback, 2010*)

Type of Rock	*a*
Shales	0.7
Sandstones	0.9
Carbonates	0.7

Tensile Strength and UCS Correlations:

Table G-3: Typical Correlations between the Tensile Strength and UCS *(Jaeger et al.,2007)*

Type of Rock	Tesnile Strengtgh	Tensile Strength (Mpa)
Shales, Siltstones, & Mudstones	$T_s \approx \frac{UCS}{10}$ *[Eq.G-1]*	0.2–2
Sandstones	$T_s \approx \frac{UCS}{15}$ *[Eq.G-2]*	5
Carbonates	$T_s \approx \frac{UCS}{m}$, *m=7-15* *[Eq.G-3]*	10

Young's Modulus E and UCS Correlations:

Table G-4: Typical Correlations for Young's Modulus E as a Function of UCS (*Chang et al., 2006*)

Lithology	Correlations	
Shales	$E = \exp(\frac{1}{0.712}\ln(\frac{UCS}{7.22}))$	*[Eq. G–4]*
Sandstones	$E = \frac{UCS-2.28}{4.1089}$	*[Eq. G–5]*
Carbonates	$E = \exp(\frac{1}{0.51}\ln(\frac{UCS}{13.8}))$	*[Eq. G–6]*

UCS and ϕ Correlations:

- ✓ *Shales/Siltstones:*
  - *Vernik et al. (1998)*

    $UCS = 254(1 - 2.7\varphi)^2$ *Eq. G–7*

  - *Lashkaripour and Dusseault, (1993); Chang, (2006)* $\{used\ in\ the\ model\}$*:*

    $UCS = 1.001 \times 10^8\varphi^{-1.143}$, low porosity high strength ($\varphi < 0.1$) *Eq. G–8*

  - *Horsrud (2001):*

    $UCS = 0.28\varphi^{-1.762}$, high porosity low strength ($\varphi > 0.27$) *Eq. G–9*

- ✓ *Sandstones:*
  - *Clean sandstone (Plumb, 1994)*

    $UCS = 357(1 - 2.8\varphi)^2$, $\varphi < 0.357$ *(upper boundary for UCS)* *Eq. G–10*

  - *Zoback, (2010)* $\{used\ in\ the\ model\}$*:*

    $UCS = 277\exp(-10\varphi)$, $\varphi < 0.33$ *Eq. G–11*

- ✓ *Carbonates:*
  - *Rzhevsky and Novick, (1971); Zoback et al. (2006)* $\{used\ in\ the\ model\}$*:*

    $UCS = 135.9e^{-4.8\varphi}$, $0 < \varphi < 0.2$ *(upper boundary for UCS)* *Eq. G–12*

Thermal Expansion Coefficient α_m

Table G-5: Typical Thermal Expansion Coefficients

Lithology	*Thermal Expansion Coefficient[1/℃],* *(Gillian & Morgan, 1987)*
Shale	$2 \times 10^{-4} - 10^{-5}$
Sandstone	$1.1 \times 10^{-5} - 3.3 \times 10^{-5}$
Carbonates	$1 \times 10^{-5} - 2 \times 10^{-5}$

Thermal Diffusivity Coefficient η_T:

Table G-6: Typical Thermal Diffusivity Coefficients-Based on Lithology

Lithology	**Thermal Diffusivity [m2/s]** (Eppelbaum et al., 2014; *Huotori et al., 2004*)
Shale	7.3e-7
Sandstone	9.57e-7
Carbonates	10.92e-7